CANADIAN THESES ON MICROFICHE

THÈSES CANADIENNES SUR MICROFICHE

National Library of Canada
Collections Development Branch

Canadian Theses on
Microfiche Service

Ottawa, Canada
K1A 0N4

Bibliothèque nationale du Canada
Direction du développement des collections

Service des thèses canadiennes
sur microfiche

NOTICE

The quality of this microfiche is heavily dependent upon the quality of the original thesis submitted for microfilming. Every effort has been made to ensure the highest quality of reproduction possible.

If pages are missing, contact the university which granted the degree.

Some pages may have indistinct print especially if the original pages were typed with a poor typewriter ribbon or if the university sent us an inferior photocopy.

Previously copyrighted materials (journal articles, published tests, etc.) are not filmed.

Reproduction in full or in part of this film is governed by the Canadian Copyright Act, R.S.C. 1970, c. C-30. Please read the authorization forms which accompany this thesis.

AVIS

La qualité de cette microfiche dépend grandement de la qualité de la thèse soumise au microfilmage. Nous avons tout fait pour assurer une qualité supérieure de reproduction.

S'il manque des pages, veuillez communiquer avec l'université qui a conféré le grade.

La qualité d'impression de certaines pages peut laisser à désirer, surtout si les pages originales ont été dactylographiées à l'aide d'un ruban usé ou si l'université nous a fait parvenir une photocopie de qualité inférieure.

Les documents qui font déjà l'objet d'un droit d'auteur (articles de revue, examens publiés, etc.) ne sont pas microfilmés.

La reproduction, même partielle, de ce microfilm est soumise à la Loi canadienne sur le droit d'auteur, SRC 1970, c. C-30. Veuillez prendre connaissance des formules d'autorisation qui accompagnent cette thèse.

THIS DISSERTATION
HAS BEEN MICROFILMED
EXACTLY AS RECEIVED

LA THÈSE A ÉTÉ
MICROFILMÉE TELLE QUE
NOUS L'AVONS REÇUE

Canada

NL 339 (r. 85/09)

0-315-19513-4

National Library of Canada
Canadian Theses Division
Ottawa, Canada
K1A 0N4

Bibliothèque nationale du Canada
Division des thèses canadiennes

67421

PERMISSION TO MICROFILM — AUTORISATION DE MICROFILMER

• Please print or type — Écrire en lettres moulées ou dactylographier

Full Name of Author — Nom complet de l'auteur

DENNIS JOSEPH SIMEONI

Date of Birth — Date de naissance	Country of Birth — Lieu de naissance
APRIL 4, 1954	CANADA

Permanent Address — Résidence fixe

2098 LANSDOWNE ROAD
VICTORIA, B.C. V8P 1B3

Title of Thesis — Titre de la thèse

OPERATING AND PLASMA EXPULSION CHARACTERISTICS OF THE COAXIAL SPARK IGNITER

University — Université

UNIVERSITY OF ALBERTA

Degree for which thesis was presented — Grade pour lequel cette thèse fut présentée

Ph.d.

Year this degree conferred — Année d'obtention de ce grade	Name of Supervisor — Nom du directeur de thèse
1985	DR. PETER R. SMY

Permission is hereby granted to the NATIONAL LIBRARY OF CANADA to microfilm this thesis and to lend or sell copies of the film.

The author reserves other publication rights, and neither the thesis nor extensive extracts from it may be printed or otherwise reproduced without the author's written permission.

L'autorisation est, par la présente, accordée à la BIBLIOTHÈQUE NATIONALE DU CANADA de microfilmer cette thèse et de prêter ou de vendre des exemplaires du film.

L'auteur se réserve les autres droits de publication; ni la thèse ni de longs extraits de celle-ci ne doivent être imprimés ou autrement reproduits sans l'autorisation écrite de l'auteur.

Date	Signature
Jan. 28/1985	Dennis Simeoni

NL-91 (4/77)

THE UNIVERSITY OF ALBERTA

OPERATING AND PLASMA EXPULSION CHARACTERISTICS OF THE COAXIAL SPARK IGNITER

by

(C) DENNIS JOSEPH SIMEONI

A THESIS

SUBMITTED TO THE FACULTY OF GRADUATE STUDIES AND RESEARCH

IN PARTIAL FULFILMENT OF THE REQUIREMENTS FOR THE DEGREE

OF DOCTOR OF PHILOSOPHY

DEPARTMENT OF ELECTRICAL ENGINEERING

EDMONTON, ALBERTA

SPRING, 1985

THE UNIVERSITY OF ALBERTA

RELEASE FORM

NAME OF AUTHOR DENNIS JOSEPH SIMEONI

TITLE OF THESIS OPERATING AND PLASMA EXPULSION CHARACTERISTICS OF THE COAXIAL SPARK IGNITER

DEGREE FOR WHICH THESIS WAS PRESENTED DOCTOR OF PHILOSOPHY

YEAR THIS DEGREE GRANTED SPRING, 1985

Permission is hereby granted to THE UNIVERSITY OF ALBERTA LIBRARY to reproduce single copies of this thesis and to lend or sell such copies for private, scholarly or scientific research purposes only.

The author reserves other publication rights, and neither the thesis nor extensive extracts from it may be printed or otherwise reproduced without the author's written permission.

(SIGNED) Dennis Simeoni

PERMANENT ADDRESS:

2098 Lansdowne Road

Victoria, B.C.

V8P 1B3

DATED Jan. 28, 1985

THE UNIVERSITY OF ALBERTA

FACULTY OF GRADUATE STUDIES AND RESEARCH

The undersigned certify that they have read, and recommend to the Faculty of Graduate Studies and Research, for acceptance, a thesis entitled OPERATING AND PLASMA EXPULSION CHARACTERISTICS OF THE COAXIAL SPARK IGNITER submitted by DENNIS JOSEPH SIMEONI in partial fulfilment of the requirements for the degree of DOCTOR OF PHILOSOPHY.

Peter R Smy
.....

Supervisor

.....

.....

.....

.....

External Examiner

Date..December 14, 1989.

Dedication

To my parents, Giuseppe and Gemma Simeoni

Abstract

Experiments were performed in an attempt to obtain a better comprehension of a coaxial spark igniter's operating characteristics and its plasma ejection process.

The erosion rate of typical igniter component materials was monitored as a function of various experimental parameters. For optimum conditions it was found that working lifetimes of the order of ten hours could be expected and this was consistent with previous arc erosion measurements. From direct calibration of the thermal energy transferred by the igniter to the ambient gas it was found that overall efficiencies ~ 10% could be attained. The criterion required to minimize erosion and still maintain a substantial thermal energy transfer was determined to involve the use of low initial voltages on the energy storage capacitor.

Igniter plasma efflux measurements were performed and revealed that the plasma exits the jet cavity in a substantially supersonic condition. Measurements were obtained of the arc electric field within the cavity and the plasma expulsion time. Together with the efflux results they were found to correspond quite satisfactorily to established arc theory and to the concept of a plasma expansion from the cavity where the latter is assumed analogous to the high-pressure section of a conventional shock tube. There was strong evidence that the region adjacent to the luminous plume propagating from the igniter contained intense turbulence.

To determine the extent and growth of this turbulent 'mixing zone', photographs were taken of the induced motion of a tracer column of smoke. Simultaneous Schlieren photographs were also taken and when compared with the former it was evident that the turbulent region was coincident with a sharply defined warm gas distribution. Indications from previous studies were that the igniter was capable of distributing both particles and heat at greatly enhanced rates compared to those pertinent to molecular diffusion or heat conduction. The consequent implications were that this augmentation of the respective coefficients was turbulence-induced. Measurements obtained from a unique smoke-scattered light technique in conjunction with a photomultiplier/raster system yielded values of these coefficients which were consistent with the above deductions.

Acknowledgements

I consider myself very privileged to have worked under the excellent supervision of Dr. Peter Smy. He always found time to provide advice or assistance on the project and his encouragement, sympathy, and sense of humour were invaluable during the difficult periods of the research.

I am very grateful to Doug Way-Nee who provided his technical expertise in the course of the experiments. I could also rely upon him for support and kind advice on any matter and appreciated his companionship while jogging or playing racquetball.

Dr. Jamie Santiago provided many valuable suggestions and much assistance during this work. I am indebted to the research assistants: Salman Ghufran and Lin Duquette, for their contributions during the latter portions of the research.

My thanks go to the Electrical Engineering machine shop staff who were very perceptive to my requirements and produced high calibre work. Those particularly involved with my project were: Konrad Doerrbecker, Herb Gans, Bernie Munawich, Herbert Dexel, and the late Steve Gomez.

I wish to acknowledge the valued friendship of Ed Sumbar who provided his support throughout these years and whose sense of humour brightened some dreary days. My appreciation goes to Farouk Soliman, Bill Tighe, Steve Au, and Rajender Razdan for their friendship, encouragement, and the many pleasant hours spent on the racquetball courts.

I express my utmost gratitude to Paul and Simonne Rogiani who shared their house with me for five years and treated me as part of their family. They played a major supportive role in the realization of this work.

Finally I wish to thank my family who always had faith that I would attain this lifelong goal and who with their love, spiritual and financial support sustained me through these years.

Table of Contents

Chapter Page

1. Introduction 1

1.1 The Ignition System 1

1.2 Past Research 4

1.2.1 Automotive Applications 4

1.2.2 Studies Of Chemical And Gas Dynamic Igniter Characteristics 6

1.3 Commercial Applications Of The Plasma Jet System 12

1.4 Topics Of The Thesis Research 12

2. Coaxial Spark Igniter Erosion And Efficiency Investigations 16

2.1 Erosion Considerations 16

2.2 Efficiency Considerations 20

2.3 Erosion Experiments 22

2.4 Discussion Of The Erosion Results 27

2.5 Efficiency Experiments 30

2.6 Discussion Of The Efficiency Results 32

2.7 Conclusions 32

3. Plasma Expulsion Processes In The Plasma Jet Igniter 36

3.1 Introduction 36

3.2 Characteristic Times For The Ejection Process 37

3.3 Determination Of The Plasma Heating Time 38

3.4 Plasma Expulsion Time Considerations 41

3.5 Heating Time Experiments 49

3.6 Streak Photograph Experiments 50

3.7 Plasma Exhaustion Time Measurements 58

3.8 Observations Of The Plasma Expansion Process Within The Cavity 58

3.9 Two Dimensional Still Photographs Of The Plasma Jet 62

3.10 Discussion And Conclusions 65

4. Diffusion And Heat Conduction Enhancement By Coaxial Spark Igniters 70

4.1 Introduction 70

4.2 Turbulent Transport Considerations 72

4.3 Smoke-Scattered Light Technique 85

4.3.1 System For The Determination Of The Enhanced Diffusion And Heat Conductivity Coefficients 85

4.3.2 Theoretical Aspects Of The Smoke Column Expansion 89

4.3.3 Experimental Determination Of The Eddy Diffusivity 95

4.3.4 Discussion Of The Eddy Diffusivity Results 100

4.4 Studies On The Relative Heat Wave And Smoke Plume Motions 107

4.5 Heat Conductivity Experiments 110

4.6 Conclusions 115

5. Summary Of Conclusions 117

References 121

Vita 125

List of Tables

Table	Page
4.1 Turbulent Diffusion Coefficients	102

List of Figures

Figure		Page
1.1	Cross-Section Of The Igniter	2
1.2	Ignition Circuit	3
2.1	Mass, Momentum, And Energy Transfer In An Evaporation Dominated Arc	18
2.2	Demountable Component Igniter	23
2.3	Graph Of The Erosion Rate Versus The Initial Capacitor Stored Energy	25
2.4	Graph Of Erosion Rate Versus Current	26
2.5	Erosion Rate Versus Gas Pressure	28
2.6	Efficiency Cell	31
2.7	Graph Of Overall Efficiency Versus Stored Energy	33
2.8	Graph of E_E/E_s Versus Initial Capacitor Voltage	34
3.1	Graph Of Axial Temperature And Electric Field Versus Current	39
3.2	Graph Of Heating Time And Ejection Time Versus Current	42
3.3	Shock Wave Parameters	46
3.4	Calculated And Measured Flow Velocities Versus Current	48
3.5	Streak Photography Setup	51
3.6	Parameters Used In Streak Photo Analysis	54
3.7	Proposed Model Of The Pulsed Plasma Jet	68
4.1	Variation Of $E(k,t)$ With Wavenumber k	83
4.2	Smoke-Scattered Light Detection System	86
4.3	Oscilloscope Raster Display System	88
4.4	Scan Of Aperture Across Spherical Control Volume	92
4.5	Log-Log Plot Of Normalized Scattered Light Intensity Decay With Scanning Time Period	101
4.6	Log-Log Plots Of Shifted Data For Various Distances	103

Figure Page

4.7 Log-Log Plots Of Shifted Data For Various Voltages 104

4.8 Log-Log Plot Of D Versus x 106

4.9 Optical Configuration For Obtaining Simultaneous Smoke And Schlieren Photographs 108

4.10 Schlieren/Mirror/Lens Configuration 109

4.11 Schlieren Technique For Measuring Heat Flux Near A Wall 112

4.12 Graph Of Q And K/K_0 Versus Distance From Wall 114

List of Plates

Plate		Page
3.1	Oscillograms Of The Pulsed Current To The Igniter And The Associated *E* Field	52
3.2	Streak Photograph Of The External Plasma Jet	55
3.3	Oscillogram Of Probe Current Versus Time For The Laser Spark Experiments	57
3.4	Ceramic Channel Model	60
3.5	Plasma Expansion Within The Igniter Channel	61
3.6	Composite Streak Photograph	63
3.7	Two Dimensional Photograph Of The External Plasma Jet	64
4.1	Photographs Of Smoke Dispersion At Various Delay Times	96
4.2	Photograph Of A Single Smoke Dispersion Event	97
4.3	Photograph Of The Scope Raster Display For A Single Diffusion Event	99

1. Introduction

In recent years, rising world oil prices have inspired significant research efforts to improve the efficiency of spark-ignition engines, particularly under lean-burn conditions. The reliable ignition of lean mixtures is more difficult than for stoichiometric mixtures and the corresponding flame speeds are much slower. Attempts to accomplish this complex task have directed considerable attention to one particular technique: use of the coaxial spark igniter as opposed to a conventional spark plug. The research described in the succeeding pages is an attempt to achieve a better understanding of the coaxial spark igniter's operating characteristics and its plasma ejection process.

1.1 The Ignition System

The coaxial spark igniter, also described as a plasma jet ignition plug ('plasma plug'), is a modified version of a standard surface discharge igniter and is similar to the Lodge He 1/2 igniter used for the ignition of fuel oil.[1] Specifically the modification involves the welding of a steel disk with a small hole in its centre to the end of the igniter. A small cylindrical cavity is then formed by drawing back the centre electrode. This cavity is the site of the electrical discharge which manifests itself as a narrow jet of plasma of two to three centimetres length and a few millimetres in diameter. The cross-section of the igniter is illustrated in Figure 1.1.

The supply circuit consists of a low voltage energy storage stage which is coupled to a high voltage stage, the latter initiating breakdown in the igniter cavity. The circuit schematic is shown in Figure 1.2. Operation of the system consists of a standard SCR discharge pulser which delivers a 600 volt pulse to the ignition coil primary. The resulting induced high voltage charges the capacitor C_1 until spark gap breakdown occurs. In turn, a rapidly rising high voltage pulse is produced which initiates breakdown in the igniter cavity. The capacitor C_1 and the spark gap are oriented such that the latter pulse is of such rapidity that it is not shorted out through the inductance L ($\simeq 35\mu H$). With igniter breakdown, the low voltage energy storage capacitor C_2 discharges through the cavity.

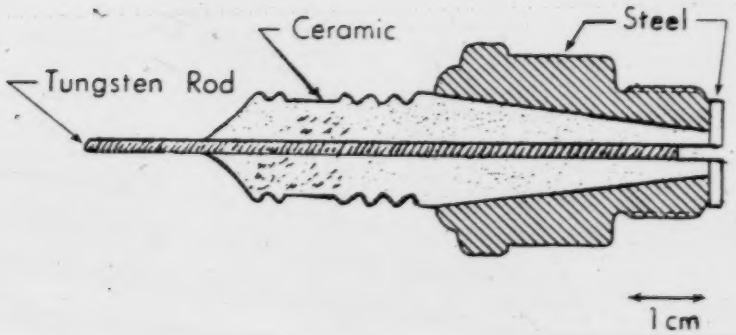

Figure 1.1 Cross-Section Of The Igniter

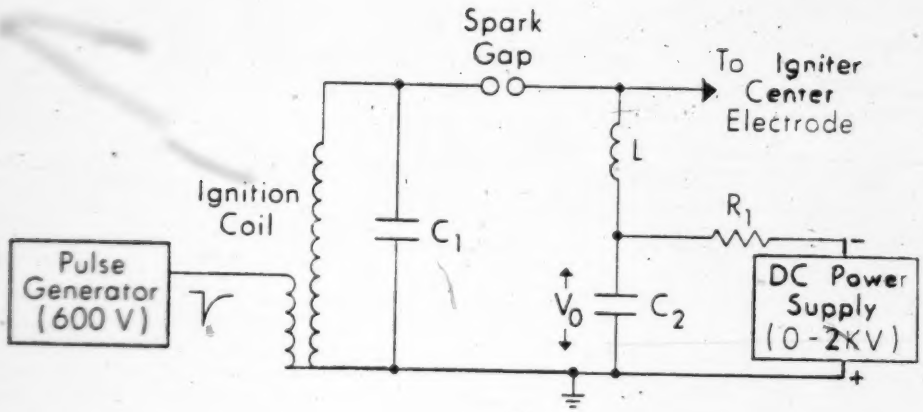

Figure 1.2 Ignition Circuit

The electrical energy delivered causes Joule heating of the gas in the cavity and raises its temperature, partially ionizing it. With the sudden increase in temperature there is a corresponding increase in pressure of the partially confined plasma and it is consequently ejected out of the cavity in the form of a jet. This plasma consists of highly energetic and chemically active free electrons and ions which are at temperatures of the order of 10^4 °K. There is also an undetermined fraction of neutral ions or molecules.

1.2 Past Research

1.2.1 Automotive Applications

Research on the plasma jet igniter has proceeded in several directions. Most of this work has focussed on automotive applications and many patents related to this system exist.

The earliest intensive research on plasma jet igniters occurred during the 1950's where their applicability for producing high energy plasmas for propulsive purposes was explored.[2] The first attempt to improve engine emission characteristics and efficiencies by employing a pulsed plasma jet was the thesis project of K. Waterson.[3] He used a plasma jet igniter which was made by modifying a conventional spark plug. His research compared plasma jet ignition with conventional ignition sources and those by focussed laser beam plasmas. Two years later Topham *et al.*[1] applied the igniter to experiments with single and multi-cylinder engines. Although not conclusive, their data implied that the lean mixture limit for a single-cylinder i/c engine was extended while there were minimal improvements with the multi-cylinder engine. Wyczalek *et al.*[4] used a similar experimental system but the cavity diameter of their igniter was much larger. This resulted in a much weaker plasma jet with less penetration into the combustion chamber. Their findings for single and multi-cylinder engines were that the plasma jet did not extend the lean flammability limit, increased hydrocarbon emissions, decreased horsepower, and reduced the NO_x pollutant concentrations. However, Fitzgerald[5] using a modified version of the plasma igniter demonstrated that the lean limit

could be increased in single-cylinder engines. Asik *et al.*,[6] using an igniter cavity diameter similar to that of Topham and associates, worked with single and multi-cylinder engines and reported that for the former case plasma jet ignition increased NO emissions, reduced the ignition delay and increased torque compared to conventional systems. They found that plasma jet action depended on the cavity diameter and minimal improvements resulted with the multi-cylinder engine. Dale *et al.*[7] found when the igniter was applied to a single cylinder engine burning either gasoline or propane that: the exhaust temperature generally decreased; the output power increased and the specific fuel consumption decreased; the range of air/fuel ratios for engine operation was extended; hydrocarbon and CO emissions were not significantly altered but NO concentrations always increased. They also found that with the plasma plug, the ignition volume was orders of magnitude greater and engine timing was less critical than for conventional systems. Dale and Oppenheim[8] indicated that the plasma jet at an air/fuel ratio greater than 18 produces a power output and specific fuel consumption which are definitely superior to those of a standard spark plug. In wide-open throttle and partial throttle operation combustion was found to start at about the same time using the two types of igniter but it was observed to end definitely earlier using the standard plug. In the work of Tozzi and Dabora[9] using a single-cylinder engine the lean misfire limit and the power output were observed to be extended and increased respectively using a plasma jet system. They also found that the plasma cavity size can affect the gains which casts some light on the incongruous results reported above by Wyczalek *et al.*[4] Pitt and Clements[10] applied the plasma jet system to a single-cylinder engine burning propane and found that ignition delay was reduced.

Evidently in the majority of the foregoing experiments using single and multi-cylinder engines operating with a lean charge (air/fuel>18), the plasma jets were shown to extend the lean misfire limit. There was shown to be an improvement in engine output power for specific fuel consumption, and it was greatly enhanced for operation on lean mixtures. Generally the CO and hydrocarbon pollutant concentrations were not significantly affected whereas the NO emissions were usually higher.

For the plasma jet ignition systems Dale *et al.*[9] found that the engine performance was unaffected by timing as opposed to standard systems. This follows since the volume in which ignition occurs for the plasma jet igniter was found to be greater by orders-of-magnitude than for a conventional spark plug. Hence for stoichiometric fuel mixtures the timing of an engine utilizing the plasma plug would not have to be altered.

1.2.2 Studies Of Chemical And Gas Dynamic Igniter Characteristics

The mechanisms by which plasma jet igniters produce the observed improvements in engine performance described in the preceding section are complex and not clearly understood. Plasma expulsion is affected by electromagnetic as well as aerodynamical effects. The latter effects manifested as turbulence and jet penetration as well as the chemical effects of radicals are definitely responsible in large part for the performance improvements. There is evidence that these effects are correlated and linked by a thermal stratification of the jet. Lawton and Weinberg[11] regarded the wake of plasma jets originating from magnetically spun d.c. arcs as a 'spiral staircase' of radical-rich hot gas embedded in a cooler ambient stream. Turbulence converts this stratified structure into one of isolated pockets of hot gas. Behbahani *et al.*[12] likened the distribution of these hot pockets by the plasma jet to that of pellets from a shot gun.

For many years chemists working in flame kinetics have considered the pertinent conversion reactions in terms of radicals (active molecular fragments) and their respective reactions.[13] Radicals have low activation energies and hence the overall flame reaction rate depends on their concentration. Flame reactant conversion processes proceed through steps involving a variety of radicals which are capable of rapid multiplication through branching reactions such as:

$$H + O_2 \longrightarrow HO + O \qquad (1.1)$$

For normal hydrocarbon flames in the presence of nitrogen the dissociation equilibria are[14]:

$$CO_2 \rightleftharpoons CO + 1/2O_2$$
$$H_2O \rightleftharpoons H_2 + 1/2O_2$$
$$H_2O \rightleftharpoons 1/2H_2 + OH \qquad (1.2)$$
$$1/2H_2 \rightleftharpoons H$$
$$1/2O_2 \rightleftharpoons O$$
$$1/2N_2 + 1/2O_2 \rightleftharpoons NO$$

Premixed flames are dependent upon the intensity of the turbulence.[15] The flame front is disrupted completely for very large intensities and burning occurs in isolated pockets.[11] For very small scales of turbulence less than the flame thickness, the flame is subjected to larger heat and diffusion losses by transport processes. The flame chemistry is not likely affected and the transport coefficients for laminar propagation are modified by the eddy diffusivity. Small scale turbulence greater than the flame thickness corrugates the instantaneous flame front shape.[11]

The augmentation of combustion rates by radicals and turbulence generated by the discharge of the igniter has been the subject of many studies. The possibility of long-range radiation effects in improving flame initiation in hydrocarbon plasmas was discounted as insignificant by Orrin *et al.*[16]

Harrison and Weinberg[17] observed the effect of a magnetically rotated continuous flow plasma jet on methane in air flame reaction rates and stability. A subsidiary stream of different gases was added to the igniter cavity to carry the enthalpy from the arc to the main reaction zone. The carriers consisted of argon, nitrogen, and the OH, O, and H radical producing species: H_2O, O_2, and CH_4. They found that flame stability and reaction rates greatly increased when a small proportion of electrical energy was added and N_2 in argon was the most effective carrier. Argon and water were found to be the least effective. Hilliard and Weinberg[18] used a much smaller plasma jet in the absence of a magnetic field and added significantly less proportions of electrical energy than the preceding work. Once again nitrogen containing plasmas were utilized and it was found that flame stability was greatly increased to the point

where the flame could be maintained on mixtures too lean and flow velocities too rapid for normal flame stabilization. The effect of the N_2 plasma on concentrations of the pollutant NO was found to decrease the latter by a very significant factor.

Topham *et al.*,[1] Bradley and Critchley,[19] and Oppenheim *et al.*[20] used a constant volume bomb for their studies. The combustible mixture was initially stationary and at ambient temperature and pressure. The results were summarized by Dale and Oppenheim[8] as follows:

1. "The plasma jet entered the combustion chamber in the form of a turbulent plume which was imbedded in a blast wave headed by a hemispherical shock front.
2. The gasdynamic effects of the blast wave were dissipated by the time combustion started, after a delay typically of an order of 1 msec, so that ignition took place in the turbulent zone of the plume.
3. The depths of penetration of the jet were solely a function of its initial velocity; it could be thus controlled by the amount of energy deposited in the cavity, as well as its size and that of the exit orifice.
4. In direct contrast to spark ignition that produces a laminar flame which later becomes turbulent, here combustion was initiated in the form of a turbulent flame which upon leaving the plume tended to acquire a laminar character; the normal burning speed was, as a consequence, initially quite high decreasing monotonically as the flame kernel expanded.
5. With provisions made to fill the cavity with different feedstock, the most effective for ignition were hydrocarbons, among which those initially in liquid state were particularly effective-a phenomenon interpreted as due to the action of hydrogen atoms, of which there was an abundance in the plasma created from the feedstocks.
6. Plasma jets were shown to be capable of igniting gaseous mixtures below the normal flammability limit."

Cetegen *et al.*[21] also utilized a combustion bomb in their experiments and proposed that the observed flame speed enhancement by the plasma jet was due to an enlarged flame surface area created by the jet generated turbulence. They also found that jet penetration was proportional to the ratio of the volume of the igniter cavity to its orifice area. Orrin *et al.*[22] performed experiments with a combustion chamber for various igniter designs. They used shadowgraphy and C_2 emission spectroscopy as two independent methods of assessing flame propagation rates and geometry. Their findings were that the H content of the plasma medium correlated with the enhancement of the burning velocity of very lean mixtures. They also indicated that turbulence generated by the plasma jet was most likely responsible for the increased flame speeds. Two years later Carleton *et al.*[23] compared the plasma jet radical injection and turbulence effects on flame propagation and ignition enhancement. They

proposed that chemical effects (i.e. due to radicals) were dominant for lean mixtures whereas the generation of maximum turbulence was most favourable for stoichiometric conditions. They also considered radical losses to the walls in the vicinity of the igniter. For a bomb with walls within 1.3 cm of the plasma jet it was found that there was a definite narrowing of the ignitability limits except at high pressures. With respect to the thermal efficiency of the igniter they found that approximately 10% of the initially stored energy is available to the plasma jet itself. This value was also presented in the work of Topham *et al.*[1] Likewise Clements *et al.*[24] verified the above igniter efficiency value.

In the latter work a systematic study was performed of the various designs of injection-type igniters. They found that the dominant plasma ejection mechanism was pressure dependent with insignificant contributions from electromagnetic forces. A low voltage high capacitance discharge was found by them to be more thermally efficient than a high voltage low capacitance discharge.

In their investigations of design parameters for the optimization of igniter performance, Grant *et al.*[25] using various cavity diameters, were unable to obtain the jet penetration relationship to orifice area of Cetegen *et al.*[21] They investigated the effect of input energy on jet penetration and found no correlation between them while the volume of the jet was found to be energy dependent. Their combustion chamber work using propane-air mixtures indicated that combustion enhancement was dependent on the igniter orifice area and accordingly adjustment of the latter parameter for higher pressures than atmospheric could maintain optimal flame spread conditions in engines.

In an attempt to elucidate the turbulence mechanism generated by the igniter, Topham *et al.*[26] suggested a similarity between the Schlieren photographs of the turbulent patches of fluid before combustion and atmospheric buoyant thermals or 'puffs'. Their experimental results indicated that the two phenomena were mathematically similar.

Zhang *et al.*[27] performed studies on the plasma jet augmentation of the burning velocity of a methane-air fuel mixture. Their method involved the separation of the ignition and

velocity enhancement processes. The jet-induced turbulence was found to augment the burning velocity and for moderate mixture strengths turbulence rather than radical effects were found to dominate.

Behbahani *et al.*[12] continued the work of Hilliard and Weinberg[18] in the removal of NO using N_2 generated by the plasma jet. Using a novel design of plasma jet igniter their results yielded surprisingly high efficiencies for the destruction of NO and these efficiencies were found to prevail at considerable distances downstream of the igniter orifice. This phenomenon could not be reconciled by any plug flow model which assumes a half life for sonically injected N atoms at distances of the order of a centimetre downstream. They proposed that jet induced turbulence causes the magnetically spun spiral of the radical rich hot gas embedded in the external colder stream to disintegrate into pockets of unmixed hot gas which would transport and preserve radicals far downstream. The previous work of Jagoda and Weinberg[28] using Schlieren-Doppler velocimetry methods also indicated evidence of the existence of these 'hot pockets' of gas.

In further studies of the work in the preceding paragraph Behbahani *et al.*[29] suggested that plasma jets act similarly to atomizers which disperse minute 'droplets' of high temperature gas encapsulating highly dissociated, reactive species. They did not use a magnetically spun arc as in their preceding work but rather a high velocity vortex which was generated by the plasma medium injection method. The resulting plasma jet was thermally more stratified than that for a standard plug. They found that the NO removal efficiency was highest for a maximum flow rate and minimum power input and when the igniter was applied to a simulated exhaust system there were very marked efficiencies of NO removal.

The recent work of Cavolowsky *et al.*[30] concluded that the results of Behbahani and associates were due to a thermal stratification in the plasma jets which in turn resulted in the heating of a very small proportion of the gas to extremely elevated temperatures. These small pockets of very hot gas were evident on Schlieren and shadowgraphs although this could not be taken as conclusive evidence since the latter optical methods are very sensitive to extremely

small temperature fluctuations. Further confirmation of the existence of the pockets was obtained by the use of ionization probes connected to an oscilloscope. As the pockets reached the probes, voltage spikes appeared on the oscilloscope and these were found to disappear for probe separations in excess of 1.5 mm and at measurement sites beyond 2.5 cm downstream. The former distance defined the maximum size of the hot pockets and the latter their maximum times of duration.

Continuing on the subject of the dispersion of these hot pockets by plasma jets, the recent work of Clements *et al.*[31] indicated that the quantity of nitrogen atoms produced by the igniter was considerably in excess of the value from equilibrium dissociation predictions and that the average temperature of the plume was quite low to justify this. They performed experiments to measure the thermal energy propagation (temperature) and convective velocities within the turbulent puff generated by the plasma jet. The results were found to be consistent with the predictions of Topham *et al.*[26] In addition the convective velocity measurements indicated the existence of a substantial turbulent velocity component. They found that the gas beyond the jet was heated abruptly to temperatures of the order of 10^2 °C and this was too low to explain the intense persistence of chemical activity throughout the puff. It was proposed that some form of convective or turbulent transport of the particles was responsible for the anomalies and that a knowledge of the local hydrodynamic flow field was critical in the determination of the role of radicals in the observed flame speed enhancements.

The majority of the foregoing studies have dealt with the plasma jet ignition of lean mixtures. Vince *et al.*[32] examined the effects of the plasma plug on flame propagation and sooting at the rich limits of flammability. This is particularly relevant to recent diesel engines where plasma ignition is presently being considered. They found that plasma jet ignition extended the rich limits of flammability and soot formation was greatly reduced. The flame propagation velocity was found to be increased for plasmas in certain media. As opposed to lean mixtures, the chemical effects were not found to be greatest for plasmas producing only hydrogen atoms. The most effective media for the rich mixtures involved the interaction of

oxygen and hydrocarbons.

Very recently Pitt *et al.*[33] have devised a new ignition concept which is a device incorporating the features of a conventional spark plug, a plasma jet and direct-injection stratified charge ignition. Their 'puff-jet' ignition functions by injecting a small volume of combustible mixture which produces a turbulent plume in the region of the standard spark gap. Here the plume rapidly mixes the gas and the surrounding medium and results in a near stoichiometric turbulent 'puff'. Stratification of the charge in the combustion chamber is produced. It was found that this device reduces ignition delay and combustion time similarly to the plasma plug system.

1.3 Commercial Applications Of The Plasma Jet System

Aside from the obvious applicability of the plasma jet igniter to internal combustion engines there are several other situations where it may be useful. It could be utilized for starting diesel engines involving some of the proposed new fuels especially in very cold climates. It would provide more reliable ignition in furnaces where a major explosion hazard exists if rapid ignition fails. Plasma plugs would be useful in jet engines following flame-out. Although the igniters in the latter case would not prevent flame-out for jet engines flying through rain clouds they could provide reliable re-ignition following the re-establishment of fuel flammability. Studies are proceeding to test the feasibility of applying the plasma jet igniter to pilot sour gases in flare stacks.

1.4 Topics Of The Thesis Research

It is interesting to note that none of the research described in the preceding sections has dealt with the erosion characteristics of the plasma jet igniter. This important aspect of its operation was given cursory mention in the work of Topham *et al.*[1] and Tozzi and Dabora.[9]

Although repetitive pulsed energies of the order of a Joule typically required by the igniter are feasible in an automobile engine, this places a very considerable increase in demands

of the battery charging system. There is also an inherent increase in plug erosion and therefore in servicing frequency.

With respect to the latter erosion, consider a four cylinder engine running at 6000 r.p.m. with each plug firing every two revolutions. The revolution rate is 100 rev/sec and in turn there will be 50 sparks/plug/sec. At a speed of 50 km/hr the time required to travel 1600 km will be 33.3 hours. Therefore the number of sparks produced will be: $5.94 \cdot 10^6$. From the erosion data obtained from this experimental work under ambient conditions, using $14\mu F$ capacitance; 700 volts and $1.142 \cdot 10^5$ firings, ablation of a soft steel plug end amounts to an average value of .030 grams. Hence, the expected erosion after 1000 miles of use in the four-cylinder engine would be 1.60 grams. At $14\mu F$; 700 volts, the corresponding erosion for plugs fitted with hard steel ends would be .80 grams. These erosion values represent a significant percentage of the initial mass of the plug ends and qualitative observations reveal that the bulk of the ablation manifests itself in enlargement of the plug end aperture. This effect would result in a definite change in the plasma jet ejection characteristics and would undoubtedly reduce the igniter channel back pressure and penetration depth of the jet as is indicated in the work of Wyczalek *et al.*[4] The data used in the above example were obtained from erosion tests in air and hence can only provide a rough estimate of the corresponding erosion in an engine's cylinders where conditions differ greatly from the ambient. Nevertheless this problem seems at present to be severe enough to pose a major obstacle to implementation of high energy igniters in conventional automobile engines.

Chapter 2 deals with the investigation of the igniter erosion with variations of such parameters as pressure, energy/pulse, and component materials. The corresponding values of igniter efficiencies for these variations were also studied. From the efficiency and erosion considerations the limits of igniter operation were determined and the operating conditions where both parameters would be optimal were ascertained.

Chapter 3 describes experiments performed in an attempt to elucidate the plasma ejection mechanism and with the intent that the results would assist in the optimization of the

igniter design. Measurements were performed of the flow velocity, exhaustion time and electric field within the igniter cavity. In order to obtain more definitive results of the external plasma column structure and streaming velocities, streak photographic work similar to that of Topham *et al.*[1] was undertaken.

Although the past research described above presents definite evidence that the igniter improves engine performance by a corresponding increase in flame speed there is no clarification of the mechanism responsible for this increase. Even though recent studies have proposed the propagation of hot pockets of gas and thermal stratification of the plasma jet as likely mechanisms, they are still based largely on conjecture.

Most of the papers published in recent years suggest chemical and aerodynamic mechanisms were most likely responsible for the increase in flame speeds. Studies of the separate contributions of these two effects stress the importance that they be considered as acting together.[22,31] These two complementary mechanisms may also compete against each other. For mixtures near stoichiometric the turbulence mechanism appears to be dominant. Near the limits of flammability, however, turbulence can be unfavourable as it tends to disrupt and extinguish the flame front. The free radicals, on the other hand, produce marked increases in the laminar burning velocity for this situation. Hence for very lean mixtures the chemical mechanism is advantageous whereas for conditions near stoichiometric, plug design considerations will involve the generation of maximum turbulence.

Association of turbulence with the stratified volumes encapsulating active species (i.e. hot pockets) facilitates the explanation of the unusually great diffusion paths and times of radical interactions and also the major role of turbulence in promoting combustion. From photographs of the luminous plume ejected from the igniter cavity in the work of Chapter 3 it is evident that regions of intense turbulence exist adjacent to the plume.

A major portion of this work was devoted to the further investigation of the nature of the turbulence mechanism and its related transport properties. Particularly, the main experiment involved the determination of a turbulent diffusion coefficient for various

parameter variations using a unique system involving the tracking of the induced motion of tracer columns of smoke. This work is contained in Chapter 4.

Chapter 5 contains a summary of the conclusions of the thesis research work.

2. Coaxial Spark Igniter Erosion And Efficiency Investigations

This chapter deals with the investigation of igniter efficiency and erosion with respect to the variation of several parameters which might be encountered in automotive applications. These parameters include spark energy, ambient gas pressure, and igniter component materials (specifically in the case of erosion).

2.1 Erosion Considerations

Research on electrode erosion has been performed for many years especially in switchgear applications. Cathode evaporation rates have been reported by Cobine[34] for copper and mercury of 87 and 250 $\mu g\ C^{-1}$ respectively. Turner *et al.*[35] determined an empirical relation for currents less than 1000 A and durations over 10 msec of:

$$\frac{dM_e}{dt} = ki^{1.6} \quad \mu g\ s^{-1} \tag{2.1}$$

where k is a constant, M_e is the eroded mass, and i the current is in amps. Turner and Turner[36] give the erosion rates for a 100 A copper cathode discharge of 250 μsec duration of 13 $\mu g\ C^{-1}$. Extrapolation of equation (2.1) ($k=2.4$ for copper) to this situation yields a value of 38 $\mu g\ C^{-1}$ which is approximately three times the experimental value. Application of equation (2.1) to a typical situation encountered in the experiments of this chapter with $i \simeq 200$ A and $t \simeq 5 \cdot 10^{-5}$ sec yields a value for the erosion rate of $\simeq 58\ \mu g\ C^{-1}$. Assuming as in the past case an approximate threefold disparity with the experimental value results in a rate of $\simeq 19\ \mu g\ C^{-1}$. Other rates varying between .1 and $10^{-3}\ \mu g\ C^{-1}$ have been reported.[37,38,39] Erosion rates of 10-100 $\mu g\ C^{-1}$ have been measured in previous studies for conditions similar to those in this thesis work (i.e. currents $<10^3$ A for discharge times $\simeq 10^{-4}$ sec).

Niemeyer[40] in his study of high current density arcs in channels of solid material developed from first principles an integral arc model relating the arc characteristics to the arc current, the channel geometry, and the properties of the channel material. The latter work describes a steady-state situation and the processes involved for these evaporation dominated

arcs are defined as: induced evaporation of wall or electrode material, axial convection, and radiative transfer. For wall evaporation to become dominant, he shows that the current density j must be ≥ 10 A mm^{-2} which is certainly the case for the experiments performed in this chapter (i.e. $j \simeq 10^2$ A mm^{-2}). The production and transfer of mass, momentum, and energy for an evaporation dominated arc are shown schematically in Figure 2.1. The parameter $\dot{q}_0$ represents the fraction of the ohmic power generated in the arc zone which is transferred to the wall material and in turn provides the vapourization energy for the material. The channel wall in consequence ejects a mass flux $\dot{\mu}_{21}$. The vapour injection and ohmic heat input creates an overpressure which causes an expansion flow through the open channel ends. For a channel of uniform diameter along its length the overpressure $\hat{p}$ attains a maximum value at the channel mid-point and the negative pressure gradients produced towards the channel exits accelerate both the plasma and surrounding vapour at the cross-sectional velocities v_{e1} and v_{e2} respectively.

The relation for the mass ablation rate $\dot{M}$ is given by Niemeyer as:

$$\dot{M} = .55 V_1 \left[\beta + (1-\beta)\frac{c_1}{c_2}\right] \frac{\pi R^2 \hat{p}}{h_1} \tag{2.2}$$

where $V_1 = V(T_1)$ is a combined material function:

$$V(T_1) = V(p,T) = \rho(p,T)c(p,T)h(p,T)p^{-1} \tag{2.3}$$

where p is the pressure, T is the temperature (°K), ρ is the density, c is the acoustic speed, and h is the enthalpy. These values are all in SI units. The following parameters apply to equation (2.2):

c_1 is the arc zone acoustic speed
c_2 is the vapour layer acoustic speed
R is the channel radius ($7.9 \cdot 10^{-4}$ metres)
h_1 is the arc zone enthalpy
$\hat{p}$ is the central channel stagnation pressure
β is the arc contraction ratio $= \pi r_1^2 / \pi R^2$ where r_1 is the radius of the arc zone

As stated in the paper an average value of $\beta \simeq .8$ may be taken as a reasonable approximation.

The stagnation pressure $\hat{p}$ is determined from:

$$\hat{p} = \left[\frac{I}{\pi R^2}\right]^2 \frac{l}{\sigma_1} \frac{1-(\Delta h_v/(h_2+\Delta h_v))}{V(T_1)M_e(p_e\hat{p}^{-1})(\beta+(1-\beta))(h/c)_2/(h/c)_1} \tag{2.4}$$

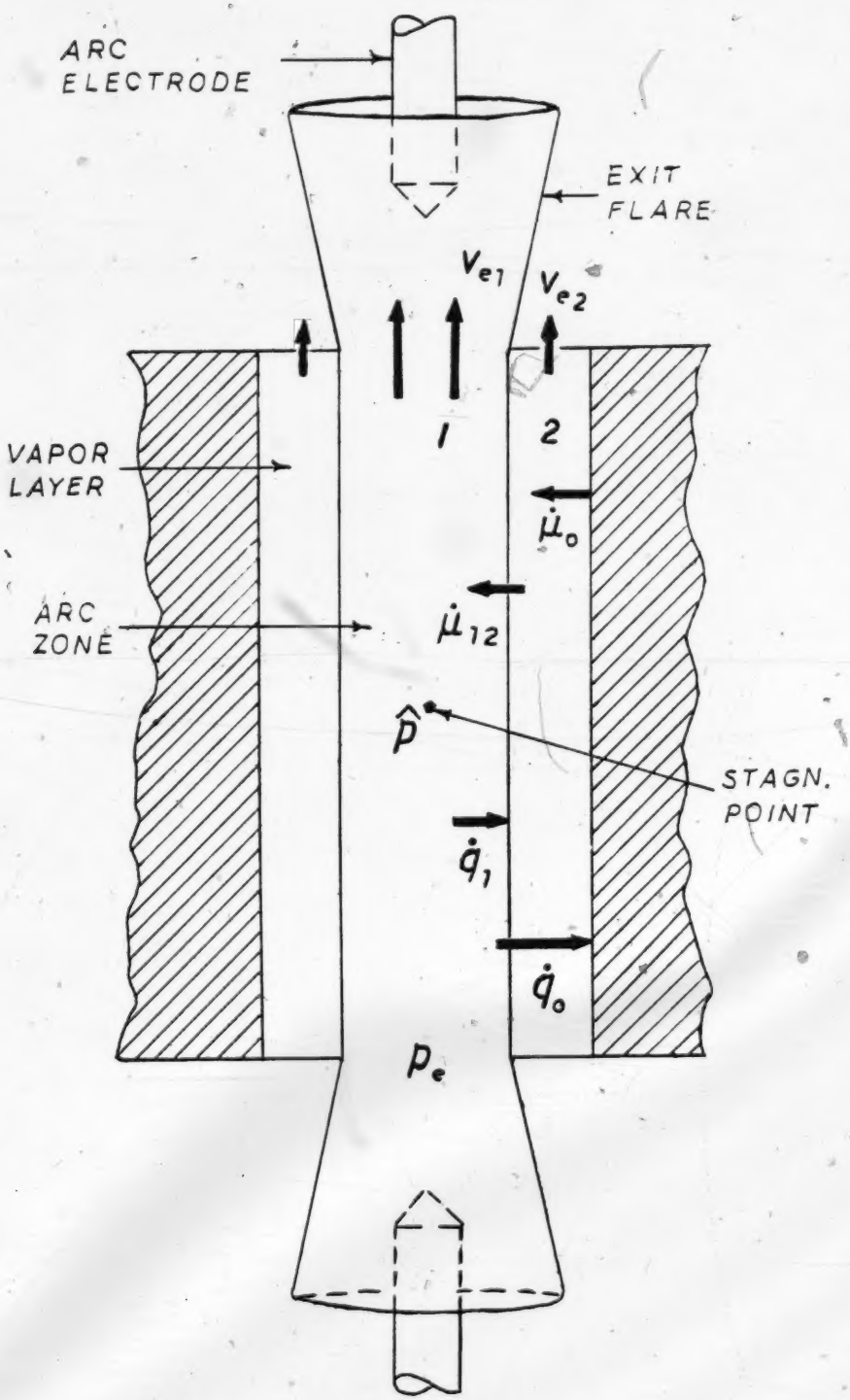

Figure 2.1 Mass, Momentum, And Energy Transfer In An Evaporation Dominated Arc

The symbol definitions are:

Δh_v represents the vapourization enthalpy of the channel material (for Fe it is $6.36 \cdot 10^6$ J kg^{-1})
h_2 is the vapour layer enthalpy
M_e is the Mach number in the channel end sections: $M_e = v_e c_e^{-1}$ where v_e is the plasma jet exit velocity
p_e is the pressure at the exit zone. The paper presents a value of $p_e \hat{p}^{-1} = .55 \pm .05$ for $1 < \gamma < 1.67$ (γ is the specific heat ratio and is taken to be $\simeq 1.3$ for the plasma under consideration)
l is the channel length $= 1.6 \cdot 10^{-3}$ m for the steel end section
σ_1 is the plasma arc zone conductivity ($\simeq$ 5000 Siemens/m from Topham *et al.*[1])
I is the arc current($\simeq 10^2$ A)

The acoustic speeds can be determined from the relation: $c = (\gamma RT)^{1/2}$ where R is the universal gas constant (287.0 J kg^{-1} °K^{-1}). Therefore $c_1 = (1.3(287.0)10^4)^{1/2} = 1.932 \cdot 10^3$ m sec^{-1} and $c_2 = (1.3(287.0)5000)^{1/2} = 1.366 \cdot 10^3$ m sec^{-1}. It is to be noted that the plasma temperature $T_1 = 10^4$ °K was determined experimentally by Topham *et al.*[1] and T_2 was arbitrarily taken as 5000 °K. The paper of Niemeyer[40] states that $1000 < T_2 < 5000$ °K. The vapourization temperature of iron occurs at 3008 °K. Hence, this imposes the condition $T_2 > 3000$ °K. Ogurtsova *et al.*[41] give the temperature dependence of the enthalpy ΔH of a unit mass of plasma up to $2.5 \cdot 10^4$ °K as $\Delta H = 4 \cdot 10^{-4} T^2$ J g^{-1}. Hence $h_1 \simeq 4 \cdot 10^7$ J kg^{-1} and $h_2 \simeq 1 \cdot 10^7$ J kg^{-1}. From Topham *et al.*[1] the exit velocity of the plasma from the igniter cavity was estimated to be $\simeq 5 \cdot 10^3$ m sec^{-1}. Therefore $M_e \simeq 2.4$ at the channel exit cross-section.

Comparing equations (2.2) and (2.4) it becomes evident that if (2.4) is substituted into (2.2) the term $V(T_1)$ is eliminated and hence its evaluation is unnecessary. Substitution of the appropriate values of the various parameters into (2.4) yields $V(T_1)\hat{p} = 7.1 \cdot 10^8$ Jsec^{-1} and in turn (2.2) results in $\dot{M} = 210$ μg C^{-1}. For the erosion of ceramic channels, Niemeyer[40] supplies the relation: $N = 1 - (\Delta h_v / (h_2 + \Delta h_v)) \simeq .25$. Substitution of this value into relation (2.4) yields $V(T_1)\hat{p} = 2.43 \cdot 10^8$ Jsec^{-1} and $\dot{M} = 71$ μg C^{-1}. These values are an order of magnitude greater than those obtained in the following experiments.

It is necessary to take into account once again that the foregoing model represents a steady-state situation. For the igniter cavity, the heating process is very transient and its various fluid flow, evaporative, and heat conduction processes could not be expected to

establish steady-state conditions. Specifically for an initially cold surface to reach a temperature T when it is subjected to a steady heat flux F, the time t required would be[42]:

$$t = kT^2c/\pi F^2 \tag{2.5}$$

where k and c are the specific heat and thermal conductivity of the solid respectively. From measurements of the longitudinal electric field within the cavity (see Chapter 3) the upper limit of the heat flux to the wall is 10^9 W m^{-2}. This value assumes 100% losses and the flux would be in the form of conduction or radiation losses. At the electrode or the casing if a typical voltage drop of 30 V at these conducting surfaces is assumed, the heat flux is $\simeq 10^{10}$ W m^{-2} over the channel cross-section. Using these heat flux values, for iron to reach its boiling point, equation (2.5) yields heating times of $3 \cdot 10^{-3}$ sec (10^9 W m^{-2}) and $3 \cdot 10^{-5}$ sec (10^{10} W m^{-2}). Similarly for tungsten the corresponding values would be 2.4 seconds and $2.4 \cdot 10^{-2}$ seconds respectively while for the ceramic, which would not develop a voltage drop at its surface, the lower flux would yield a heating time of 10^{-5} seconds.

Since the calculated heating times reflect the very highest currents used it is expected that for the erosion measurements which involved lower currents, the heating times would be at least an order of magnitude greater than the former case. An interesting aspect of the preceding calculations is that a threshold flux (i.e. igniter energy) may exist which sets a minimum limit for the occurrence of erosion. For electrodes in air, however, it has been suggested that ebullition may not be a limiting factor in the erosion process.[38]

2.2 Efficiency Considerations

Recent work has shown that the thermal energy dissipated in the plasma gases in the igniter cavity reflects an inefficient conversion of the initial energy stored in the the supply capacitor. As described in the Introduction, Topham *et al.*,[1] Clements *et al.*,[24] and Carleton *et al.*[23] in their measurements of the absorbed thermal energy concluded that in a typical situation less than about 10% of the original capacitor energy was available to the gas. There is also considerable variation of the efficiency with operating conditions. Carleton and associates

determined that most of the energy losses occurred in the external igniter circuit. Because of the nonlinearity of a confined arc it is difficult to match a capacitive source to it. There is a saturation of the arc voltage drop in the range of 100 to 200 V because of the rapid variation of the arc's electrical and thermal conductivity with temperature. For an increase of the supplied voltage above this level the transfer of energy becomes more inefficient. Spark gap triggering requires voltages in excess of 300 V and consequently electrical energy transfer efficiencies decrease for the higher voltages.

There are two separate processes involved in the conversion of the igniter input energy to the thermal energy of the gas. They are the capacitor (electrical energy) to the igniter (electrical energy) and the latter to the gas (thermal energy). As described in the preceding paragraph Carleton *et al.*[23] attribute the first process to dominate the variable efficiency losses. The efficiency of the second process is relatively constant at 25%.

In the usual situation the discharge is limited to the first half-cycle. For a capacitor initially charged to a voltage V_0, the charge flow in this cycle will be CV_0. As has been noted previously the voltage developed across the igniter electrodes is variable. However, in order to obtain a rough estimate of the energy dissipated in the cavity, assume a voltage in the area of 120 V. Approximately one third of this would consist of the anode and cathode voltage drops and the remainder would be distributed along the arc length. Therefore the energy dissipated in the igniter would be $120CV_0$ (J) and if the electrodes receive the energy dissipated in the voltage drops then approximately 60% of the initial energy would be available for plasma heating and heat losses to the igniter. The initial energy $E_s = 1/2CV_0^2$ and hence the first process efficiency would roughly be:

$$e \simeq \frac{CV_0(120)}{1/2CV_0^2} = \frac{240}{V_0} = \frac{E_E}{E_s} \tag{2.6}$$

The second process efficiency would undoubtedly amount to less than 60%.

Carleton and coworkers have also indicated that efficiency could be greatly increased by using liquid fed plugs at low stored energies. They reported that values as high as 40% of the initially stored energy could be transmitted to the plasma with an alcohol-wetted plug at

capacitor energies below one Joule. This plug is said to reduce erosion as well through transpiration cooling. However, engine temperatures may impose prohibitive complications to feeding liquid fuel. Grant *et al.*[25] have found that use of inorganic hydride cavity inserts rather than liquid feeds are apparently more viable for the active fuelling of an igniter.

2.3 Erosion Experiments

The purpose of the igniter component investigation was to determine what limit the ablation process imposed on plug operation and in turn, to deduce the operating regimes for which these limits (if significant) would be optimized.

The erosion measurements were carried out on 'conventional' overvolted coaxial spark igniters. The plug was constructed in such a way that it could be disassembled into three components for the purpose of determining by weight the three separate erosion rates. The three parts consisted of a 1.6 cm diameter tungsten electrode, a cylindrical ceramic channel, and an outer steel casing. Fittings used to assemble the plug were of the 'Swagelock' type. The plug assembly is shown in Figure 2.2. A high voltage power supply designed to accommodate the high repetitive firing frequency required for the erosion tests was used to energize the igniter.

Erosion rates were measured by operating the igniters at approximately 10 Hz for periods of several hours. The initial measurements involved observing how much component erosion could occur before the plasma jet igniter's operating efficiency was greatly reduced. To conserve an effective ejected plasma plume it was found that the maximum tolerable volume loss from the plug was of the order of 10^{-3} cm^3. For a steel density of approximately 10 gm cm^{-3}, an expected erosion rate of approximately 10^{-5} gm C^{-1} (Cobine[34]) and a typical charge flow per pulse of $2 \cdot 10^{-3}$ C it is apparent that the maximum number of ignition pulses per igniter lifetime is approximated by: $10^{-3}(10)/(2 \cdot 10^{-3}(10^{-5})) = 5 \cdot 10^5$ cycles. For a four cycle, four cylinder engine, operation at 3000 r.p.m. would require $9 \cdot 10^4$ pulses per igniter per hour which limits the lifetime to approximately five hours. Expressing the erosion rate as the quantity R (μg C^{-1}) results in a corresponding lifetime $L \simeq 55/R$ (hours).

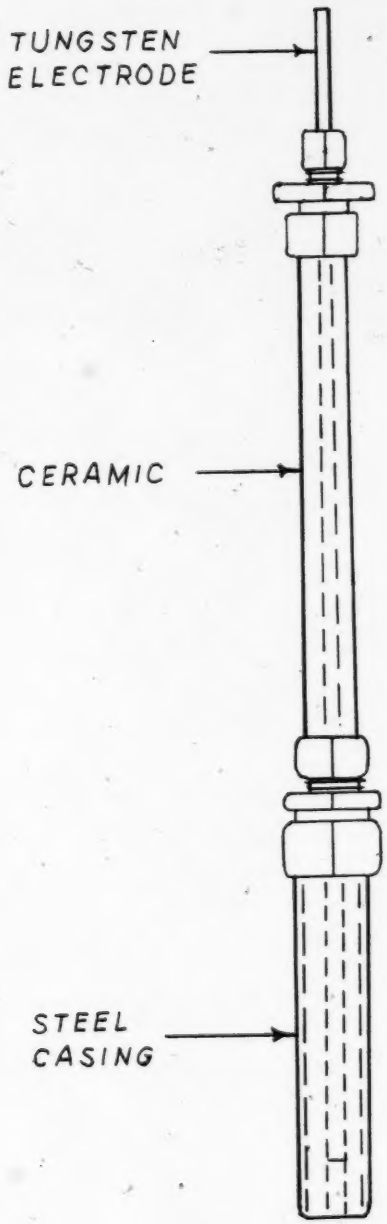

Figure 2.2 Demountable Component Igniter

Some cooling was provided for the plug during the measurement period by maintaining a weak gas flow around it. The component erosion was found to be unaffected by the gas flow rate.

A set of measurements was performed in order to determine whether the total mass eroded was proportional to the charge flow through the circuit or was more directly related to the total stored energy or some different parameter. Each erosion measurement was the average of ten or more two hour runs and the component material used was steel and tungsten. Three erosion rates are shown in Figure 2.3:—for mild and hard steel casings, and for the tungsten electrode. The erosion for the ceramic channel was found to be insignificant ($<10^{-1}$ μg C^{-1}) compared to the other components. Figure 2.3 shows the erosion rates (μg C^{-1}) as a function of the energy E_s initially stored in the capacitor. There was considerable scatter in the results. While the experimental results have considerable practical value in placing limits on the probable erosion rates, they have little significance in determining the precise variation of erosion with charge flow or initial capacitor voltage beyond demonstrating some increase of the erosion rates with energy.

In Figure 2.4 are values obtained from relation (2.1) with the constant k adjusted to .72 and .40 for the mild and hard steel ends respectively. The experimental points appear to agree fairly closely to the ones obtained from (2.1). The plotted values for the tungsten electrode indicated no correlation with this equation. The current was measured with a Pearson coil applied at the high voltage electrode of the igniter and the induced voltage trace was calibrated on an oscilloscope.

Reasons for the scatter in the erosion rates for the igniter components have not been determined. It was found that small traces of oil or grease on the metal surfaces resulted in greatly enhanced erosion rates. Accordingly the metal components were cleaned before testing. Because of the presence of the same mechanism, it can be inferred that this scatter will also manifest itself in i/c engines.

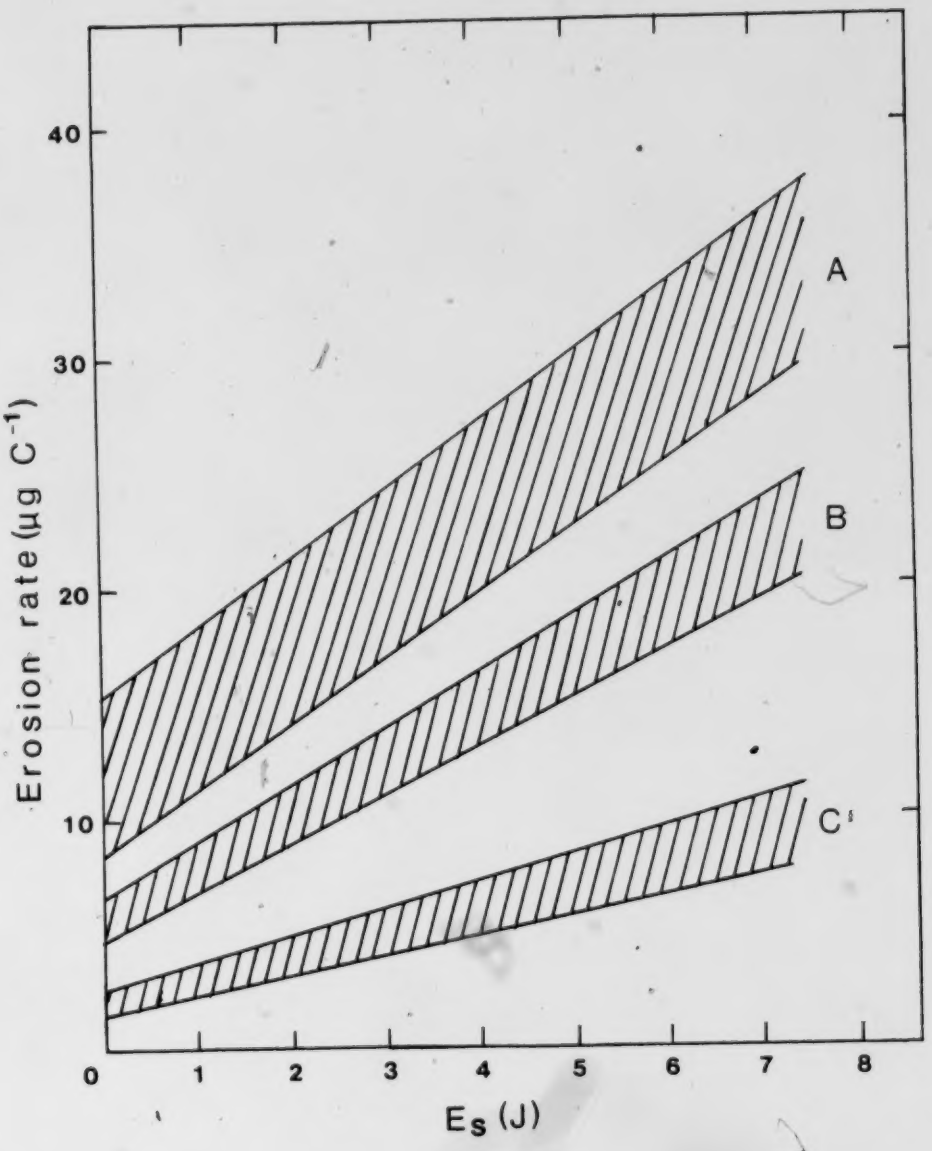

Figure 2.3. Graph Of The Erosion Rate Versus The Initial Capacitor Stored Energy. For mild (A) and hard (B) steel casings and for a tungsten electrode (C). The results were scattered in a random manner between the indicated limits.

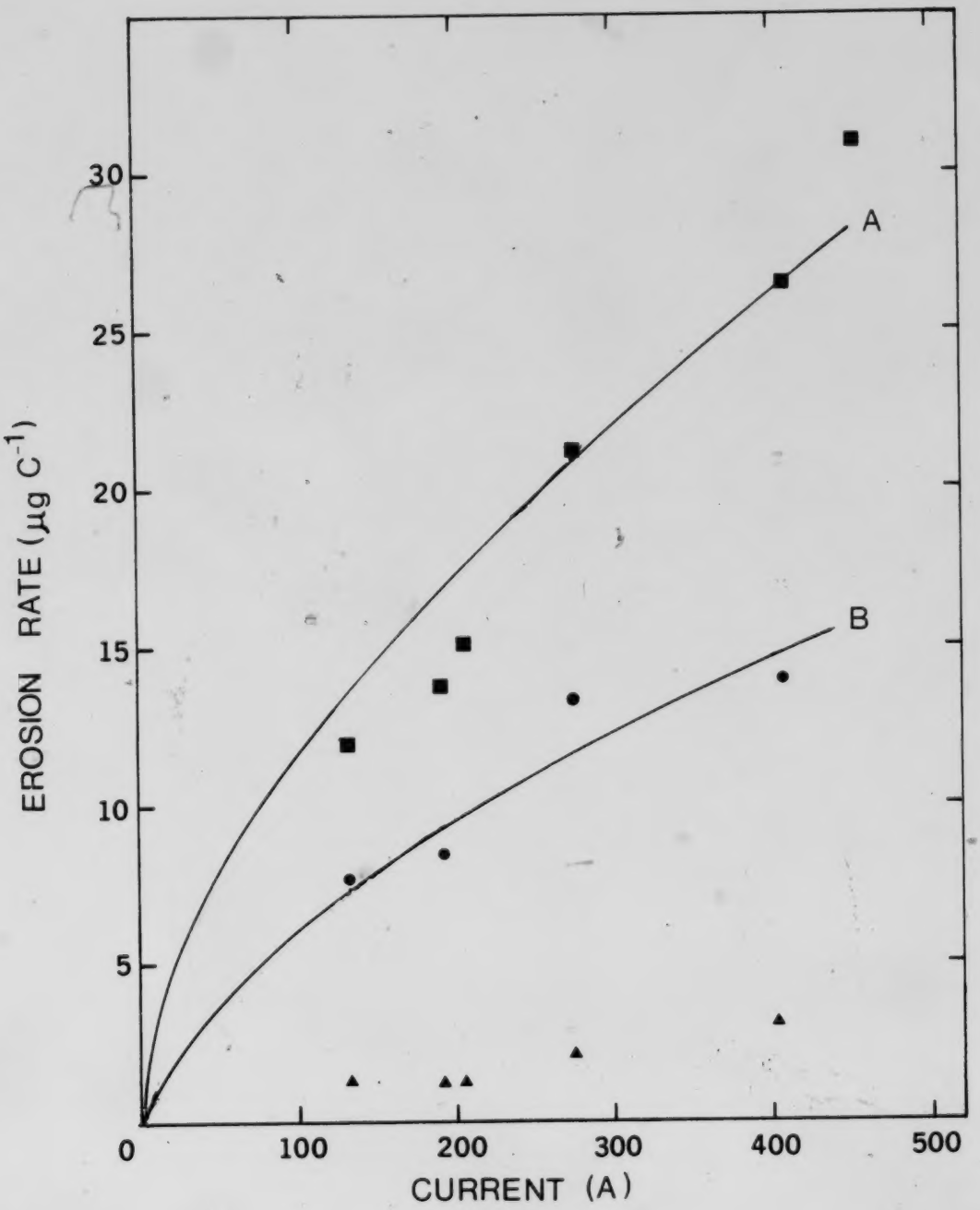

Figure 2.4. Graph Of Erosion Rate Versus Current. For the mild ■ and the hard steel ends •. Curves A and B represent values calculated from (2.1). Triangles are for the tungsten electrode.

Another set of measurements involved variation of the ambient gas pressure and these runs were performed using a small pressure chamber. For example, in an i/c engine operating at an 8:1 compression ratio the gas density can be expected to range from far below that at atmospheric room temperature air up to approximately eight times this quantity. The actual range used in this experiment varied from .1 to 8 atmospheres pressure in room temperature air. The results of these measurements are shown in Figure 2.5 and are for an igniter operating with a 14μF capacitor charged to 700 V (E_s=4.2 J).

The characteristic current waveform obtained for the igniter represented an underdamped oscillatory discharge. Because of the low capacitor voltage used in the measurements, the current did not oscillate through more than a half cycle (i.e. the triggering gap in the circuit did not restrike for a second half cycle). It was found that if the voltage was increased beyond ~ 700 V then the full cycle current was attained. Hence for the experiments, the polarity assigned to the current would be that of the first half cycle.

The effect on the erosion rates due to the polarity reversal of the high voltage and ground electrodes was investigated. No significant discrepancy was found between these results and those employing the initial polarity (i.e. the tungsten electrode h.v. biased and the steel casing earthed).

2.4 Discussion Of The Erosion Results

For the component materials used in the experiments, the erosion measurements indicate serious limitations in its applications in i/c engines. The results in Figures 2.3 and 2.5 indicate values for the erosion rates which are consistent with the previous work on electrode erosion. The reasonably close correspondence between the experimental and theoretical points in Figure 2.4 indicates that the $i^{0.6}$ dependence of equation (2.1) (in terms of μg C^{-1} and for an appropriately chosen constant k) is valid for the steel casing erosion rates.

The value for the steel erosion rates calculated from equation (2.2) was $\dot{M}$=210 μg C^{-1}. As was mentioned above, this is an order of magnitude greater than the observed rates and the

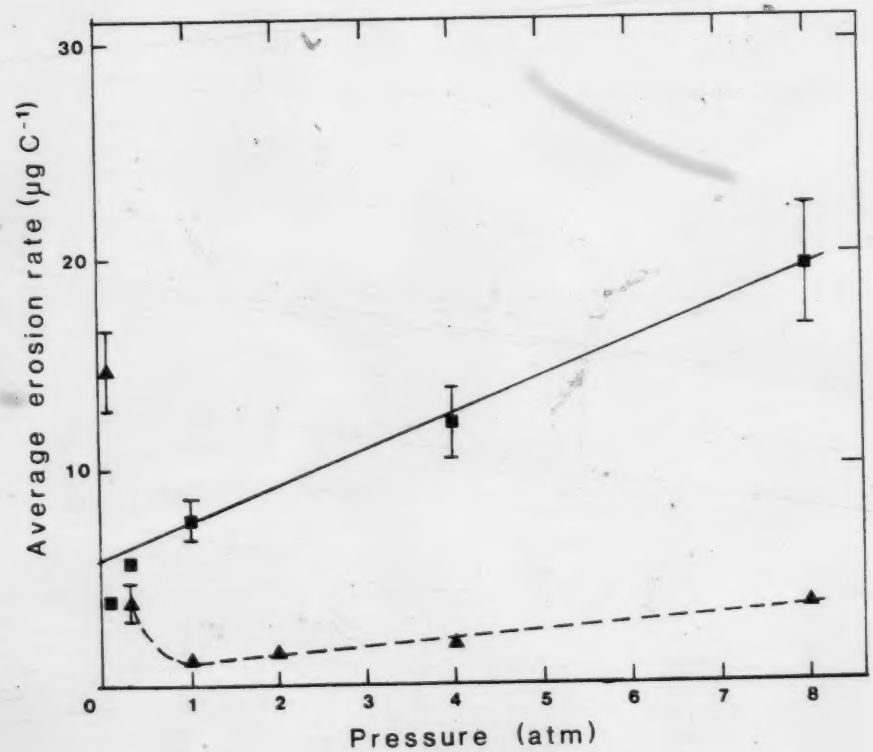

Figure 2.5. Erosion Rate Versus Gas Pressure. For the hard steel casing (solid line) and tungsten electrode (dashed line).

model from which the theoretical value was obtained represents a steady-state situation.

The calculations from equation (2.5) indicated the possibility of the existence of a threshold flux which would set a minimum limit upon the onset of erosion. No such energy threshold was observed in the experimental results. However, this is consistent with previous findings.

In the calculations using equation (2.5) the energy flux densities used ranged from 10^9 to 10^{10} W m^{-2}. The average flux density to the electrodes was calculated not to exceed these amounts and these values are also consistent with those of Cobine and Burger[38] for a high-current short term arc. Arc spot formation would possibly increase the local flux density. To investigate this premise streak photographs were taken of the luminous arc in the vicinity of the electrode and the spot size was found to be as little as 10^{-2} of the full electrode area. Recalculation of the flux for this much smaller area of the arc cross-section indicated that the electrode material would exceed its boiling point in times of the order of nanoseconds. Therefore the arc in order to sustain full conduction to the electrode surface may require an energy flux at the surface which is always greater than the calculated erosion threshold. This would explain the fact that no threshold was observed. In support of the foregoing argument, Belkin[39] in his studies of electrode erosion dependence on heat flux and duration of current flow determined that for low currents (<1 kA), the average heat flux and average temperature of the electrode covered by arc spots is small so that for discharges of short duration, vapourization occurs only from the spots.

It is also possible that the erosion mechanism may be some high pressure form of sputtering.[43] This would produce emission of particles (mass efflux) from the electrodes as a result of the impact of high energy ions from the arc discharge. Further consideration of this topic is beyond the scope of this thesis.

Figure 2.5 indicates that aside from pressures below one atmosphere the erosion rates tend to increase with pressure. Higher ambient gas pressures have a constraining influence on the arc plasma. They reduce its physical extent, increase the core temperature, and tend to

minimize the discharge path length between the electrodes. Accordingly, as this hotter plasma comes into contact with the electrode surfaces the erosion of the surface discharge material is increased.

2.5 Efficiency Experiments

The igniter thermal efficiency experiments were performed since this parameter is highly relevant to the ignition process.

The thermal energy dissipated within the gas was measured directly as opposed to obtaining the difference between the pre-discharge energy input to the plug and the residual heat energy in it after the discharge. This method was also used by Carleton *et al.*[23]

A diagram of the experimental setup is shown in Figure 2.6. The technique was basically similar to that of Offenberger *et al.*[44] which was developed to measure the energy content of very high laser pulses.

Air at various pressures was used as the ambient medium in the detector cell and the igniter was discharged into the latter. The pressure increase in the cell was monitored by a Celesco LD 25 piezoelectric pressure transducer. In turn the transducer output was connected to a Tektronix 1A7A plug-in amplifier unit on the oscilloscope. Since the resultant unfiltered trace was extremely noisy, electrical smoothing was accomplished by shunting the pressure transducer (C=.25 nF) with a much larger capacitance of .47μF and applying a 300 Hz high frequency cutoff to the subsequent signal at the amplifier. The pressure response of the complete system was calibrated by allowing transient flows of known pressure through the cell valves. The calibrated and theoretical responses were found to agree. The transient temperature increase ΔT produced by the thermal energy (E_{th}) dissipated in the gas is obtained from:

$$\Delta T = \frac{E_{th}}{\rho V c} = \frac{T_0 \Delta p}{p_0} \tag{2.7}$$

where ρ is the gas density, c the specific heat at constant volume, V ($\sim 10^{-5}$ m^3) is the volume of the detector cell and T_0, p_0 are the initial temperature and pressure.

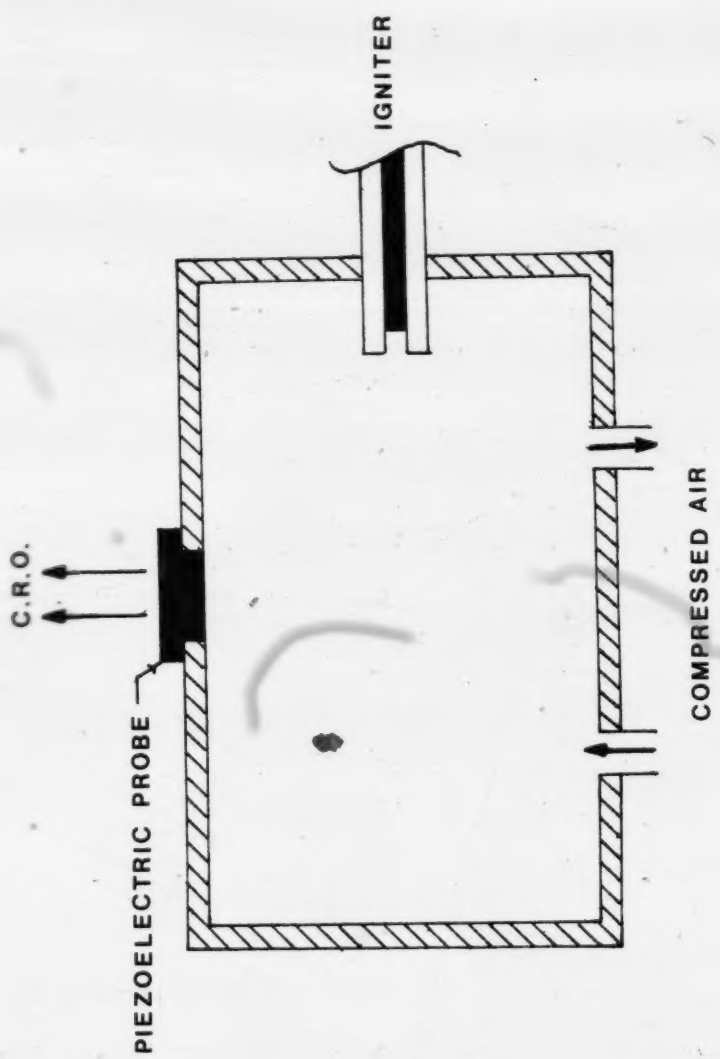

Figure 2.6 Efficiency Cell

Measurements were obtained for the plasma jet igniter for various storage capacities, initial voltages, and ambient pressures. A conventional air-gap spark plug and a standard surface gap plug were also used for comparison purposes.

For all the trials the igniter current (i) and voltage (V) waveforms were monitored and the internal energy $E_E = \int_0^\infty iV\,dt$—the energy delivered to the igniter was computed. Figure 2.7 illustrates the dependence of the overall efficiency E_{th}/E_s with E_s.

The dependence of E_E/E_s with the initial capacitor voltage V_0 is plotted in Figure 2.8. Also plotted are theoretical values obtained from equation (2.6).

2.6 Discussion Of The Efficiency Results

From Figure 2.7 it is evident that the plasma jet igniter efficiency decreases at high energies and at subatmospheric pressures. Thus the heat capacity of the gas initially in the igniter cavity will be the limiting factor in the transference of heat energy to the external gas. For sufficiently low pressures (low heat capacities) or high energies the cavity gas' insufficient heat capacity will prevent the absorption of electrical energy delivered to it and hence there will be a decreased efficiency. The results of Figure 2.7 are compatible with the previously reported overall efficiencies for the igniter in the range of 10%.

With respect to the results of Figure 2.8 the plotted theoretical curve obtained from equation (2.6) follows the trend of the experimental ones quite reasonably. These results illustrate the inherent difficulties involved in the matching of a capacitive source to the essentially constant voltage characteristics of an arc discharge.

2.7 Conclusions

From Figure 2.3 the igniter component erosion rates were found to increase with the stored capacitor energy $E_s = 1/2CV_0^2$. If the latter relationship is assumed to be approximately linear then the erosion rate $M_e/CV_0 \propto E_s$ where M_e is the eroded mass. Additionally, if the initial stored capacitor energy is maintained constant, the proportionality

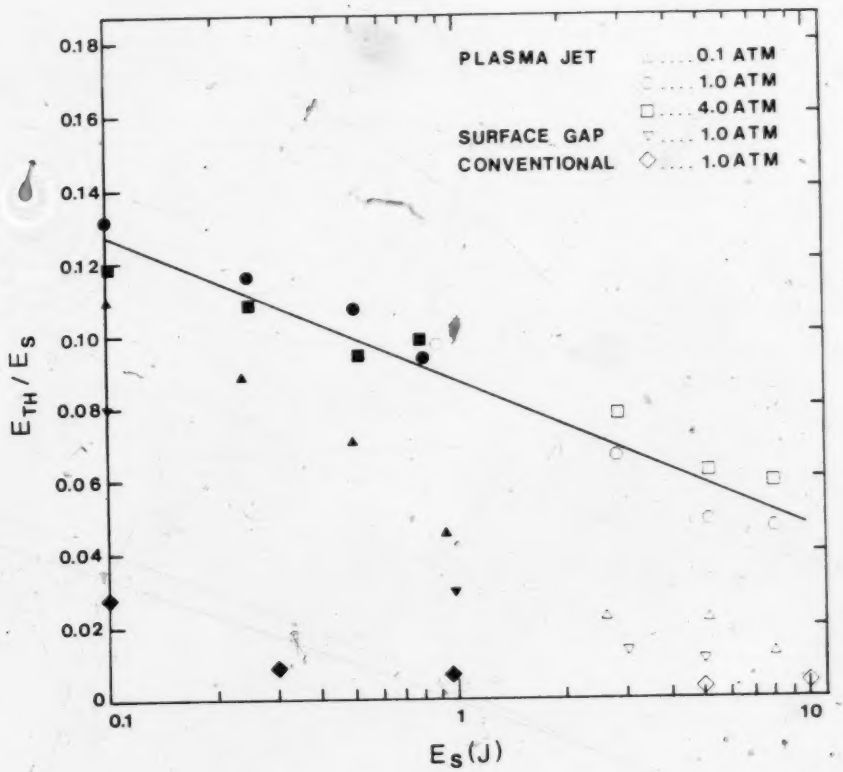

Figure 2.7. Graph Of Overall Efficiency Versus Stored Energy. Filled symbols are for 2μF capacitance while open ones are for 20μF. The curve is fitted to the atmospheric and high pressure igniter data.

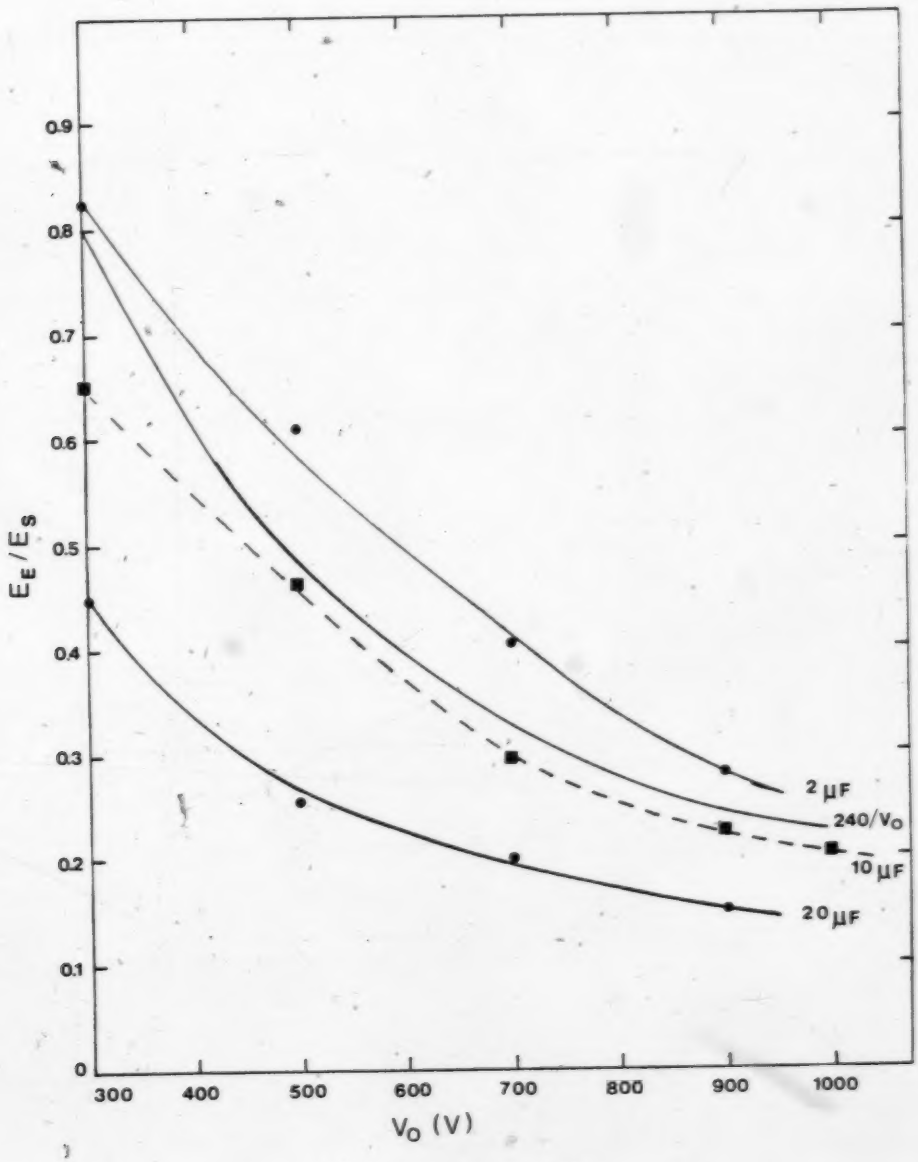

Figure 2.8 Graph of E_E/E_s Versus Initial Capacitor Voltage

becomes: $M_e \propto 2E_s^2/V_0$. This implies that the total eroded mass will be minimized for high initial capacitor voltages. If the initial capacitor charge $Q_0 = CV_0$ is also assumed constant then $M_e \propto 2E_s^2 C/Q_0$. From the latter relation it can be deduced that the total eroded mass is minimized if a low initial capacitance is used. Improved efficiency is obtained at low capacitor voltages.

For all the test conditions the erosion rates were found to be prohibitively high for applications of an igniter composed of the materials tested in an i/c engine. Expected automotive lifetimes for such an igniter were found to be less than ten hours. The plasma igniter was found to be more efficient than the two other standard types of igniter in terms of plasma heating. The measurements of Topham *et al.*,[1] Carleton *et al.*,[23] and Clements *et al.*[24] were found to be consistent with the direct thermal energies measured herein and a similar loss distribution was found between the two successive stages involved in energy transfer.

In order to minimize component erosion and maintain an effective thermal energy transfer it is necessary to maximize the relation $(E_{th}/Mass\ eroded)$. From Figures 2.3 and 2.7 it can be deduced that a high voltage low capacity situation achieves this.

The work of Carleton *et al.*[23] on high efficiency liquid fed plugs with their erosion reducing transpiration cooling shows promise for continuous operation applications. Likewise does that of Grant *et al.*[25] who used inorganic hydride cavity inserts rather than the liquid feeds. Research is still proceeding in these areas.

As described in Section 1.3, plasma jet igniters of the design described in this research work would be viable for intermittent operation.

3. Plasma Expulsion Processes In The Plasma Jet Igniter

3.1 Introduction

The work described in this chapter is an attempt to gain further insight into the coaxial spark igniter plasma jet ejection mechanism. This knowledge is relevant to the determination of an operating regime for optimum igniter efficiency.

Measurements were made of the plasma exhaustion time from the igniter cavity, the external flow velocity, and the electric field within the cavity. These results were compared with corresponding parameters derived from arc theory and a plasma expansion theory based on a model in which the plasma cavity represents the high pressure section of a conventional shock tube.

Most of the previous work directed to understanding the plasma expulsion has concentrated on relating the depth of penetration and other properties of the expanding jet to the dissipated energy and various geometries of the cavity and orifice.[8,21,22,25]

Topham *et al.*[1] focussed their attention on the structure and ejection velocities of the plasma jet. They found from streak photographs that the structure and dynamic properties of the plasma column had a strong pressure dependence which far outweighed the electromagnetic force influence parallel to the particle motions. Their photographs illustrated that the column consists of a series of curved, roughly vertical dark and light bands. Particle velocities in these bands were found to differ and measurements of the luminous front velocity yielded a value of the order of 600 m/sec. This infers a highly structured supersonic (~ Mach 2) plasma jet propagating into the cold neutral gas. Behind the luminous front, lesser quasi-stationary shocks were found to exist which were followed by an expansion region of high pressure and the motion of the shocks was found to correlate with the current pulses flowing into the igniter. Topham and associates found that the initial spread of the luminous front is proportional to voltage variations and varies inversely with pressure. Very little current was detected from Langmuir probe measurements to exist in the external region of the igniter. From theoretical

considerations the particle streaming velocity was estimated to have a value of $5 \cdot 10^3$ m/sec. The energy required to generate the precursory shock wave was estimated to be $\sim 3 \cdot 10^{-2}$ J. They calculated the energy for typical current and voltage values dissipated for the first half cycle of the discharge to be $\sim .2$ J. As mentioned in the previous chapter it was determined from blast wave measurements that the proportion of the latter energy which is expended in generating the pressure wave into the external gas is approximately 10%.

A portion of the research described in this chapter involved the repetition of the work just alluded to above in order to obtain more definitive results on the external plasma plume structure and streaming velocities. Streak photographs were taken of the internal plasma expansion (i.e. within the igniter channel) for the variation of various parameters and the qualitative results are presented below. Some longitudinal structure of the expelled plasma was observed from the streak photos and hence to pursue this in more detail, several two-dimensional time exposure photographs were taken of the jet.

3.2 Characteristic Times For The Ejection Process

Three characteristic times are involved in the operation of the plasma jet igniter. They are: the cavity plasma heating time t_H, the plasma expulsion time from the cavity t_E and the duration of the input electrical energy to the cavity t_l. After an elapsed time $t \simeq t_H$ during which the electrical energy is delivered to the cavity the plasma therein attains an equilibrium temperature in which the input power is balanced by the heat losses. If the time exceeds t_H, the electrical power will mainly be dissipated in heat losses rather than being utilized for the plasma expansion process. In consideration of this for a reasonably efficient plasma expansion it is necessary that $t \leq t_H$. Also since wastage of energy occurs if electrical energy is supplied to the cavity after the majority of the plasma therein has been expelled, there is the additional restriction: $t \leq t_E$. This limitation implies that the maximum energy input for optimum efficiency occurs with $t_l \simeq t_E$. These constraints impose the simple design criteria: $t_l \sim t_E \leq t_H$. The time t_l is dependent upon the external storage capacitor C_2 whose initial voltage and

capacitance can be varied. This reduces the plug design requirements to consideration of the appropriate quantities of t_H and t_E.

3.3 Determination Of The Plasma Heating Time

The relatively narrow radius ($7.5 \cdot 10^{-4}$ m) of the arc within the igniter cavity compared to the channel length ($1.6 \cdot 10^{-3}$ m) permits usage of the Elenbaas-Heller model to determine the maximum equilibrium plasma temperature from the radial heat losses.[45] For the low plasma temperatures generated in the cavity ($<1.2 \cdot 10^4$ °K), conduction dominates the thermal transport within the plasma.[46] Hence the heat generated by the Joule heating can be assumed to balance the heat conduction to the channel walls. For temperatures above the aforementioned value, emission and re-absorption of UV radiation becomes dominant in the energy transport.

The following theoretical considerations result in an estimate of the plasma temperature by two different methods. One utilizes the Elenbaas-Heller model to determine the temperature and subsequently the electric field as a function of the total arc current and cavity radius. The other method adopts values from detailed calculations for nitrogen (i.e. quantitatively similar to air as a conducting medium) cascaded arcs by Ernst *et al.*[46] These results are very specific as to gas, arc radius, and current combinations but though they are more reliable than those deduced from the Elenbaas-Heller model, they are not as general.

From calculations by Ernst *et al.*[46] the plasma temperature T_0 and the electric field E are expressed as a function of the arc current for an arc radius of 10^{-3} metres. Other complementary work by Ernst *et al.*[47] comprises data for $8 \cdot 10^{-4}$ m whose graphical representation corresponds extremely closely to that for $r_0 = 10^{-3}$ metres. The latter data can accordingly be applied to conditions of the subsequently described experiments using $r_0 = 7.5 \cdot 10^{-4}$ m. The values for the electric fields and temperatures obtained from the latter two publications are shown in Figure 3.1.

A fully ionized plasma possesses thermal (K) and electrical (σ) conductivities which vary as $\sigma = cT^{3/2}$ and $K = kT^{5/2}$ where $c = 1.5 \cdot 10^{-2}$ and $k = 3 \cdot 10^{-10}$ in SI units; T is the local

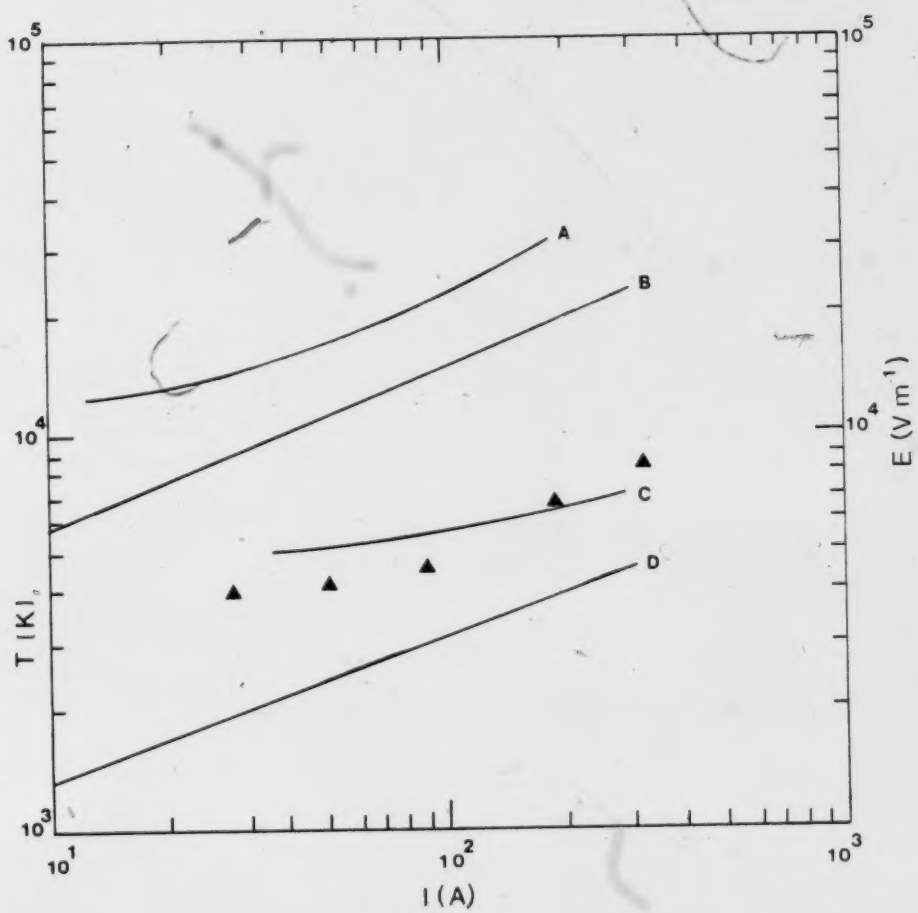

Figure 3.1. Graph Of Axial Temperature And Electric Field Versus Current. For T_0: A, Ernst *et al.*[46,47]; B, equation (3.7). For E: C, Ernst *et al.*[46,47]; D, equation (3.8). Triangles represent measured E values.

plasma temperature.[48,49] Applying now the Elenbaas-Heller model for an indefinite positive arc column in a fixed neutral gas, the Elenbaas-Heller equation yields:

$$\sigma E^2 = -\frac{1}{r}\frac{d}{dr}\left[rK\frac{dT}{dr}\right] \tag{3.1}$$

where r is the radius of a given annulus of plasma and E is the electric field. Substituting the relations given previously for σ and K yields:

$$rE^2cT^{3/2} = -\frac{d}{dr}\left[kT^{5/2}r\frac{dT}{dr}\right] \tag{3.2}$$

or

$$\frac{T^{-3/2}}{r}\frac{d}{dr}\left[r\frac{d}{dr}T^{7/2}\right] + \frac{7}{2}\frac{E^2c}{k} = 0 \tag{3.3}$$

Substitution of $\exp(x) = rE\alpha/T_0$ and $p = (T/T_0)^{7/2}$ where $\alpha = (7c/2k)^{1/2}$ and T_0 is the maximum temperature (at $r=0$) results in:

$$\exp(2x)p^{3/7} = -\frac{d^2p}{dx^2} \tag{3.4}$$

with the boundary conditions $p=1$ at $x=-\infty$ (i.e. $T=T_0$ at $r=0$) and $p \to 0$ as $\exp(x) \to Er_0\alpha/T_0$. Equation (3.4) cannot be solved analytically but a numerical method solution yields $x=.73$ at $p=0$. Hence,

$$T_0 = .48Er_0\alpha \tag{3.5}$$

If the total heat loss is balanced by the incoming power (total current I) the result is:

$$IE = 2\pi rkT^{5/2}\frac{dT}{dr} = \frac{2}{7}(2\pi k)\left[\frac{dp}{dx}\right]_{r=r_0}T_0^{7/2} \tag{3.6}$$

Solving numerically for (dp/dx) and combining (3.6) and (3.5) yields:

$$T_0 = .7(kc)^{-0.2}(I/r_0)^{0.4} = 130(I/r_0)^{0.4} \tag{3.7}$$

$$E = .8k^{0.3}c^{-0.7}(I^{0.4}/r_0^{1.4}) = 2.1 \cdot 10^{-2}(I^{0.4}/r_0^{1.4}) \tag{3.8}$$

where I is the plasma current and r_0 is the arc radius. Relations (3.7) and (3.8) are plotted in Figure 3.1 for $r_0 = 7.5 \cdot 10^{-4}$ m which is the igniter cavity radius.

From equations (3.7) and (3.8) the time t_H required to attain the plasma equilibrium temperature can be deduced. The temperature and to a lesser degree the chemical composition of the plasma determine its enthalpy H. Tables of the thermochemistry of air at approximately

10^4 °K yield the following empirical enthalpy relation of reasonable accuracy[50]:

$$H = 80T^{1.4} \tag{3.9}$$

where H is in J kg^{-1} and T is in °K.

For combustion conditions it can be expected that relatively small amounts of hydrocarbons or organic fuels would be present in the plasma. Calculations by Ogurtsova *et al.*[41] for a CH_2O plasma indicate that the latter impurities would negligibly affect equation (3.9) since their results yield enthalpies which are a factor of two greater than the latter relation (i.e. of the same order). If the hydrocarbon concentrations are assumed ~ 10% that of air the effect on the enthalpy would be insignificant.

The heating time results from the division of the enthalpy per unit length (3.9) by the input electrical power per unit length (IE) from equation (3.8). Thus,

$$t_H = 1.3 \cdot 10^7 \, r^{2.14} / I^{0.14} \tag{3.10}$$

Equation (3.10) is plotted in Figure 3.2 for $r_0 = 7.5 \cdot 10^{-4}$ m.

3.4 Plasma Expulsion Time Considerations

A previous model of the plasma expulsion from the igniter cavity by Cetegen *et al.*[21] was based on the premise that choked flow occurred at the cavity orifice and sonic velocities were attained there. Although the latter model may be appropriate for steady-state flow conditions the concept of the channel as the high pressure section of a shock tube just after diaphragm rupture has occurred would be more suitable.

Assuming the arc channel is cylindrical and symmetrically placed within the cavity, Joule heating released within the channel leads to a thickening of the arc and increase in the channel pressure. This radially thickened channel acts like a piston on the remaining gas within the cavity and causes it to be driven out of the exit.

Turning now to the conditions required to obtain critical flow in a cylindrical duct, consider the latter to be of uniform cross-section along its entire length L. Take its longitudinal axis as the x-axis and assume the fluid velocity to be in this direction. Assuming that the

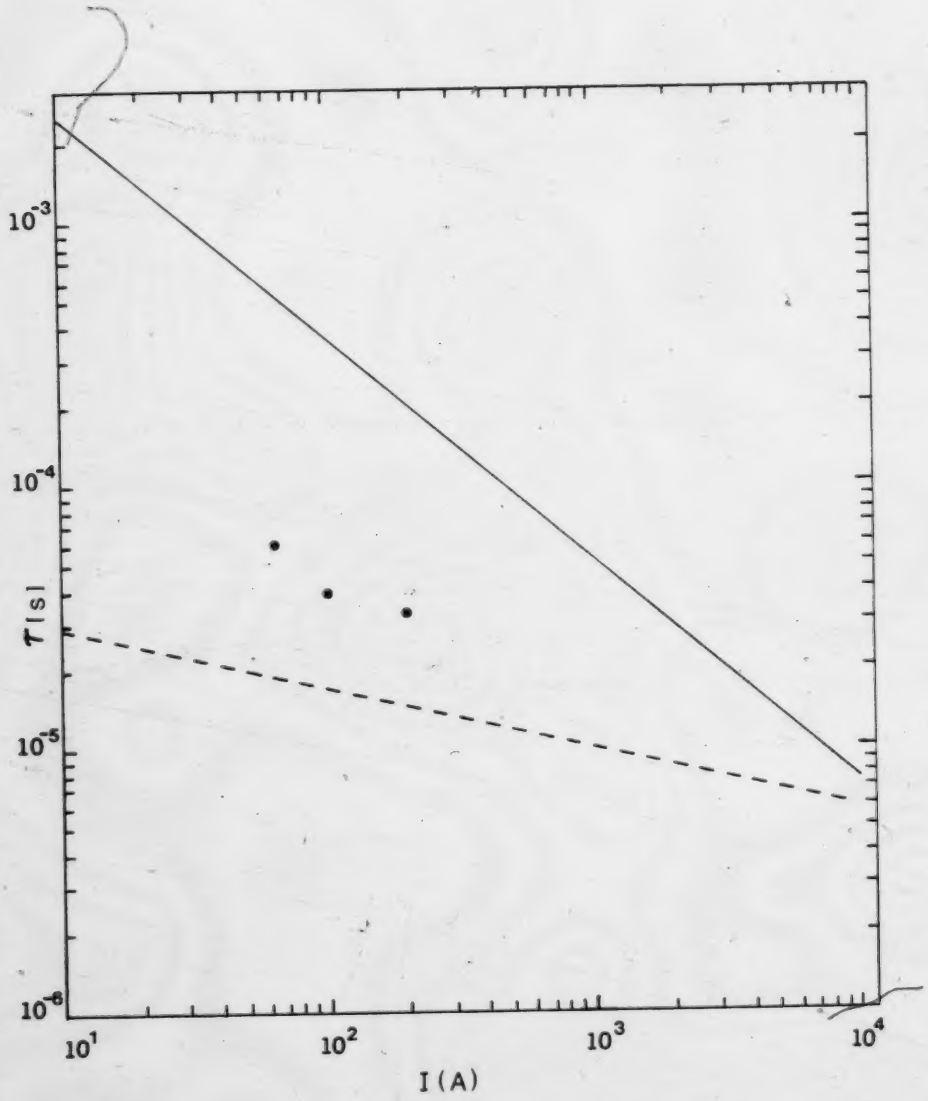

Figure 3.2. Graph Of Heating Time And Ejection Time Versus Current. Solid line represents the heating time (equation (3.10)) and the dashed line represents the ejection time (equation (3.24)). Dots represent approximate experimental values of the ejection time.

pressure p is constant over the duct cross-section yields: $\partial p/\partial y = \partial p/\partial z = 0$. Hence the x-component of the Navier-Stokes equation for a steady flow yields:

$$\frac{\partial^2 v}{\partial y^2} + \frac{\partial^2 v}{\partial z^2} = \frac{1}{\eta}\frac{dp}{dx} \tag{3.11}$$

where v is the fluid velocity, and η is its viscosity. Assuming that $dp/dx = \text{constant}$, the pressure gradient may be written $dp/dx = -\Delta p/L$ where Δp is the pressure difference between the duct ends. The boundary conditions of (3.11) require $v=0$ at $r=r_0$ where r_0 is the duct radius. Expressing equation (3.11) in polar coordinates yields:

$$\frac{1}{r}\frac{d}{dr}\left[r\frac{dv}{dr}\right] = -\Delta p/\eta L \tag{3.12}$$

Integration of (3.12) results in[51]:

$$v = -pr^2/4\eta L + a\log r + b \tag{3.13}$$

Since v must be finite along the duct axis the constant $a=0$ and the boundary condition yields $b = \Delta p r_0^2/4\eta L$. Therefore

$$v = \Delta p/4\eta L(r_0^2 - r^2) \tag{3.14}$$

If critcal flow is assumed at the duct end ($x=L$) along its axis ($r=0$) the corresponding pressure at the end cross-section would be $p = \rho a_0^2/\gamma$ where a is the acoustic speed, ρ is the density, and γ is the specific heat ratio. Assuming p at $x=L$ is much greater than p at $x=0$ results in $\Delta p \simeq \rho a^2/\gamma$. If the fluid is taken to be a plasma at a temperature exceeding 10^4 °K the value of $\gamma \to 1$. With these considerations equation (3.14) becomes:

$$v = \rho a r_0^2/4\eta L \qquad \text{or} \qquad v/a = M = \rho a r_0^2/4\eta L \tag{3.15}$$

where M is the flow Mach number $=1$ for choked conditions. Hence the critical duct length to obtain this condition would be:

$$L^* = \rho a r_0^2/4\eta \tag{3.16}$$

The gas within the igniter cavity may be assumed to be heated to $2 \cdot 10^4$ °K. This heated gas is then ejected at the corresponding sonic velocity $\sim 2 \cdot 10^3$ m sec^{-1}. If the ejected gas density is consistent with the 1 atmosphere ambient pressure (and $2 \cdot 10^4$ °K) and if η is specified, then the minimum value of L^* can be determined from (3.16). The viscosity of nitrogen varies

rather irregularly with temperature but for a maximum value of η of approximately $2 \cdot 10^{-5}$ (SI), application of (3.16) results in values of L^* in the range $3 \cdot 10^{-2}$-$3 \cdot 10^{-1}$ m which are much greater than the cavity length (i.e. $1.6 \cdot 10^{-3}$ m).[52]

The implication of the preceding paragraph is that critical flow is unattainable for a typical pulsed plasma jet cavity. However, if boundary layer formation is considered within it, the relation for boundary layer thickness $\delta \sim (\mu L/\rho v)^{1/2}$ indicates that the layer will grow from zero thickness at the inner electrode face and will extend radially across the cavity at a distance L^* from the electrode. For a cavity length L much less than L^* it can be inferred that wall friction will not be a significant factor in the plasma expansion as is the case for the pressure driven shock tube analogy.

In brief, a shock tube is a device in which a plane shock wave is produced by the sudden bursting of a diaphragm which separates a gas at high pressure from one at low pressure. The cross-section of the shock tube is generally uniform. Upon rupture of the diaphragm a compression wave propagates into the low pressure gas and steepens rapidly to eventually form a shock front. Simultaneously a rarefaction wave travels back into the high pressure gas, the wave front propagating at the sonic speed of the driver gas. The rarefaction front pressure fall is smooth unlike the discontinuities occurring at the shock front.

From Figures 3.1 and 3.2 it is evident that for typical arc currents in the range $10^2 \rightarrow 10^3$ A, equilibrium temperatures of approximately $10^4 \rightarrow 10^5$ °K will be attained by the cavity gas quite rapidly ($10^{-5} \rightarrow 10^{-4}$ sec). With the considerable temperature increase within the igniter cavity there is a corresponding pressure increase and providing that the constraint $t_H \leq t_E$ holds, the plasma flow situation will correspond to that in a shock tube.

Shock tubes are capable of generating highly supersonic flows. With the sub-critical length cavity dealt with in the igniter experiments it is possible that the plasma ejection velocities may be much greater than previous assumptions. The investigation of this possibility is very pertinent to the mechanisms affecting the igniter performance.

Returning to the behaviour of the rarefaction waves in a shock tube after diaphragm rupture, the region into which they propagate is characterized by falling temperature, pressure, and density below the initial values. As mentioned previously these parameters decrease continuously. The gas pressure decreases uniformly from its initially high value at the head of the rarefaction wave down to its value just behind the shock front. The latter value is always greater than the pressure initially present in the low pressure section ahead of the shock front. A representative diagram of the gas motion in the shock tube after diaphragm bursting is shown in Figure 3.3.

From Gaydon and Hurle,[53] the ratio between the flow velocity v_3 throughout the rarefaction wave and the corresponding acoustic speed a_3 is given by:

$$\frac{v_3}{a_3} = M_3 = \frac{2}{\gamma_4 - 1}\left[(P_4/P_2)^{(\gamma_4 - 1/2\gamma_4)} - 1\right] \tag{3.17}$$

where γ_4 is the specific heat ratio, P_4 and P_2 correspond to the pressures in the regions indicated in Figure 3.3. For an ideal gas

$$T_3/T_4 = (a_3/a_4)^2 = (P_3/P_4)^{\gamma - 1/\gamma} \tag{3.18}$$

Therefore $$a_3 = a_4(P_3/P_4)^{\gamma - 1/2\gamma} \tag{3.19}$$

Substitution of equation (3.19) into (3.17) results in:

$$\frac{v_3}{a_4} = \frac{2}{\gamma - 1}\left[1 - \left(\frac{P_3}{P_4}\right)^{(\gamma - 1)/2\gamma}\right] \tag{3.20}$$

For plasma temperatures exceeding 10^4 °K, γ is typically less than 1.1 and for these conditions, equation (3.20) can be approximated by its $\gamma \to 1$ limit of:

$$v_3/a_4 \to \ln(P_4/P_3) \tag{3.21}$$

Eventually the plasma in the cavity is exhausted to atmospheric pressure (i.e. $P_3 \to 1$ atmosphere; $T_3 = T_1$). Despite the value of γ alluded to above, this situation can be represented by assuming ideal gas behaviour ($p = \rho RT$) and that the cavity temperature increases adiabatically due to the Joule heating process. For P_4/P_3 and a_4 the approximate relations would be:

$$P_4/P_3 = T_4/T_3 \qquad \text{and} \qquad a_4 = a_0(T_4/T_1)^{1/2} \tag{3.22}$$

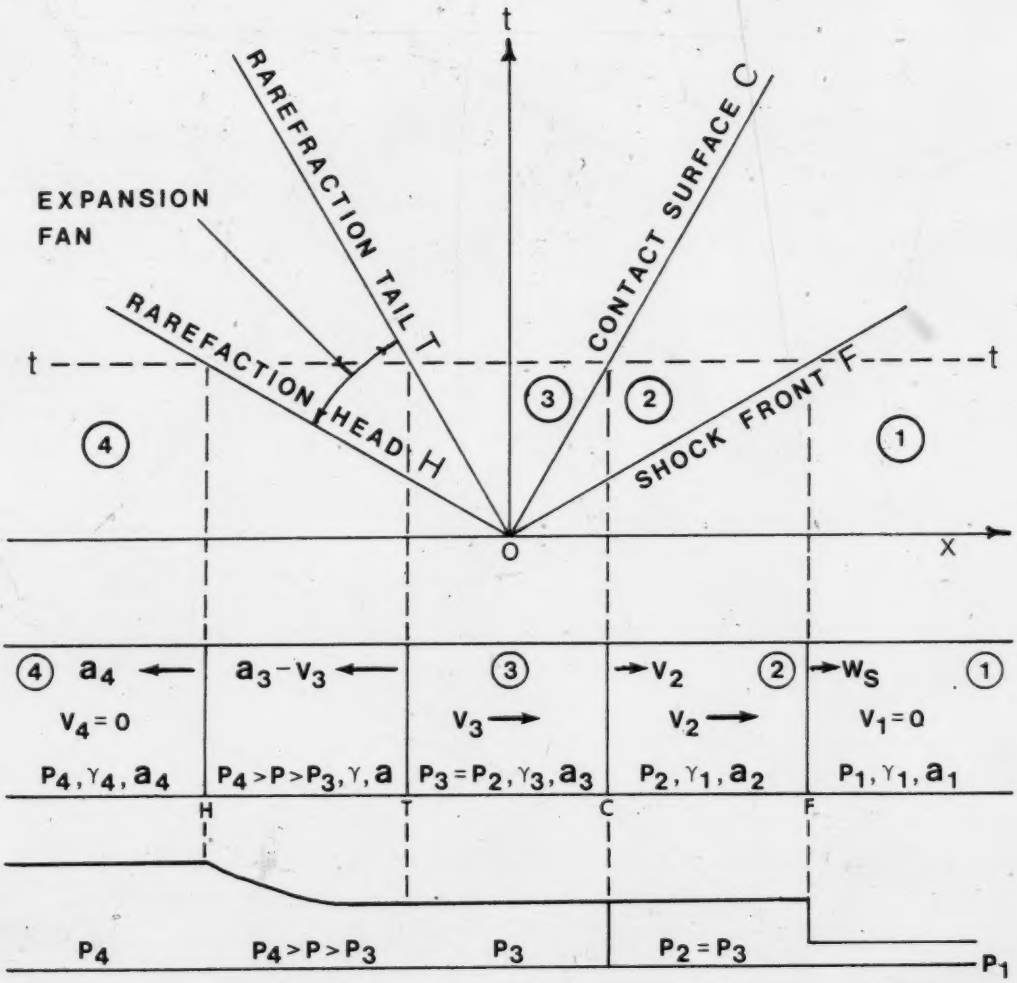

Figure 3.3 Shock Wave Parameters

where $T_1=T_0=$room temperature (300°K), $T_4=T_0$ and a_0 is the ambient acoustic speed at T_0. Substitution of the preceding relation into equation (3.21) yields:

$$v_3=a_0(T_0/300)^{1/2}\ln(T_0/300) \tag{3.23}$$

Indications from photographs of the jet plume are that after the plasma leaves the cavity its cross-section increases by approximately a factor of two. Hence this radial expansion tends to reduce the overall pressure ratio P_4/P_3 required for axial acceleration with the result that effective pressure ratios of one quarter to one tenth of the temperature ratio might be expected. The work of Resler *et al.*[54] and Alpher and White[55] indicates that the effective pressure ratio is increased by a factor of two if the shock tube cross-sectional area at the diaphragm is halved. Conversely then it would be expected that the effective pressure ratio would be proportionally decreased by a large increase in cross-sectional area. Figure 3.4 illustrates the plot of v_3 in equation (3.23) as a function of current. For comparison purposes the same quantity calculated for a more realistic pressure ratio in light of the foregoing discussion is plotted in Figure 3.4. This quantity is an order of magnitude less than that for equation (3.23).

From relation (3.18), the ejected plasma temperature is given by:

$$T_3/T_4=(P_3/P_4)^{\gamma-1/\gamma}$$

For P_3 as low as one atmosphere the near unity value of γ necessitates the temperature ratio at $T_4=T_0$: T_3/T_0 to range from 80 to 90%.

Proceeding now to estimate the plasma ejection time t_E, it is first necessary to calculate the mass efflux from the cavity. Assuming a constant cross-section of the plume external to the cavity, the mass flow through this area will be proportional to the product of density and velocity. From the thermal equation of state for an ideal gas the mass flow will vary as P_3v_3/T_3. This in turn is proportional to P_3v_3/a_3^2. At this rate if the mass flow is maintained at the orifice of the cavity of length L and temperature T_4 (proportional to a_4^2) the cavity will be exhausted in the time:

$$t_E=(P_4/a_4^2)L(a_3^2/P_3v_3) \tag{3.24}$$

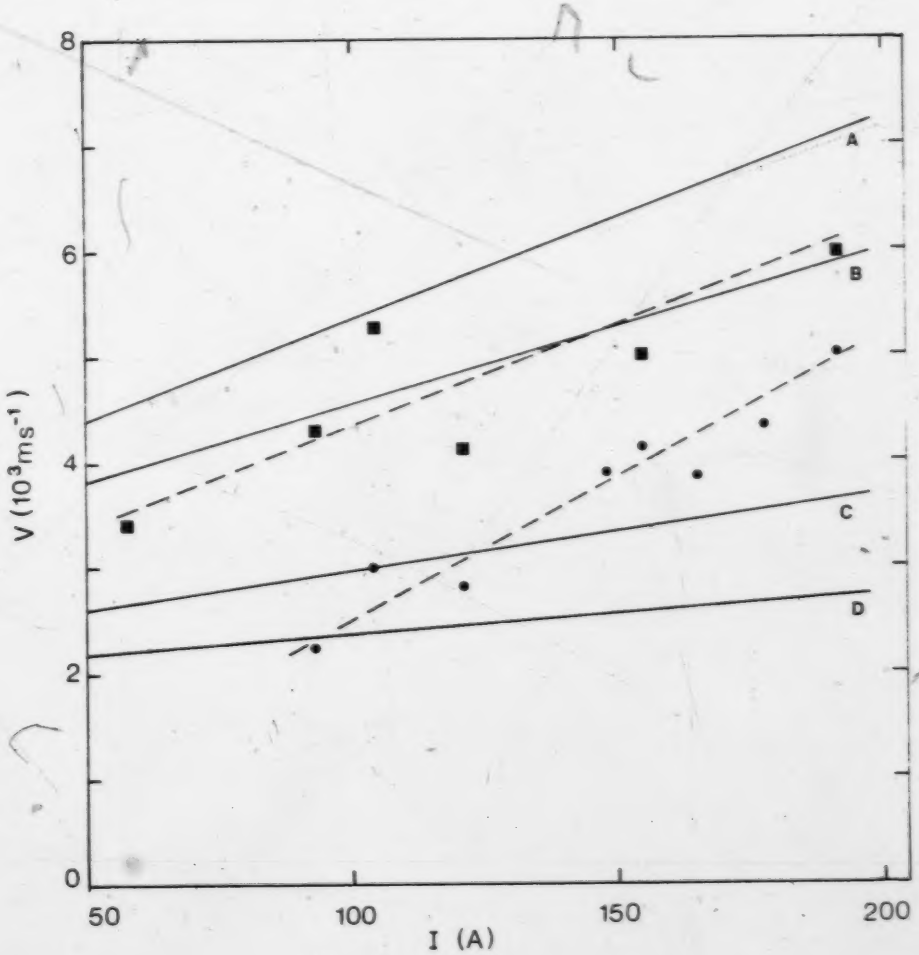

Figure 3.4. Calculated And Measured Flow Velocities Versus Current. Dots represent laser spark and squares are streak photograph results. Theoretical curves: equation (3.23) with tenfold area increase (A, Ernst *et al.*[46,47]; B, equation (3.7)) and sonic velocity (C, Ernst *et al.*[46,47]; D, equation (3.7)).

Equation (3.18) yields:

$$a_3/a_4 = (P_3/P_4)^{(\gamma-1)/2\gamma}$$

and applying (3.20), equation (3.24) becomes:

$$t_E = \frac{L}{a_4}\left(\frac{P_4}{P_3}\right)^{1/\gamma} \frac{\gamma - 1}{2[1 - (P_3/P_4)^{(\gamma-1)/2\gamma}]} \tag{3.25}$$

If $P_3/P_4=0$ or 1, then $t_E \to \infty$. For intermediate values, t_E in (3.25) reaches a minimum value when $1/\gamma=\ln(P_4/P_3)$ and consequently:

$$t_E=t_{min}=(L/a_4)e \tag{3.26}$$

For the rarefaction wave front to propagate the length of the cavity and once again upon reflection from the electrode surface the time required will be $\sim 2L/a_4$. The time expected to exhaust all the cavity plasma will be to some extent greater than this value. The quantity t_E in (3.25) is very insensitive to the ratio P_3/P_4 and for $.1<P_3/P_4<.9$ it remains less than $10L/a_4$. By inspection of (3.25) for these ranges an effective average value of t_E can be deduced to be:

$$t_E \sim 4L/a_4 \tag{3.27}$$

Equation (3.27) is plotted in Figure 3.1 where $L=1$ cm and a_4 is calculated upon application of relations (3.7) and (3.22) where $T_4=T_0$.

3.5 Heating Time Experiments

From Section 3.3 involving theoretical considerations with respect to the cavity plasma heating time the relation (3.10) was obtained using (3.7) for the plasma temperature T_0 and (3.8) for the longitudinal electric field E within the cavity. In order to test the validity of (3.10) experimentally, measurements were made of E. These results would in turn check the justification of (3.7) since it is related to (3.8) via equation (3.5).

The electric field measurements within the cavity were accomplished by the insertion of two .2 mm diameter tungsten wires into the cavity's ceramic lining. The electrodes were separated longitudinally by a distance of 2 mm and were connected via a differential amplifier to an oscilloscope where the transient potential difference between the wires was recorded. The

plasma electrical conductivity has a strong pressure dependence and hence the measurements were taken for various maximum arc currents. These currents were varied by applying different initial voltages to the energy storage capacitor C_2. The E field results were found to agree reasonably well with the expected theoretical values and the transient behaviour of the electric field provided evidence for the validity of equation (3.10). A pair of oscilloscope traces for the longitudinal E field and disharge current are presented in Plate 3.1. The oscillogram indicates that the electric field is initially high and decreases with time while the current momentarily continues to increase. At the lapse of approximately 20 μsec the electric field was found to stabilize at a value which was consistent with (3.8). After the current concluded its first and usually final half cycle the electric field magnitude decreased to zero. The measured E field results as a function of various maximum currents are plotted in Figure 3.1.

3.6 Streak Photograph Experiments

As mentioned in Section 3.1 this work involves a more detailed repetition of the work of Topham *et al.*[1] The apparatus used to photograph the external plasma jet in order to obtain its temporal variation is illustrated in Figure 3.5. The streak camera housing was of steel construction and utilized a cube having four mirrored faces to spread the image of the jet expansion across the photographic emulsion. A PMI U9M4FT d.c. motor coupled axially to the cube produced the rotation. The motor was provided with a tachometer output so that the rotational frequency of the cube could be calibrated. A magnet was mounted on one of the vertices of the cube such that its pole was aligned parallel with the axis of rotation and a magnetic pickup coil was situated on the camera structure such that an emf would be induced for each revolution of the cube.

A 0–15 volt d.c. supply was used to power the camera motor and the latter's tachometer output was connected to a Sabtronics Model 2000 DMM. The r.p.m. values corresponding to the tachometer's voltage output were calibrated by observing the period of the magnetic pickup's output on an oscilloscope at several voltage values. The streak camera's time

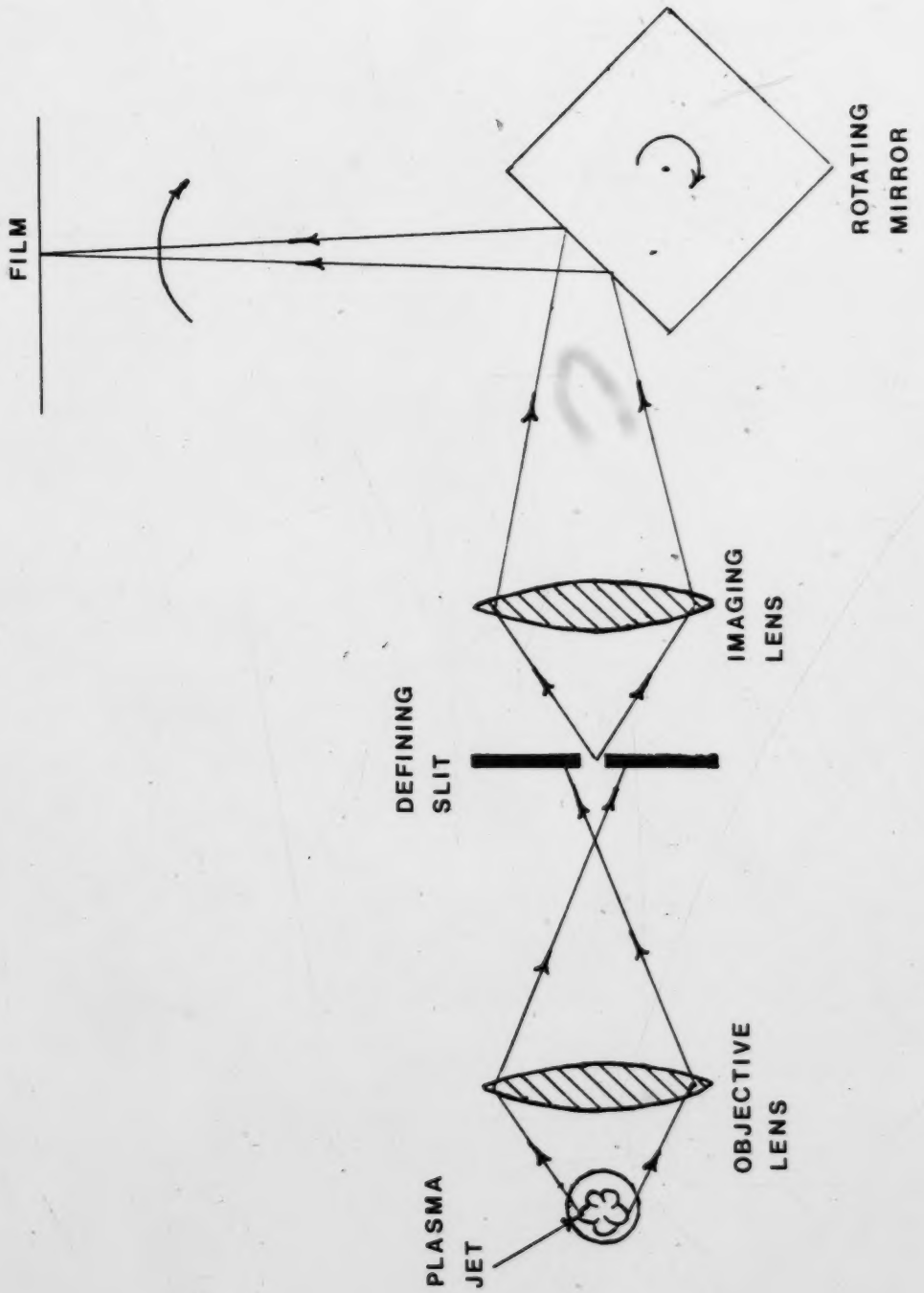

Figure 3.5 Streak Photography Setup

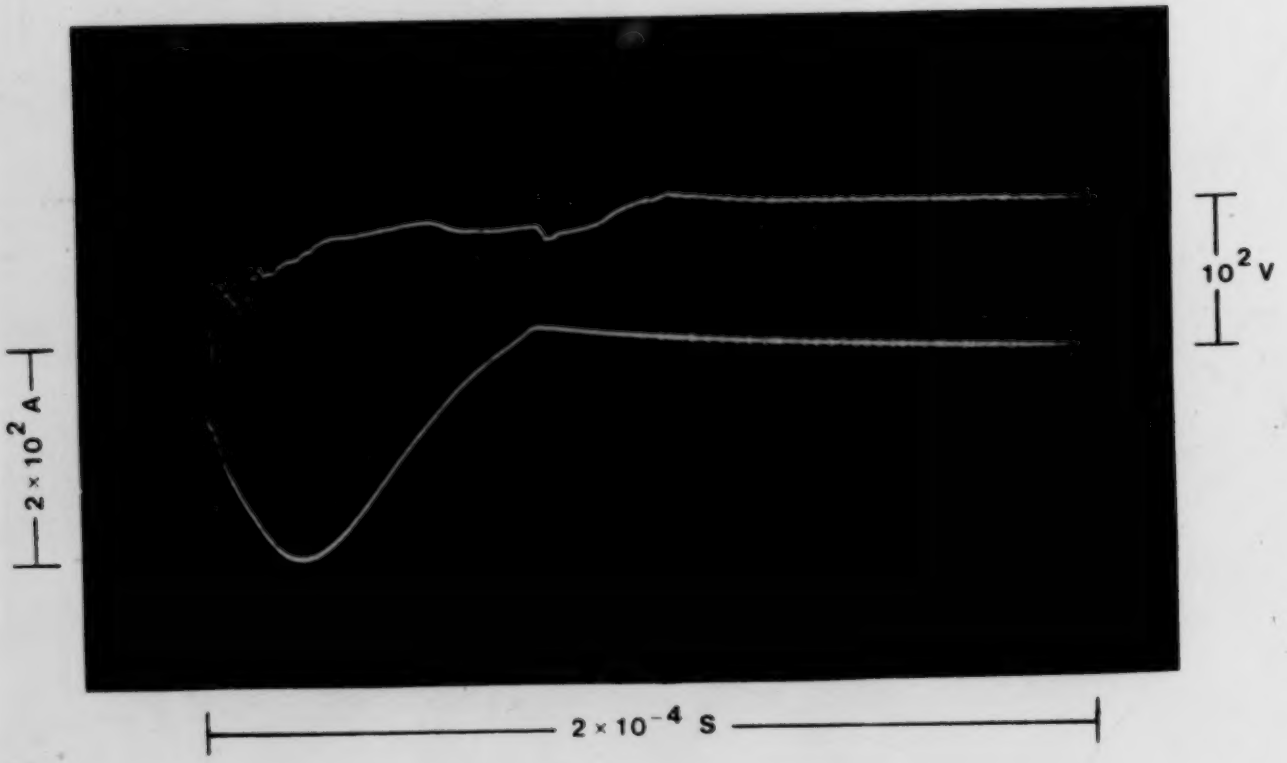

Plate 3.1 Oscillograms Of The Pulsed Current To The Igniter And The Associated *E* Field

resolution was limited by the drive motor's 15 volt rating and the cube assembly's vibrational response to higher rates of revolution. The maximum rate of rotation attainable was approximately 5000 r.p.m.

The streak camera's magnetic pickup coil output was connected to a Type 555 Tektronix Dual Beam Scope and the Time Base A mode was utilized. A coaxial cable was connected from the oscilloscope delayed trigger output to the plasma jet igniter's high voltage supply trigger input. This supply was similar to that used for the erosion experiments in Chapter 2. A high voltage cable was connected from the supply output to the plug's centre electrode. The steel end of the igniter was grounded.

The plasma plug was mounted horizontally and parallel to the streak camera's defining slit. Using a ground glass viewer, the centre of the plug end aperture was focussed onto the top streak camera plate and the optics were arranged such that the image magnification was approximately 2.5 times. The plug power supply was energized and then fired using the oscilloscope Single Sweep mode. In darkened surroundings, using a narrow defining slit width and opened shutter, the streak camera's rotating mirror was observed visually from the top plate aperture and the oscilloscope's delayed trigger setting was adjusted until the light from the plasma jet appeared centred on the mirror face coincident with the pulsing of the magnetic pickup. A Polaroid Land Camera using Type 47 (3000 A.S.A.) film was placed on the top streak camera plate, the shutter was opened and the high voltage supply was triggered. One of the many resulting photographs is shown in Plate 3.2.

It is evident that the striations and jet front are well defined on the photograph. Their respective propagation velocities were obtained from the following analysis. The vertical distance r from the centre of a mirror face to the camera plate was measured. On the photograph the ordinate represents the time axis and the abscissa is the longitudinal distance travelled by the jet. If Δs is the vertical image spread between the points t_1 and t_2 shown in Figure 3.6, then the approximate angle rotated by the mirror to subtend this distance is yielded by $\Delta\theta \simeq \Delta s/2r$ provided $\Delta\theta$ is much less than 1. For a mirror rotating at n r.p.m., the period

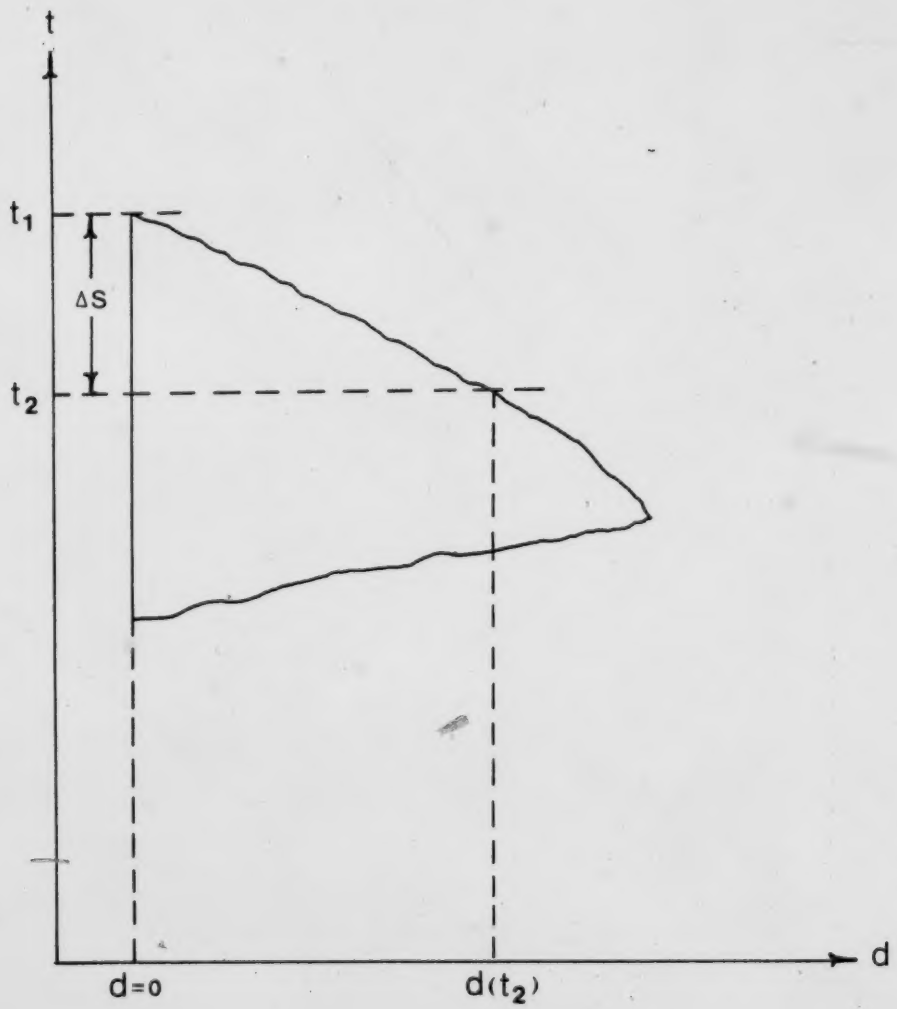

Figure 3.6 Parameters Used In Streak Photo Analysis

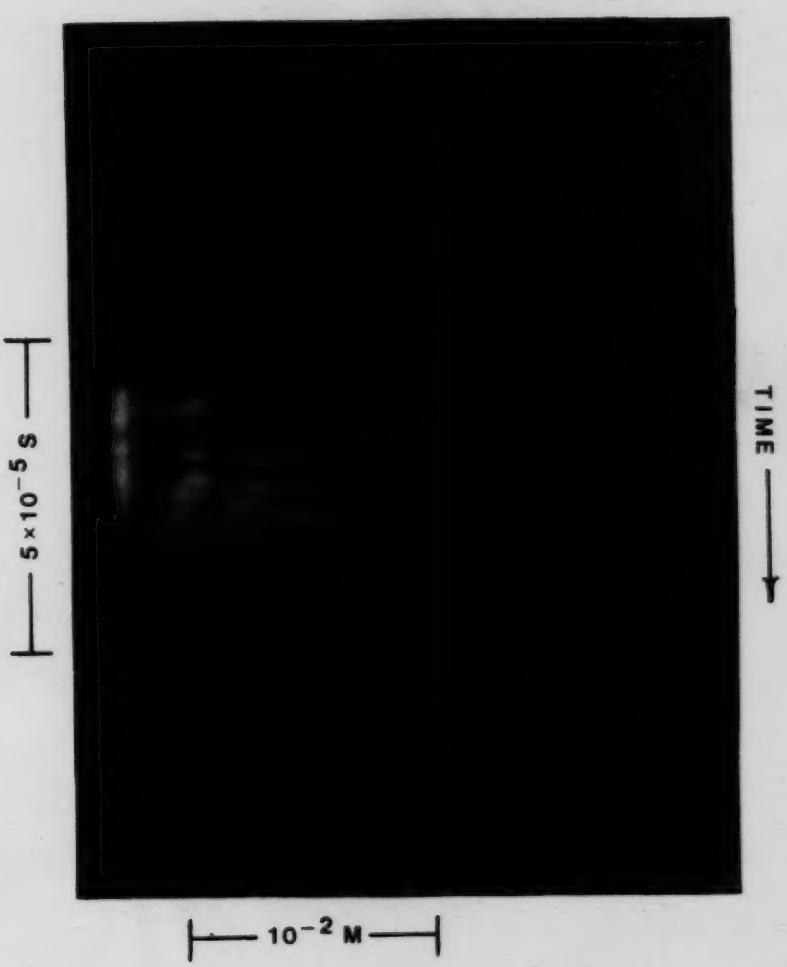

Plate 3.2 Streak Photograph Of The External Plasma Jet

$T=n/60$ rev/sec. The frequency of rotation is $f=T^{-1}$ and therefore the angular velocity is $\omega=2\pi T^{-1}$. The time period t represented by the sweep on the photograph is yielded with sufficient accuracy by: $t=\Delta\theta/\omega=\Delta sT/4\pi r$ sec. For an image magnification of M and a measured longitudinal displacement d, the jet front velocity is: $v_1=4\pi dr/M\Delta sT$ m sec^{-1}.

The striation velocities were obtained by measuring the angle from the horizontal, α. The value of the velocity was yielded by: $v_2=4\pi(\cot\alpha)r/MT$ m sec^{-1}.

Several discharge energies were used to observe the the characteristic jet velocities. Quantitative analysis of these photographs indicates that the jet front moves into the atmospheric air at near sonic velocity but the striations propagate at highly supersonic velocities (Mach 10 to Mach 20 relative to the ambient gas).

Observations of the photographs indicate that the emission of the luminous plasma from the cavity ceases abruptly. Figure 3.4 presents the measured striation velocities as a function of current along with the theoretical values from equation (3.23) based on a tenfold axial expansion and also using the plasma sonic velocity.

In order to determine whether the striations were possibly moving relative to the plasma flow itself, laser spark/probe measurements were taken of the plasma jet. These were obtained using a 40 nsec pulsed CO_2 laser beam which was focussed in the plasma jet at the cavity exit. The resulting spatially limited ionization sample was in turn entrained by the plasma jet flow and its downstream passage was recorded at a .8 cm displacement from the cavity orifice by a conventional high-pressure Langmuir probe.[56] Plate 3.3 illustrates a typical probe current oscillogram. At a time of approximately 4-5 μsec on the sweep a break is noticeable and this is caused by electromagnetic pickup from the laser. After this point there is a delay of approximately 2 μsec whereupon the probe detects a transient pulse of ionization whose magnitude peaks after an additional time in the range of 3 μsec. Flow velocity values were obtained from this technique following the method used by Dewey.[57] They are plotted in Figure 3.4 and it is apparent that their magnitudes are approximately 30% less than those corresponding to the streak camera work. However the laser spark/probe measurements were

Plate 3.3 Oscillogram Of Probe Current Versus Time For The Laser Spark Experiments

performed at a greater distance from the plug than for the streak camera and hence the above discrepancy can be accounted for by the difference in measurement locations. Striation velocities well in excess of sonic were found by this laser technique.

3.7 Plasma Exhaustion Time Measurements

The plasma exhaustion time of the cavity was estimated by replacing the energy storage capacitor (usually 1 to 12μF) with a much larger one of 300μF capacitance in series with a limiting resistor (1 to 4 ohms) and observing the consequent streak photographs of the jet. The high capacitance produced an order of magnitude increase in the duration of the discharge current (i.e. the current source was effectively of infinite duration) and hence changes in the ejected gas luminosity indicated a corresponding variation in the quantity of the ejected gas. In comparison to the streak photographs using a relatively lower capacitance an abrupt end to the plasma luminosity was observed after a much longer time period. The analysis of these photographs lacked the precision of the use of a photodensitometer but the well defined termination of the plasma luminosity provided measurements of acceptable accuracy. Results of the analysis of these photographs are also shown in Figure 3.2.

3.8 Observations Of The Plasma Expansion Process Within The Cavity

With the success of the streak camera work in obtaining high resolution photographs of the external plasma jet it was decided to apply this experimental arrangement in order to observe the plasma expansion process within the igniter cavity. It was apparent from the published research pertaining to the igniter that much less was known about the plasma characteristics within the channel than those pertaining to the external jet. The subsequent experimental approach involves qualitative observations of the internal plasma expansion process.

The channel could not be photographed directly from the actual plasma plug since it was ensconced within the the ceramic insulator and the steel casing. However a functional

model of the igniter channel which could be photographed was produced from a small cube of machinable ceramic. Channels of three widths were etched onto the cube; one of the conventional cavity width (1.6 mm diameter); one of 3.6 mm gauge; and one of .8 mm diameter. A moveable 1.6 mm diameter tungsten electrode was incorporated into the design and the channel was sealed using a plain glass microscope slide which was secured in place with nylon screws. Movement of the glass slide was necessary after each arc discharge since etching resulted from the latter. The channel model is shown in Plate 3.4.

The experimental setup to obtain streak photos of the channel was virtually identical to that for the observation of the external plasma jet with the exception that the igniter was replaced by the ceramic cube and the image of a channel section aligned vertically was focussed onto the top camera plate. An external capacitance of 12μF biased to 300 V was used in the igniter supply. The resulting streak photographs for the three channel widths are shown in Plate 3.5.

It is evident from these photographs that the plasma does not fill the entire channel for the 1.6 mm and 3.6 mm diameters during the current discharge period. However the .8 mm channel fills very rapidly. Also an oscillatory motion of the plasma is apparent during the first several microseconds of the discharge in all the channels and although not discernible in the photos presented, a similar movement of much higher frequency is faintly visible during the latter stages of the expansion process. The exact mechanism responsible for this movement is a matter for conjecture.

Observation of this oscillatory phenomenon suggested further investigation as to whether this movement noticed in conditions similar to those within the channel manifested itself somehow in the external plasma jet. Hence work proceeded on obtaining a composite streak photograph exhibiting the plasma expansion within the channel as well as the simultaneously occurring plasma ejection.

To achieve this end a successful arrangement was obtained using a small total reflection prism interposed between the collecting lens and the streak camera shutter. With this

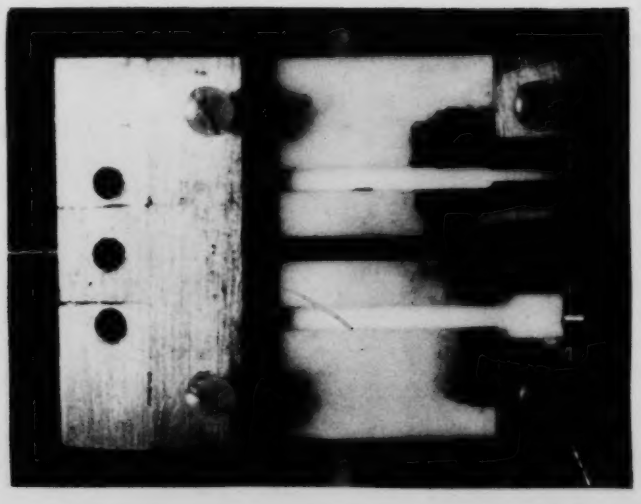

Plate 3.4 Ceramic Channel Model

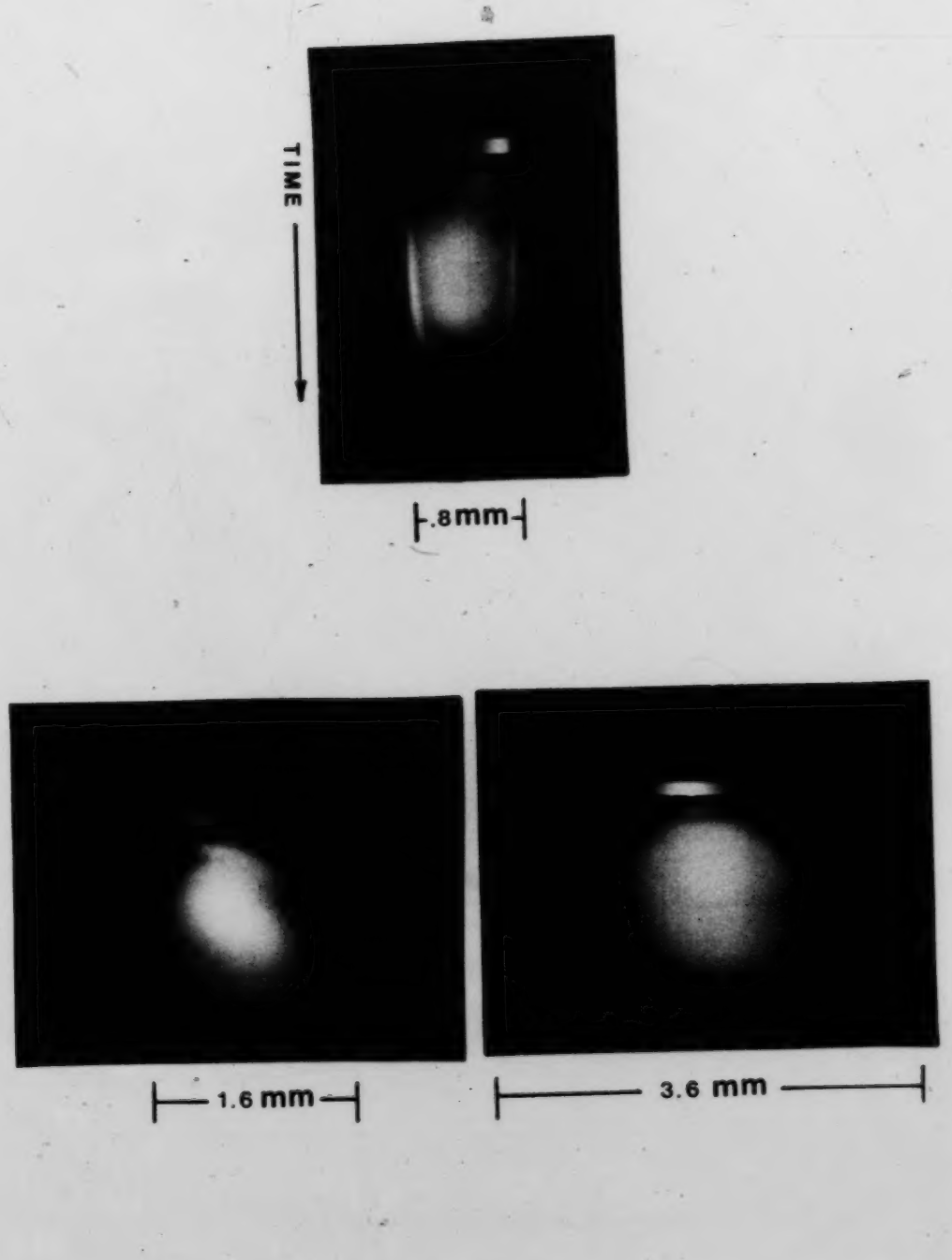

Plate 3.5 Plasma Expansion Within The Igniter Channel

configuration the channel section image was rotated through 90° (i.e. horizontal to vertical) by the prism while the external jet image was unaffected. A composite streak photograph is shown in Plate 3.6. Although the image definition is not optimum, the oscillatory movement observable in the channel section seems to occur coincidentally with a striation-like structure in the downstream plasma jet. As mentioned above these experiments were intended to yield qualitative observations. However for the initial arc discharge times these streak photographs were useful in obtaining an estimate of a typical cathode spot area for the erosion analyses of Chapter 2.

3.9 Two Dimensional Still Photographs Of The Plasma Jet

As mentioned in the introductory section to this chapter some longitudinal structure was evident in the external plasma jet displayed on the streak photographs in addition to the characteristic striations. To investigate this, several two dimensional time exposure photographs of the jet were taken using a Calumet pictorial camera. Since the light intensity radiating from the jet was very high it was necessary to mask either its top or bottom half and observe the remaining portion. One of the resulting photographs appears in Plate 3.7. There is definite evidence of flow reversal on the photograph.

Retaining the camera arrangement, photographs were also taken of the jet impinging upon a stationary barrier (i.e. a 1.6 mm diameter tungsten rod whose axis was aligned transverse to the flow direction) in order to seek further support for the streak photograph measurements which indicated a supersonic plasma streaming velocity. Indeed the photograph exhibited the well known diamond pattern associated with rocket and jet exhausts and the angle and spacing of the diamonds indicated a flow Mach number of approximately 2 which supported the streak camera measurements. This photograph was not suitable for reproduction.

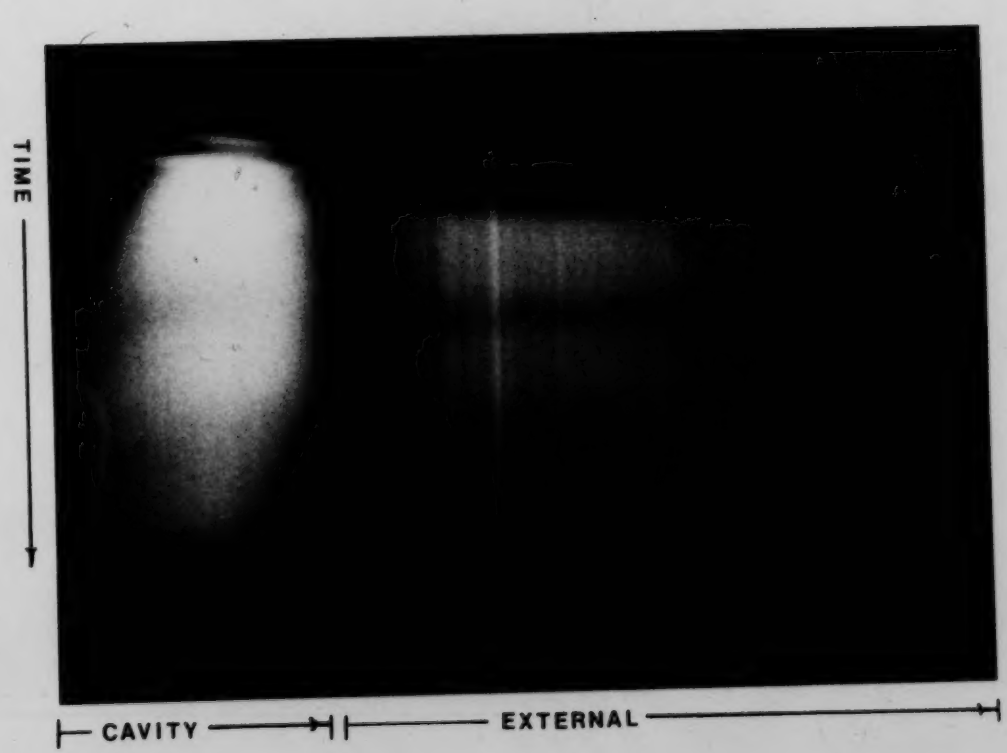

Plate 3.6 Composite Streak Photograph

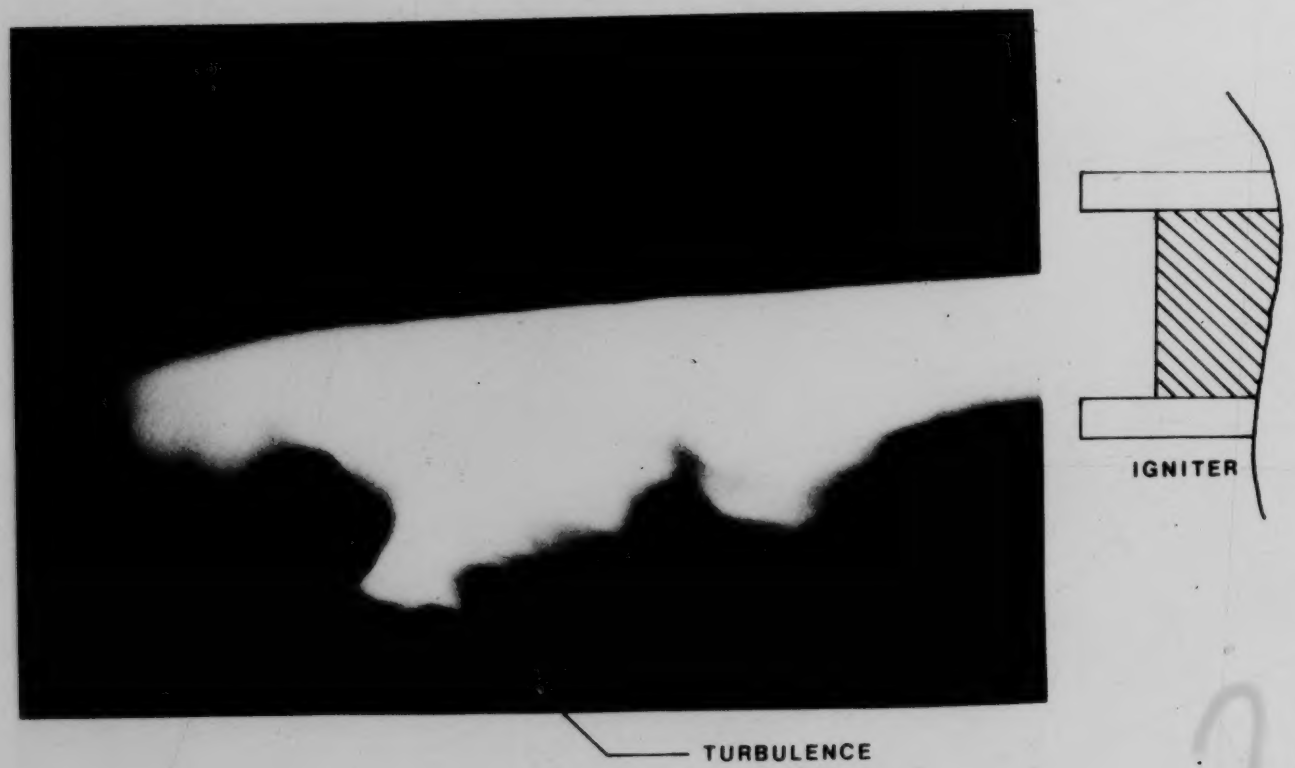

Plate 3.7 Two Dimensional Photograph Of The External Plasma Jet

3.10 Discussion And Conclusions

The experimental electric field measurements indicated that equation (3.10) for the plasma heating time was of reasonable validity. The transient behaviour of the electric field with time and the abrupt termination of jet luminosity supported very strongly the concept of the existence of a plasma heating time and ejection time respectively. Considering all the simplifying theoretical assumptions made the correspondence between the experimentally determined ejection times and the theoretical values was quite satisfactory.

The streak photograph work concurred with that of Topham *et al.*[1] and the existence of striations travelling at highly supersonic velocities was supported by the laser spark/probe measurements.

Recent streak photography work of Cavolowsky *et al.*[30] on the external plasma jet for an igniter orifice of 1.6 mm diameter found the jet front velocities to range from 125 to 300 m sec^{-1}. The discharge energy was maintained at 2.5 J. These values are consistent with the experimental results discussed in the preceding paragraph for this energy input and provide conclusive support for their validity. The findings of their studies also acknowledged the existence of the standing wave patterns observed in the streak photograph work of this chapter and that of Topham and co-workers for a similar igniter orifice diameter.

In addition Cavolowsky and associates proposed that the light streaks (striations) represented the movement of individual pockets of high temperature plasma containing excited species. They suggested that the striations are related to the dispersion of radicals formed at initially high temperatures to considerable distances downstream (as indicated previously by Behbahani *et al.*[12]) where in turn they promote chemical reaction.

Streak photographs obtained from the plasma expansion within the igniter channel model revealed that the luminous plasma did not reach the channel walls for the 1.6 mm and 3.6 mm diameters during the current discharge period. For the development of a spark channel in air, Braginskii[51] derives the channel radius a as: $a = .93\rho_0^{-1/6} J^{1/3} t^{1/2}$ where $\rho_0 = \rho\rho_{air}^{-1}$ is the density unit (ρ_{air} at atmospheric pressure $= 1.29 \cdot 10^{-3}$ gm cm^{-3}). Therefore $\rho = \rho_{air}$ and $\rho_0 = 1$;

J is the arc current (kA) $\simeq$ .16 kA for the parameters used in the experiment and t is the discharge time (μsec) and was approximately 64 μsec. With these approximate values the equation yields $a \simeq 4$ mm. The widest channel radius was 3.6 mm. Hence the relation for a is not consistent with the observed results where the plasma only reached the .8 mm diameter channel walls. Perhaps the cavity plasma radius is constrained by a magnetic pinch effect past a certain critical value of the radius. Further investigation of this phenomenon is beyond the scope of this thesis.

For the composite streak photographs the oscillatory motion which was observed in the internal channel model was found to produce coincident striations in the external plasma jet. The exact mechanism responsible for this motion has not been determined.

With the satisfactory correspondence between the theoretical models and the experimental results an overall representation of the plasma jet may be formulated which accounts for the generation of very pronounced turbulence in the gas beyond the jet. The earlier work of Topham *et al.*[1] indicated that the advance of the plasma jet into the ambient surroundings occurs with an effectively constant cross-section which is as large as an order of magnitude greater than that of the cavity. The plasma streams outwards in an envelope at velocities of the order of $5 \cdot 10^3$ m sec^{-1} as indicated in Figure 3.4. From equation (3.18) it is evident that for values of γ in the range $1.05 \rightarrow 1.1$ for the cavity plasma, the adiabatic expansion of the latter from its initial pressure to atmospheric exhaustion would involve a temperature decrease of only 10%. Hence the acoustic speed would vary slightly from that of the initial propagation of the rarefaction front (i.e. a_4) and as indicated by Figure 3.4, the effective Mach number of the flow within the plasma stream would be in the region of 1 to 2. It is expected that under these conditions the ambient pressure of 1 atmosphere would be attained by the plasma after it travels one or two cavity diameters downstream. This is indeed verified by the aforementioned appearance of the shock diamonds at a distance of approximately one cavity diameter downstream from the orifice.

The theoretical considerations described above implied that for efficient igniter operation the plasma heating and expulsion processes would have to be similar in duration. This constraint gives consistency to the shock-tube analogy for initial times but for later stages of the plasma expansion process a steady-state flow model such as that of Cetegen *et al.*[21] may be more suitable.

The plasma jet structure could be represented by that of Figure 3.7. From the streak photographs it is evident that the plasma streams at low pressure and a constant high velocity from the cavity orifice to the jet front. Since the photographs indicate that the front velocity is approximately 5% of the streaming velocities, a cooling compression of the plasma must occur in the region of the front. The deceleration of the $\sim 2 \cdot 10^4$ °K plasma at the ambient air density from a velocity in the range of $5 \cdot 10^3$ m sec^{-1} will impart substantial momentum to the surrounding gas. This impulse is probably the mechanism which causes the external plume expansion at the observed near-sonic velocities. For a density of approximately 1% of atmospheric and a flow velocity in the ambient air of approximately Mach 16, the product of density $\cdot$ velocity^2 yields values in the order of atmospheric pressure and hence this would produce enough impulse to drive the front at near-sonic velocity.

As mentioned in the introduction of this chapter most of the previous work focussing on the plasma expulsion concentrated on the depth of penetration of the jet. From the work of Oppenheim *et al.*[20] it has been determined that combustion is not initiated at the jet front but in the cooler region ahead of it. All the streak photographs of the external jet indicate that the front propagation continues until either termination of the input power occurs or the cavity is exhausted of gas.

Figure 3.2 is basic in relating the three characteristic times for efficient repetitive plug operation in i/c engines. The criteria so obtained when applied to the curves of Figure 3.1 indicate that the arc can effectively absorb only relatively low voltages. For most of the plasma igniter supply circuits described to date the time of energy input has typically been $t_l \simeq 50$ μsec. Figure 3.2 shows that this time period is consistent with the experimentally determined values

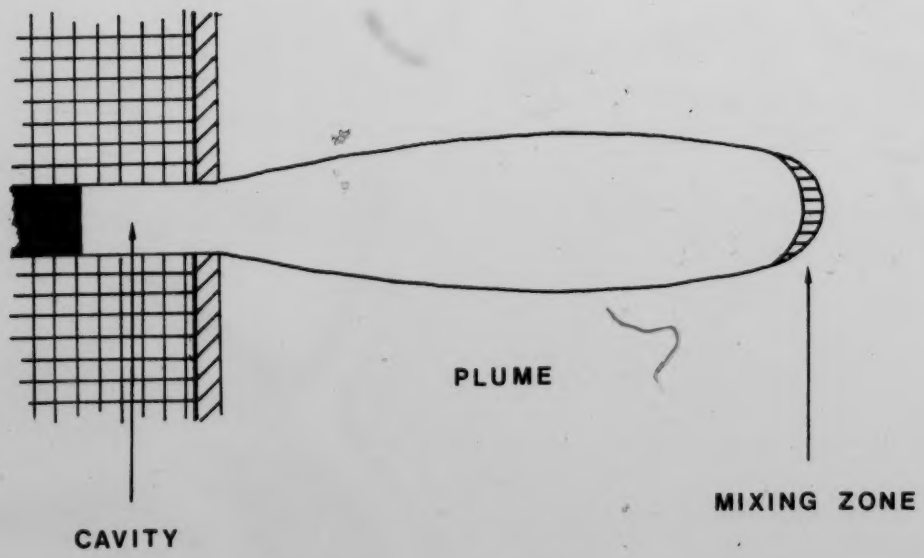

Figure 3.7 Proposed Model Of The Pulsed Plasma Jet

of t_E for currents of ~ 10^2 A.

As was mentioned in the preceding paragraph, the arc discharge in the igniter cavity is very limited in its ability to absorb voltage. Hence along with the careful matching of the characteristic times of igniter operation, the use of a high-voltage trigger with a low voltage energy reservoir would provide most efficient plug operation. The results of Chapter 2 also indicated that optimum efficiencies could be realized using low capacitor voltages.

4. Diffusion And Heat Conduction Enhancement By Coaxial Spark Igniters

4.1 Introduction

As mentioned in Chapter 1, the work of Behbahani *et al.*,[12,29] Cavolowsky *et al.*,[30] and Clements *et al.*[31] found that the quantity of nitrogen atoms produced by the igniter was considerably in excess of values from equilibrium dissociation predictions and this could not be justified by the low plume temperatures. It was proposed that these results were due to a thermal stratification in the plasma jet resulting in small pockets of very hot radical-rich gas. The existence of these pockets was experimentally verified and it was further suggested that jet induced turbulence was responsible for both the creation and transport of the pockets downstream to the relatively cold region of the flame front.

The measurements of Clements *et al.*[31] have shown that while the plasma plume extends only 10 mm from the igniter orifice and is only of 10^{-4} s duration, there is a sharply delineated wave of tepid gas (i.e. having temperatures less than 100 °C above the ambient) which propagates 50 mm downstream of the plug during the ensuing 10^{-2} s. 'Spot' interferometer measurements illustrate that the wave front thickness can be as narrow as 10^{-1} mm while from calorimetric methods it has been determined that the excess thermal energy in the wave is approximately equal to the total energy impressed upon the gas. The heat originating within the plug cavity is fairly uniformly distributed throughout the wave during its propagation time and this implies heat conductivity or diffusion constants many orders of magnitude greater than those of a stationary gas. Since flame speed is proportional to the square root of heat conductivity it is probable that the observed enhancement of the former quantity produced by plasma plugs may be correlated with the augmentation of one or both of the transport processes above.

Considering now the diffusion of particles and heat flow in a stationary gas, the speed of the particles is determined by the local gas diffusion constant D, while heat flows at a rate related to the heat conductivity K. If the number density and temperature gradients are

constant over the length L, then simple kinetic theory shows that both the particles and heat propagate at a speed v defined by:

$$v = \bar{v}\lambda/3L \tag{4.1}$$

where λ is the molecular mean free path and $\bar{v}$ is the r.m.s. molecular velocity.

For room temperature air, $\lambda \sim 10^{-7}$ m and $\bar{v} \sim 5 \cdot 10^{2}$ m sec^{-1}. If the distance L travelled by the wave in 10^{-2} s is $\sim 5 \cdot 10^{-2}$ m then the preceding equation yields a propagation speed v of 10^{-3} m sec^{-1}. The observed speed is generally much greater: $5 \cdot 10^{-2}$ m/10^{-2} sec and therefore the heat propagation is enhanced by $\sim 10^{3}$.

As mentioned in Chapter 1 the possibility of radiation absorption being the enhancement mechanism has been discounted in the work of Orrin *et al.*[16] Therefore the gas motion within the wave is most likely responsible. Indeed the measurements of Clements *et al.*[31] indicate that substantial convection velocities exist throughout the wave volume. However the measurements do not reveal whether the transient velocity field is composed of sufficiently fine scale turbulence to intimately mix the hot and cold gases and transport this mixture to the wave front.

Turning now to the igniter generated turbulent plume structure, the work of Topham *et al.*[26] described in Chapter 1 indicated that the plume is mathematically similar to atmospheric buoyant thermals or 'puffs'. The experimental results of Clements *et al.*[31] on the thermal energy propagation and convective velocities within the puff were found to be consistent with the Topham's predictions. A recent study by Batt *et al.*[59] obtained temperature measurements within rising buoyant thermals (fireballs) created by the detonation of large diameter gas-filled balloons. Their convection velocity results for the fireball thermal wake illustrate that the magnitudes were as high as twice those of the core. To a first approximation their data indicates that for early times the rising fireball is defined by a highly intermittent irregular top or cap, a relatively constant high-temperature core and a thermal wake which approximately exhibits a linear mean temperature decay. This smooth temperature decay was found in the above work of Clements and associates. The temperature fluctuations in the vicinity of the 'top'

and 'bottom' of the fireball were found to be higher at the fireball's leading edge as compared to the trailing edge. Specifically, a rather 'sudden' growth in temperature intensity was found at the top of the fireball in contrast to the gradual decay of the bottom. It was found that the leading edge of the 'hot' eddies and fireball core generally possess steep temperature gradients in contrast to the relatively shallow gradients of the trailing edge. A hot fluid motion at the top of the fireball was found to consist of large-scale structure combined with pockets of intense turbulent activity. Ambient air eddies were found to be embedded/entrained within the fireball top and wake. These results support strongly the existence of a mechanism to transport the mixed hot and cold species to the cap (wave front).

The work discussed in this chapter is an attempt to clarify the role of the internal gas motion and turbulence in these transport processes and to measure the related effective coefficients of diffusion and heat conductivity directly.

4.2 Turbulent Transport Considerations

It is not intended to give a comprehensive and rigorous exposition of turbulent flow theory which has grown during this century into a vast field of study but to focus particularly on concepts which are relevant to turbulent transport processes.

The phenomenon of turbulence is essentially analyzed by statistical dynamic methods. It can be defined as the superposition of an irregular eddying motion on a mean stream and the former motion is not reproducible in detailed configuration in identical experiments nor is it theoretically predictable. Its statistical properties are significant and for theoretical analysis a probability average can be defined to separate the mean and fluctuating flow quantities. By the ergodic theory in probability this average is equivalent to an ensemble average obtained from a large number of macroscopically identical experiments provided that the flow is stationary in time and homogeneous in one or more spatial directions.[60,61]

A stationary field of turbulence is one in which the statistical characteristics are independent of time and homogeneity occurs when the statistical characteristics of the field are

unchanged by a translation of the flow axis.[62] If the turbulence is additionally isotropic, the statistical characteristics will also be invariant under a rotation or reflection of the axes.[62] In actuality turbulent flows are neither completely stationary nor homogeneous and hence averaging procedures with respect to time or space must be taken for finite values.[61]

The Eulerian velocity time average for a homogeneous turbulence can be defined as[61]:

$$\bar{U}(x_0)=\lim(T\to\infty)(2T)^{-1}\int_{-T}^{+T} dt\, U(x_0,t) \tag{4.2}$$

The space average is yielded by[61]:

$$\bar{U}=\lim(x\to\infty)(2x)^{-1}\int_{-x}^{+x} dx\, U(x,t_0) \tag{4.3}$$

The ensemble average of N identical experiments is given by[61]:

$$\bar{U}(x_0,t_0)=N^{-1}\sum_{1}^{N} nU_n(x_0,t_0) \tag{4.4}$$

The Cartesian components of the instantaneous turbulence velocity field can be represented by: $U_i=\bar{U}_i+u_i$ where $\bar{U}_i$ is the mean field and can be a function of x and t; the fluctuation u_i is a random function of these variables and possesses zero mean. The pressure field can similarly be represented by: $P=\rho(\bar{P}+p)$ where ρ is the fluid density.

Turbulence may be described as the superposition of progressively decreasing periodic motions or alternatively the superposition of successively decreasing eddy sizes. There is a statistical lower limit to these eddy sizes since as they decrease, the velocity gradient across them increases and in turn the viscous shear stresses increasingly counteract the eddying motion. In other words, a minimum scale of turbulence exists which corresponds to a maximum frequency for the turbulent motion. Although in real turbulent motions, distinct frequencies are not permanently present, it is generally possible to allocate particular amounts of the total kinetic energy of the motion to specific frequencies. This energy distribution is defined as the energy spectrum.

As mentioned in the preceding paragraph, viscosity dominates the flow in the smallest eddies and hence molecular effects become prevalent in the diffusion process for this case. However, for moderate flow velocities the magnitude of the smallest eddies is still very large compared to the corresponding molecular mean free path for gases under ambient conditions.

Consequently gases and liquids in these flows may still be treated as continua and there exists a large difference between the domains of the turbulent and molecular magnitudes.[61]

The basic transport equation of the turbulent fluid flow is the Navier-Stokes equation.[63] For an incompressible fluid (i.e. $\partial U_i/\partial x_i=0$) the equation becomes:

$$\frac{DU_i}{Dt}=-\frac{1}{\rho}\frac{\partial P}{\partial x_i}+\nu\frac{\partial^2 U_i}{\partial x_j^2} \tag{4.5}$$

where ν is the kinematic viscosity and ρ is the density. With the additional turbulent fluctuating velocity component this equation may be written:

$$\frac{\partial}{\partial t}(\bar{U}_i+u_i)+(\bar{U}_j+u_j)\frac{\partial}{\partial x_j}(\bar{U}_i+u_i)=-\frac{1}{\rho}\frac{\partial}{\partial x_i}(\bar{P}+p)+\nu\frac{\partial^2}{\partial x_j^2}(\bar{U}_i+u_i) \tag{4.6}$$

The continuity equation is:

$$\partial(\bar{U}_j+u_j)/\partial x_j=0 \tag{4.7}$$

By averaging equations (4.6) and (4.7) with respect to time the momentum and continuity equations for the flow may be obtained. The momentum equation is:

$$\frac{\partial\bar{U}_i}{\partial t}+\bar{U}_j\frac{\partial\bar{U}_i}{\partial x_j}=-\frac{1}{\rho}\frac{\partial\bar{P}}{\partial x_i}+\nu\frac{\partial^2\bar{U}_i}{\partial x_j^2}-\frac{\partial}{\partial x_j}\overline{u_iu_j} \tag{4.8}$$

Since the ensemble averaging and differentiation processes are commutative, the continuity equation (4.7) yields $\partial\bar{U}_j/\partial x_j=0$ and hence $\partial u_j/\partial x_j=\partial\bar{u}_j/\partial x_j=0$. The right-hand side of (4.8) may be written as[64]:

$$\frac{1}{\rho}\frac{\partial}{\partial x_j}\bar{P}_{ij}=\frac{\partial}{\partial x_j}\left(-\bar{P}\delta_{ij}+\nu\left(\frac{\partial\bar{U}_i}{\partial x_j}+\frac{\partial\bar{U}_j}{\partial x_i}\right)-\overline{u_iu_j}\right) \tag{4.9}$$

where δ_{ij} is the Kronecker delta. This equation represents the divergence of the sum of the stress tensor associated with the mean flow plus the term $\tau_{ij}=-\overline{u_iu_j}$. The latter term is designated as the Reynolds stress and represents a virtual stress generated by the turbulent fluctuations and acts upon the mean flow. Its definition implies that it is a symmetric second-order tensor. Contracting equation (4.6) with u_i and averaging it with respect to time results in the turbulent energy equation:

$$\left(\frac{\partial}{\partial t}+\bar{U}_j\frac{\partial}{\partial x_j}\right)\frac{1}{2}\overline{u_i^2}+\overline{u_iu_j}\frac{\partial\bar{U}_i}{\partial x_j}+\frac{\partial}{\partial x_j}\left(\frac{1}{2}\overline{u_i^2u_j}+\frac{\overline{p\,u_j}}{\rho}\right)$$

$$=2\nu \frac{\partial}{\partial x_j}(\overline{u_i e_{ij}})-2\nu\overline{e_{ij}^2} \qquad (4.10)$$

The turbulent motion rate of strain tensor $e_{ij}=1/2(\partial u_i/\partial x_j+\partial u_j/\partial x_i)$ is used to express the right-hand side of the equation. As expressed by Phillips,[44] equation (4.10) expresses the rate of change of kinetic energy per unit mass of the turbulence following the mean motion in terms of:

1. "The rate of working of the Reynolds stresses against the mean velocity gradient.
2. The divergence of the energy fluxes in physical space associated with the turbulent convection of the kinetic energy and the covariances between the velocity and stress fields (both pressure and viscous).
3. The rate of energy dissipation per unit mass $\epsilon=2\nu\overline{e_{ij}^2}$."

The energy flux terms represent a redistribution of the turbulent motion energy in physical space in which no net loss or gain of the latter quantity occurs. The viscous dissipation rate is effectively positive and represents a continual fluid motion energy drain which is balanced by the energy supplied by the Reynolds stresses $\tau_{ij}=-\overline{u_i u_j}$ on the mean velocity gradient. Thus the Reynolds stresses play a dual role in the flow: they interact with and modify the mean velocity field and provide the mechanism by which the turbulent energy is maintained. Recent theoretical work suggests that Reynolds stresses result from the direct interaction between the turbulent fluctuations and the mean shearing motion of the flow."[44]

Considering now the turbulent diffusion of fluid particles, a Lagrangian description is necessary to analyze this motion. In real turbulence the motions of fluid particles are randomly distributed. This is analogous to the motions of molecules in a gas where two arbitrary molecules are statistically separated by an increasing distance with time. If the subsequent positions of a number of neighbouring particles or molecules are viewed at various instants a gradual spread of the particles is observed throughout space and this is the basic concept of diffusion.

The diffusion of fluid particles by the turbulent motion of the fluid is distinct from the diffusion process described by the kinetic theory of gases. In contrast to the latter theory, the fluid particle motions are continuous. There exists an intensive interaction between the fluid

particles and consequently a continuous exchange of a transferable property may occur. A correlation in time may be defined between fluid particle properties at subsequent instants and hence the turbulent diffusion process may not be considered to be a Markov process as opposed to motions on the molecular scale.

To represent this temporal correlation of fluid particle properties, the Lagrangian auto-correlation coefficient was defined by Taylor[65]:

$$R_L(\tau)=\overline{v_2(t)v_2(t+\tau)}/v_2'^2 \tag{4.11}$$

where v_2 is in this case the turbulent particle velocity in the x_2 direction, $v_2'^2=\overline{v_2^2}$, and $\tau=\Delta t$. The variance of $y_2(t)$, the distance travelled by a marked particle in the time t is given by:

$$\overline{y_2^2}(t)=2v_2'^2\int_0^t d\tau(t-\tau)R_L(\tau) \tag{4.12}$$

The properties of the Lagrangian correlation coefficient are: $R_L(0)=1$; and $R_L(\tau)$ is symmetrical with respect to τ because of the flow field homogeneity and decreases with increasing τ to an eventual value of zero.

For very small values of τ, $R_L(\tau)\simeq 1$ and (4.12) reduces to:

$$\overline{y_2^2}(t)\simeq v_2'^2t^2 \quad \text{or} \quad y_2'(t)\simeq v_2't \tag{4.13}$$

For much longer time periods, $t>>t'$ where t' represents the time where $R_L(t')\simeq 0$, the Lagrangian integral time scale is defined as:

$$L_t=\int_0^\infty dt\ R_L(t) \tag{4.14}$$

It is usually considered a measure of the longest time during which a particle on the average moves in a given direction.

There is also a relation defining the Lagrangian dissipation time:

$$\tau_L^{-2}=-1/2(\partial^2R_L/\partial t^2)_{t=0} \tag{4.15}$$

where τ_L is the Lagrangian dissipation time scale and is a measure of the most rapid changes that occur in the fluctuations of $v_2(t)$.

Application of equation (4.14) to (4.12) for large values of t results in the expression[66]:

$$y_2'\simeq v_2'(2L_tt)^{1/2} \tag{4.16}$$

Hence for this case it is evident that the diffusion is proportional to $t^{1/2}$.

A coefficient of eddy diffusion ε is defined for these large times:

$$\varepsilon = \overline{y_1^2}(t)/2t = v_2'^2 L_t = v_2'^2 \int_0^\infty dt\, R_L(t) \tag{4.17}$$

The coefficient may alternatively be written:

$$\varepsilon = v_2' \Lambda_L \tag{4.18}$$

where $\Lambda_L = v_2' \int_0^\infty dt\, R_L$ and may be interpreted as a space scale for particle motion in only one particular direction. The latter term is designated as the Lagrangian or diffusion-integral length scale.

In theories describing turbulent transport processes, those based upon the concept of a 'mixing length' have yielded useful and practical semiempirical relations. This concept was arrived at independently by Taylor and Prandtl.[67]

Prandtl's reasoning follows from the kinetic theory of gases where the kinematic viscosity is yielded by the product of the root-mean square molecular velocity and the mean free path. By analogy he assumed that the turbulent eddy viscosity coefficient was equal to the product of a 'mixing length' and some appropriate velocity.

Continuing with Prandtl's theory, consider a two-dimensional flow of mean Eulerian velocity $\bar{U}_1$ in the x_1 direction, and the average transport through a plane parallel to $\bar{U}_1$ of a transferable property P per unit mass caused by the velocity u_2 of the turbulent motions. Define a 'fluid lump' as a large part of the fluid continuum consisting of a coherent conglomerate of fluid particles.[67] It may be comparable in size to the larger turbulence eddies and smaller scale turbulence in addition to molecular effects will affect the exchange process with the surroundings. If each of these fluid lumps subjected to the turbulent motion is considered to be autonomous and the property P of this lump is conserved for a certain time period (i.e. over a certain distance) then in analogy to molecular diffusion in the kinetic theory of gases, the eddy diffusion coefficient ε_P may be defined as:

$$\varepsilon_P = \text{const.}\, u_2' \Lambda \tag{4.19}$$

where Λ is an integral length scale. The following assumptions were made by Prandtl in order

to evaluate u_1' and Λ:

1. "The distance L_P across which the fluid lumps transport a transferable property during their motions perpendicular to the control plane till adaptation with the new environment has taken place, is relatively small. So consistent with the assumption of a gradient type of diffusion, the gradient of the mean property is constant across the distance L_P.
2. The axial and transverse components of the turbulence velocities are roughly of the same magnitude."[67]

If p is the fluctuation of the property P with respect to the mean value $\bar{P}$ at the control plane (at $x_2=0$), the average flux or transport per unit area and of time through the control plane is:

$$(T_P)_2=\rho\overline{u_2 p} \tag{4.20}$$

where this average is taken over a large ensemble of fluid lumps passing the control plane.

From assumption (1) immediately above it may be deduced:

$$p=L_P \mathrm{d}\bar{P}/\mathrm{d}x_2 \tag{4.21}$$

The ensemble of fluid lumps may be divided into subensembles such that the distance L_P from which the lumps of each subensemble originate is the same. From (4.21) the transport of all these sub-ensembles together is:

$$(T_P)_2=\rho\overline{u_2 L_P}\,\partial\bar{P}/\partial x_2 \tag{4.22}$$

Assumption (2) above yields the relations:

$$u_2=\text{const.}\ u_1=-\text{const.}\ L_P\left|\mathrm{d}\bar{U}_1/\mathrm{d}x_2\right| \tag{4.23}$$

where the negative sign results from the fact that the lump originates from the negative x_2 direction. Substituting the relation (4.23) into (4.22) results in:

$$(T_P)_2=-\text{const.}\ \rho\overline{L_P^2}\left|\partial\bar{U}_1/\partial x_2\right|\left|\mathrm{d}\bar{P}/\mathrm{d}x_2\right| \tag{4.24}$$

Introduction of a new length parameter $l_P^2=\text{const.}\ \overline{L_P^2}$ and since by definition $(T_P)_2=-\rho\varepsilon_P\,\partial\bar{P}/\partial x_2$ yields:

$$\varepsilon_P=-\overline{u_2 L_P}=l_P^2\left|\mathrm{d}\bar{U}_1/\mathrm{d}x_2\right| \tag{4.25}$$

Prandtl's mixing length theory, though derived for one-dimensional turbulent transport can be extended to the three-dimensional case.[67] Consider the transport of a property P through a control plane perpendicular to the x-direction. This transport may be expressed as:

$$\overline{U_i P} = \overline{U}_i \overline{P} + \overline{u_i p} \tag{4.26}$$

The transport by turbulent motions is represented by: $\overline{u_i p}$. Suppose there is a fluid lump which passes the control plane with a velocity u_i and originates from the centre of a region which is a distance $(L_P)_j$ away from the point in the control plane where the fluid lump centre passes. If a gradient-type of diffusion is assumed then:

$$p = (L_P)_j \, \partial \overline{P} / \partial x_j \tag{4.27}$$

Whence follows:

$$(T_P)_i = \rho \overline{u_i (L_P)}_j \, \partial \overline{P} / \partial x_j \tag{4.28}$$

A coefficient of eddy diffusion, $(\varepsilon_P)'_{ij} = -\overline{u_i (L_P)}_j$ may again be introduced and it is a non-symmetric second order tensor. Substituting this coefficient into (4.28) and taking the divergence results in:

$$\partial (T_P)_i / \partial x_i = -\partial \{ (\varepsilon_P)'_{ij} \, \partial \overline{P} / \partial x_j \} / \partial x_i \tag{4.29}$$

Retaining the fact that the indices i and j in $(\varepsilon_P)'_{ij}$ correspond to u_i and $(L_P)_j$ respectively, (4.29) may be re-written as:

$$\partial (T_P)_j / \partial x_j = -\partial \{ (\varepsilon_P)'_{ji} \, \partial \overline{P} / \partial x_i \} / \partial x_j \tag{4.30}$$

For a cubical volume, if only the turbulence transport contribution to the rate of change of $\overline{P}$ is considered, then:

$$\frac{\partial \overline{P}}{\partial t} = \frac{\partial}{\partial x_i} (T_P)_i = -\frac{1}{2} \left[\frac{\partial}{\partial x_i} \{ (\varepsilon_P)'_{ij} \frac{\partial \overline{P}}{\partial x_j} \} + \frac{\partial}{\partial x_j} \{ (\varepsilon_P)'_{ji} \frac{\partial \overline{P}}{\partial x_i} \} \right] \tag{4.31}$$

If the turbulence is homogeneous, then:

$$\frac{\partial \overline{P}}{\partial t} = -(\varepsilon_P)_{ij} \frac{\partial^2 \overline{P}}{\partial x_i x_j} \tag{4.32}$$

where $(\varepsilon_P)_{ij} = 1/2[(\varepsilon_P)'_{ij} + (\varepsilon_P)'_{ji}]$ and is symmetric in i and j. Equation (4.32) is Fick's second law of diffusion and reduces to the heat conductivity equation if $(\varepsilon_P)_{ij} = K$ (constant) where K is the thermal conductivity.[61]

A connection may be made between the mixing-length theory just described and Taylor's theory of fluid particle diffusion.[69,70] Consider a control plane perpendicular to the x_2-direction at x_2. If the fluid particles are assumed to travel in this direction while

transporting with them the property P, the transport of this property through the control plane is:

$$\overline{v_2 p(t)} = T^{-1} \int_0^T dt_0 \; p(t_0,t) v_2(t_0) \tag{4.33}$$

where t_0 is the instant the particle passes the plane at x_2, t is the diffusion time, and v_2 is the Lagrangian turbulent particle velocity in the x_2-direction. From the mixing-length theory the property has been carried by a fluid particle a distance y_2 to the plane at x_2. If $\overline{P}$ is assumed to vary linearly with x_2 and any exchange of the fluid particle with the surroundings along its path is neglected, then:

$$p(t_0,t) = -y_2(t_0,t) d\overline{P}/dx_2 \tag{4.34}$$

If $v_2(t_0) = dy_2(t_0,t)/dt$ then:

$$\overline{v_2 p} = -d\overline{P}/dx_2 \; T^{-1} \int_0^T dt_0 \; y_2(t_0,t) dy_2(t_0,t)/dt = -d\overline{P}/dx_2 (1/2) d\overline{y_2^2(t)}/dt \tag{4.35}$$

If by definition: $\overline{v_2 p} = -\varepsilon_p d\overline{P}/dx_2$, it is evident that the fluid particle eddy diffusivity $\varepsilon_p(t) = \varepsilon(t) = 1/2 \; d\overline{y_2^2(t)}/dt = \overline{y_2(t) v_2(t)}$. Use of equation (4.17) yields:

$$(\varepsilon_p)_{t=\infty} = \varepsilon = \overline{v_2^2} \int_0^\infty dt \; R_L(t) \tag{4.36}$$

For homogeneous turbulence without shear, experimental evidence indicates that the probability density distribution of y_2 is Gaussian for all diffusion times. Aside from a slightly negative skewness the axial concentration probability distribution of a round free methane jet was found experimentally to be approximately Gaussian.[71] This approximation may be assumed to apply to regions fairly close to the axis of the turbulent plume generated by the plasma igniter since it is a similar phenomenon.[44]

Proceeding now with the reasoning of Hinze,[72] assume that at the time $t = t_0$ marked fluid particles are concentrated in the region $-a \leq x_2 \leq a$. Let $B(x_2,t)$ be the probability that a marked fluid particle is at the point x_2 at time t. Then $B(x_2,t)$ is identical with the marked fluid particle concentration and neglecting any molecular diffusion effects it also represents any scalar property transferred by the fluid particles at time t. At $t = t_0$, the initial condition is:

$B(x_2,t_0) = 1$ if $-a \leq x_2 \leq a$

$B(x_2,t_0) = 0$ outside this region

and for all times:

$$_{-\infty}\int^{\infty} dx_2\ B(x_2,t) = _{-\infty}\int^{\infty} dx_2\ B(x_2,t_0) = 2a$$

If $Q(y_2,t;t_0)$ is the probability that the fluid particle has travelled a distance y_2 during $t-t_0$, then:

$$B(x_2,t) = _{-\infty}\int^{\infty} dx_2' Q(x_2-x_2',t;t_0) B(x_2',t_0)$$

since $y_2(t-t_0) = x_2-x_2'$ and because the integral is contributed to only by marked fluid particles which were at $-a \leq x_2' \leq a$ at $t=t_0$. Assuming that $B(x_2,t)$ satisfies Fick's second law then:

$$\partial B/\partial t = \epsilon_{22}(t)\partial^2 B/\partial x_2^2 \tag{4.37}$$

If instead of $B(x_2,t)$, the mean concentration $\bar{s}_0(x,y,z,t)$ at a point x,y,z and time t is considered, equation (4.37) becomes:

$$\partial \bar{s}_0(x,y,z,t)/\partial t = \epsilon(t)\nabla^2 \bar{s}_0(x,y,z,t) \tag{4.38}$$

For large dispersion times (i.e. $t >> L_t$), the eddy diffusivity becomes independent of the dispersion time and $\epsilon(t) \to \epsilon$. For this situation:

$$\overline{y^2} = 2\epsilon t \quad \text{or} \quad \overline{y^2} \to 2\nu^* t \tag{4.39}$$

where $\nu^* = \overline{v^2} L_t$ is defined as the turbulent viscosity.[73]

Contributions from molecular diffusion have thus far been neglected in this discourse. This phenomenon obeys Fick's second law with the exception that the eddy diffusivity for the case of turbulence is replaced by the molecular diffusion coefficient D.[73] The coefficient D is related to the kinematic viscosity ν by the relation $D = c\nu$ where c is a numerical coefficient. Usually the simplification $D \doteq \nu$ is used. The molecular diffusion variance $\overline{y^2}_{mol}$ is $\overline{y^2}_{mol} = 2Dt$ where t is the dispersion time.[73]

Comparing the molecular and turbulent diffusion effects, consider an instantaneous point source in a turbulent flow. If $\overline{y^2}_{tot}$ is the variance of the dispersing cloud produced by the flow and molecular agitation and assuming no correlation exists between the two processes, then:

$$\overline{y^2}_{tot} = \overline{y^2}_{turb} + \overline{y^2}_{mol} \tag{4.40}$$

While $\overline{y^2_{mol}}$ is an explicit function of t, $\overline{y^2_{turb}}$ depends on t according to (4.12). For dispersion times very small in comparison to the Lagrangian scale of turbulence (but large compared to molecular magnitudes), $\overline{y^2_{turb}} \simeq \overline{v}^2 t^2$ as stated previously in equation (4.13). Also $\overline{y^2_{mol}} > \overline{y^2_{turb}}$ if $t < 2D/\overline{v}^2$.[73]

Applying the effects of both turbulence and molecular agitation to the definition of the eddy diffusion coefficient ε, then $\varepsilon = \nu^* + D$ or $\varepsilon \rightarrow \nu^* + \nu$. Likewise for the turbulent convection of heat: $\varepsilon \rightarrow \nu^* + K$.

The major portion of the theoretical work on turbulence deals with the behaviour of wavenumber spectra and the transfer of turbulent energy from low wavenumbers (large wavelengths) to the high wavenumbers (small wavelengths) where it is dissipated.[74] A qualitative description from Hinze[75] of the three-dimensional energy spectrum in the various wavenumber ranges is given in Figure 4.1.

For a high ratio of the wavenumbers in the dissipating range to those in the energy containing range (minimally 10) the eddies in the dissipating range are isotropic and statistically independent of the energy-containing range, the latter which may be significantly anisotropic.[74] In this regime the dissipating range structure depends only on the energy-containing range (equal to the energy dissipation rate e) and on the wavenumber, viscosity, and density. The dissipating eddies are defined by typical length and velocity scales designated as the Kolmogoroff scales.[74] The latter are yielded by dimensional analysis and are the length scale $\eta = (\nu^3/e)^{1/4}$ and the velocity scale $v = (\nu e)^{1/4}$. The dissipating range begins at approximately $\mathbf{k} = 0.1/\eta$ and terminates near $\mathbf{k} = 1/\eta$ where $\mathbf{k}$ is the wavenumber.

For dissipating wavenumbers which are much greater than the energy-containing ones ($\mathbf{k}_d/\mathbf{k}_e$ is greater than or approximately equal to 100) the isotropy conditions and statistical independence from the energy-containing eddies would be satisfied for a wavenumber range below the dissipating range and the corresponding eddy structure would be viscosity independent.[74] This range is defined as the inertial subrange and its spectrum is dependent only upon $\mathbf{k}$ and the transfer of energy across the wavenumber range (i.e. equal to e). By

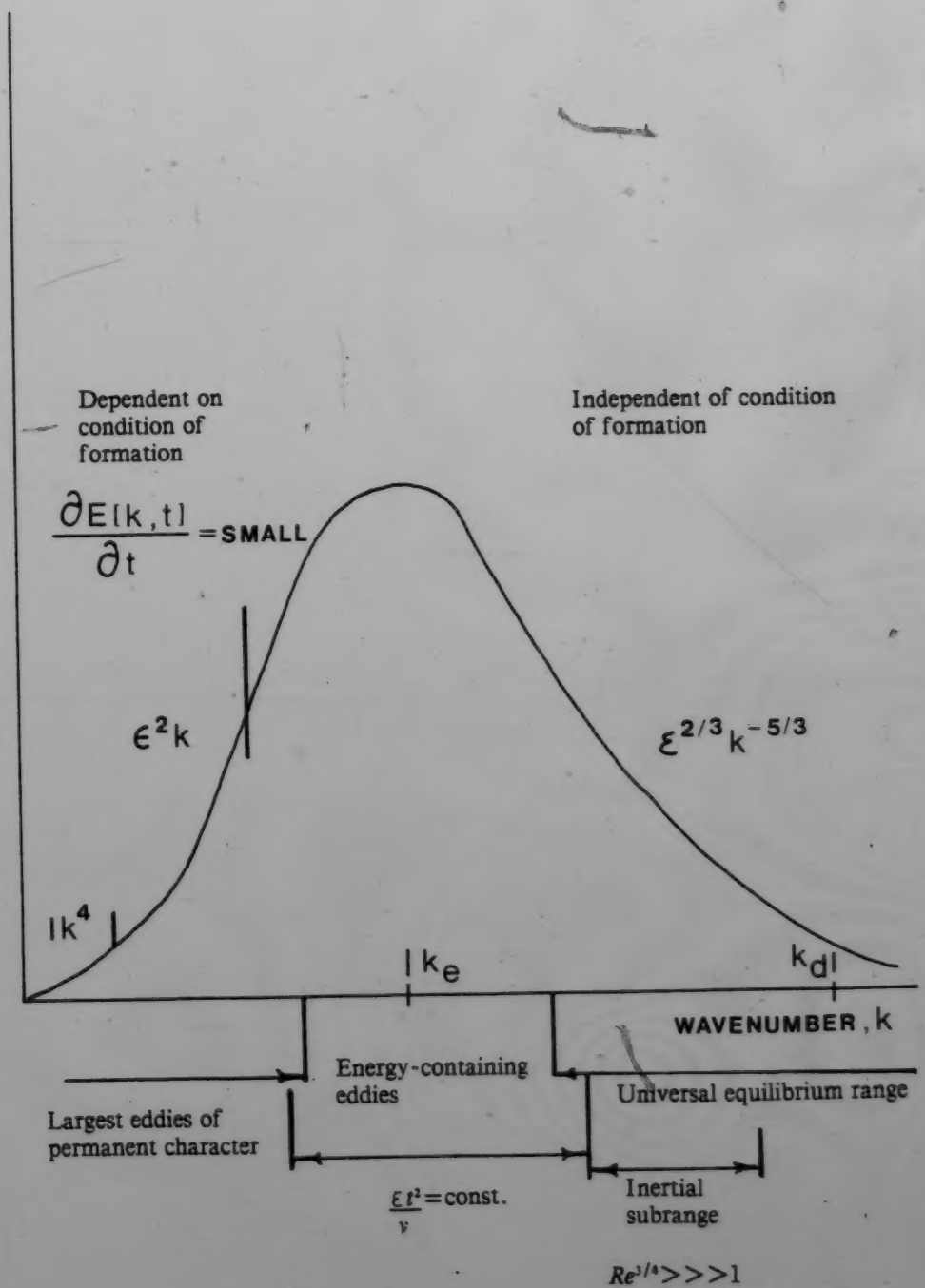

Figure 4.1 Variation Of $E(k,t)$ With Wavenumber k

dimensional analysis the one-dimensional spectral density $\phi(\mathbf{k}_1)$ and the wavenumber magnitude spectral density $E(\mathbf{k})$ for this subrange are:

$$E(\mathbf{k}) = \alpha e^{2/3}\mathbf{k}^{-5/3}$$
$$\phi(\mathbf{k}_1) = \mathbf{k}' e^{2/3}\mathbf{k}_1^{-5/3} \tag{4.41}$$

where α and $\mathbf{k}'$ are experimentally determined constants. For an isotropic dissipation range, the dissipation rate $e = 15\nu(\partial u/\partial x)^2$.[70] The length $\lambda = [\overline{u^2}/(\partial u/\partial x)^2]^{1/2}$ is designated as the turbulence microscale and is much greater than the length scale η of the dissipating eddies.

For the inertial subrange, when marker sols such as smoke particles are present in the flow field, molecular diffusion effects are negligible and hence $\varepsilon \to \nu^*$.[76] Since the ratio $\sigma = \nu/K \simeq 1$ for air, then for turbulent heat convection $\varepsilon \to \nu^*$ also.[77] The particle diffusivity D^* of marker sols in a suspending medium is generally much smaller than the kinematic viscosity ν of the medium. Hence the effective Schmidt number of the particles, $\nu/D^* >> 1$.

Beyond wavenumbers in the range of $(e/\nu^3)^{1/4}$ the eddies are rapidly dissipated by viscosity and particle diffusion remains insignificant until a second 'convection' subrange is attained where the spectral density varies as $\mathbf{k}^{-1}$. For wavenumbers in the region $(e/\nu D^{*2})^{1/4}$, particle diffusion begins to play a role in the dissipation of the marker concentration eddies and from this point there is a rapid fall of the spectral density. The experimental work of Becker *et al.*[76] was unable to attain the upper-wavenumber limit of the (-5/3)-power region of the spectrum and since this thesis work though different in objective, utilized a fundamentally similar experimental configuration it was assumed that particle diffusion effects could be neglected in the determination of the eddy diffusivity in the following pages. Furthermore Batt *et al.*[59] found that the fireball temperature spectra follow approximately a $(\mathbf{k})^{-5/3}$ falloff behaviour.

From the considerations of this section it can be deduced that regions close to the axis of fireballs (buoyant thermals) and plasma 'puffs' approximate a homogeneous turbulence velocity field and thus the transported properties may be assumed to follow a Gaussian probability distribution therein.

4.3 Smoke-Scattered Light Technique

4.3.1 System For The Determination Of The Enhanced Diffusion And Heat Conductivity Coefficients

The experimental set-up for studying the plasma jet induced turbulence is shown in Figure 4.2. The particles suspended in a vertically rising cylindrical smoke column functioned as scatterers of the horizontal beam of He-Ne laser light impinging upon the column. An eight milliwatt laser was used and was aligned in such a way that it was incident upon the coaxial igniter channel and also perpendicularly intersected the optical axis of the collecting lens.

Since the plasma 'puff' propagated a significant number of trials in directions which were not parallel to the igniter-laser axis, consequently rendering difficult the tracking of the decay process, a larger beam diameter than the one issuing from the laser (~ 1 mm at the $1/e^2$ points) was required to illuminate the centrally entrained smoke particles. To achieve this, a concave lens was interposed in the beam path, the effect of which was the illumination of a region much thicker than the spheroid-like structure evident at 1 ms in the photographs of Plate 4.1.

The plasma plug was mounted on a rack and pinion and was movable in the horizontal plane such that the distance between the plug end and smoke column was variable. Alignment of the smoke column was such that it simultaneously intersected both the laser beam and the optical axis of the collecting lens. The plasma plug assembly and smoke column were contained within a 25 cm diameter glass 'T' chamber in order that the column could be isolated from ambient air currents. The two horizontal ports of the chamber were sealed with clear plexiglass disks (i.e. one supported the 75 cm focal length collecting lens and the other provided access for photography and component adjustment). The top vertical port supported a small chimney enclosed exhaustion fan regulated by a Variac, the latter which provided a means of varying the vertical smoke flow rate.

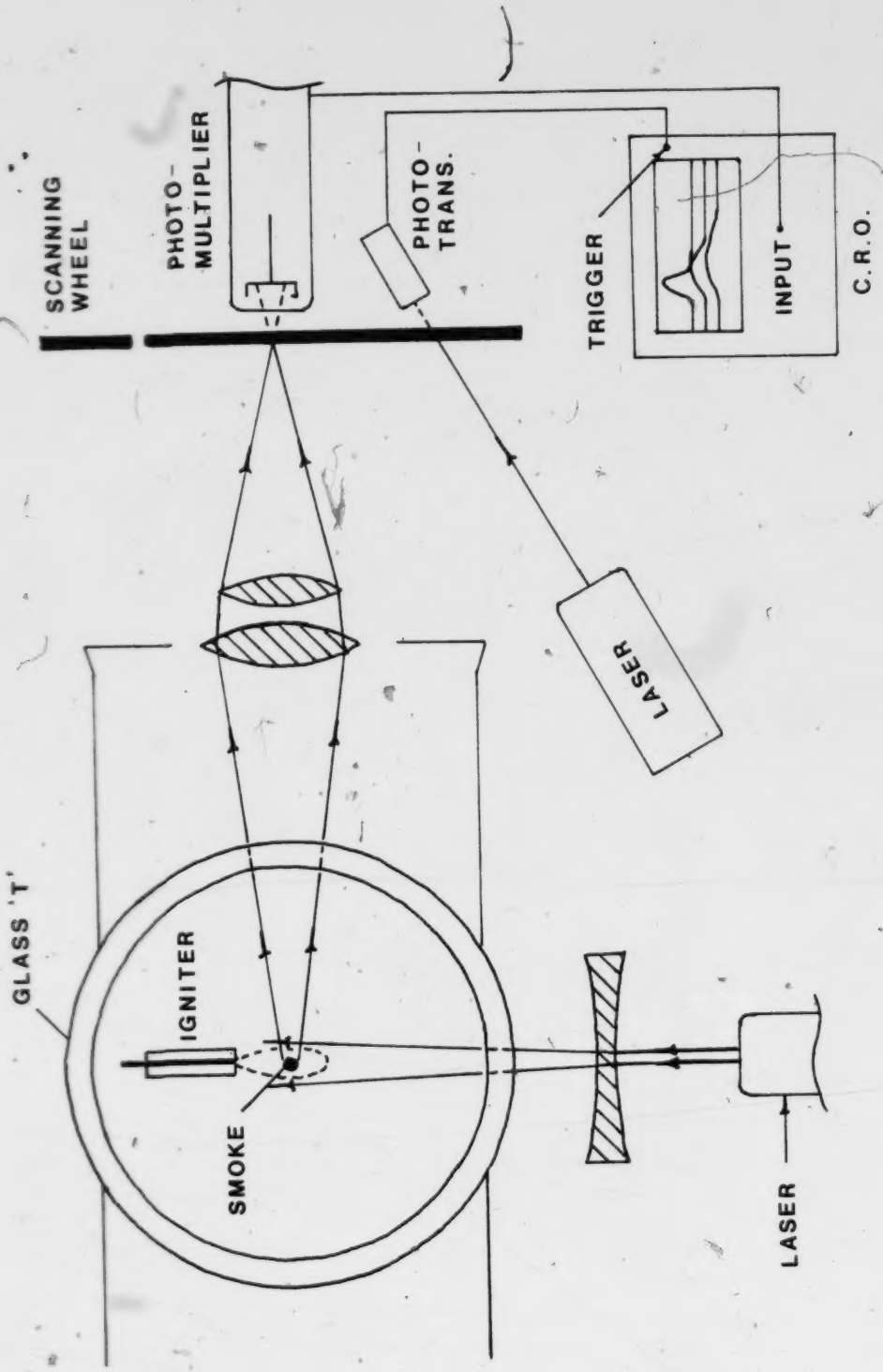

Figure 4.2 Smoke-Scattered Light Detection System

The smoke originated from an incense stick which was housed in a glass tube chimney. The top portion of the chimney tapered to a narrow aperture upon which nozzles of various diameters could be appended. This provided a rudimentary means of varying the diameter of the exiting smoke column. Only the top portion of the chimney projected into the centre of the glass 'T' chamber's base. This prevented any excessive smoke which flowed out of the chimney bottom from entering the 'T'.

The incandescent portion of the smoke column (i.e. the portion intersected by the laser beam) was projected onto a 30.5 cm diameter chopper wheel which was driven by a 62 W d.c. motor. The chopper wheel was provided with sixty .9 mm diameter holes along its circumference. Its maximum temporal resolution was approximately .3 msec at 3000 Hz. Behind the wheel there was a photomultiplier tube with an interference filter situated at the tube aperture to screen out all but the scattered laser light wavelength. A Fluke 412B High Voltage Power Supply provided the photomultiplier operating voltage in the one kilovolt negative bias range. The photomultiplier output was coupled to a Tektronix Type 556 Dual Beam Scope via a Type 1A7A High Gain Differential Amplifier and a 46 kΩ terminating resistor. The oscilloscope was housed in an earthed metal box to shield it from noise generated by the plasma plug power supply. The latter was also shielded and earthed as were all the electrical components of the system.

A .95 mW He-Ne laser was aligned such that its beam travelled through the chopper wheel holes periodically and impinged upon an FPT100 phototransistor. The latter was connected to a pulse shaping circuit which provided a trigger signal to the oscilloscope and also a means of calibrating the wheel's rotation rate.

In order to differentiate in time between the successive pulses which resulted from the photomultiplier as the chopper wheel apertures exposed the smoke scattered light to it, a raster system was devised for the oscilloscope display. A diagram of the system is presented in Figure 4.3. The raster permitted the display of numerous scans across the dispersing smoke column during a single event. It is appropriate at this point to address the theoretical aspects of the

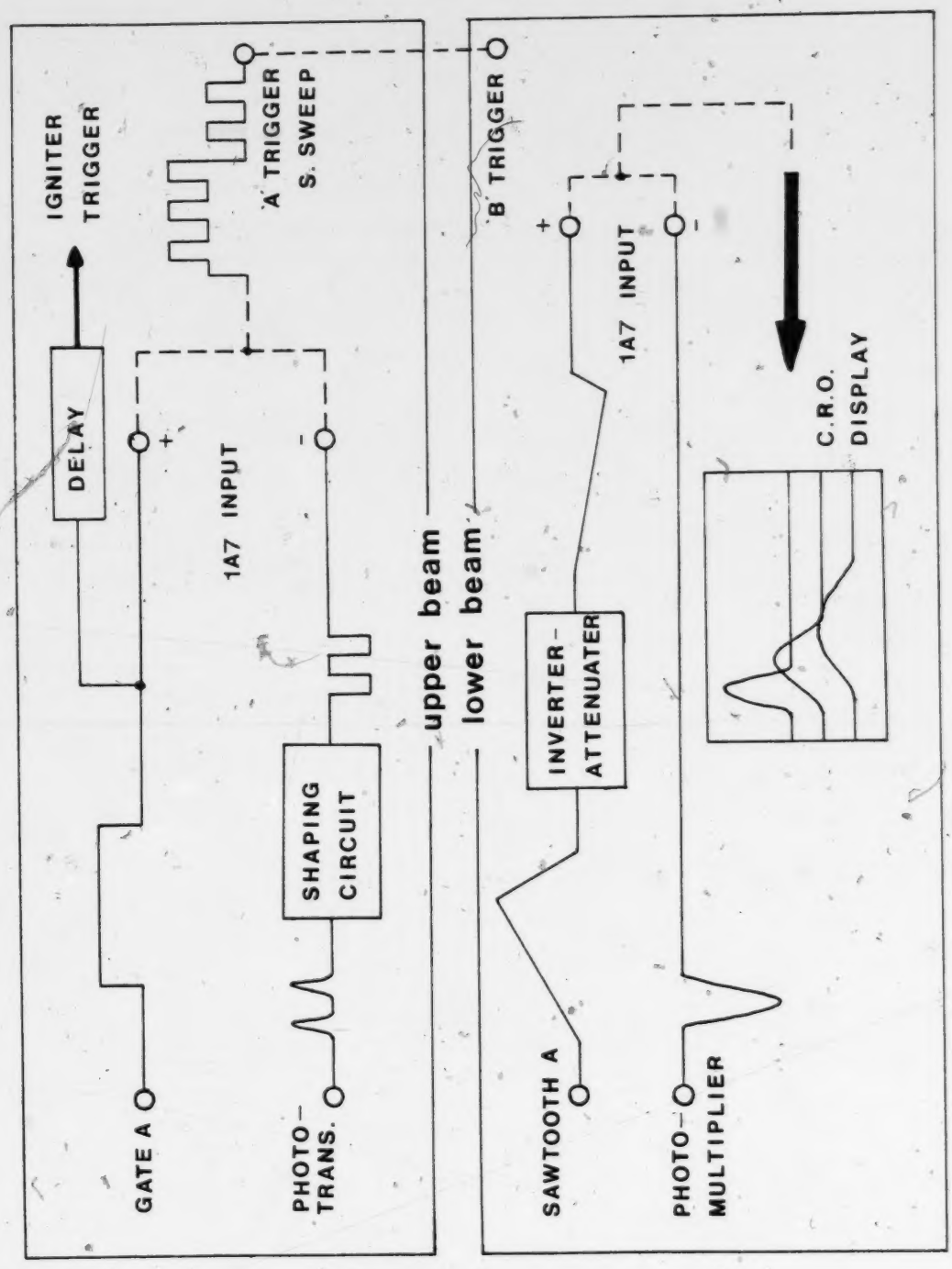

Figure 4.3 Oscilloscope Raster Display System

smoke column light scattering and the plasma jet induced dispersion of the smoke particles.

4.3.2 Theoretical Aspects Of The Smoke Column Expansion

As was mentioned in the preceding section, the smoke particles scatter the impinging laser light. The scattering intensity is proportional to the particle concentration and thus the latter property of the turbulent disturbance may be directly examined and quantified from the photomultiplier signal. The primary scattering is very weak and the smoke so dilute that secondary scattering may be considered to be negligible.[71]

Although its evaluation is very complex and beyond the scope of this work the response of the phototube to light scattered by particles inside an object control volume V is given by Becker *et al.*[76] as:

$$\bar{I}_s = S/V \int \bar{T}\, dV \tag{4.42}$$

where $\bar{I}_s$ is the mean phototube anode current to light scattered from the object control volume and $\bar{T}$ is the mean smoke concentration (i.e. $\bar{T}=\lim(V\to 0)\bar{N}/\bar{V}$). S is the overall system sensitivity and is given by: $S=1/4\pi D_p^2 V \omega_l \omega_s \int_0^\infty s\, \psi_{av} \tau_1 \tau_2 J_e\, d\lambda$, where D_p is the particle diameter, ω_l and ω_s are the solid angles of divergence of the incident and scattered beams, s is the overall radiant sensitivity of the phototube, ψ_{av} is the average scatter function given generally by Mie's equations, τ_1 is the spectral transmittivity of the projection optics, τ_2 is the spectral transmittivity of the viewing optics, J_e is the source intensity, and $d\lambda$ is the wavelength interval.

Continuing with the description of Becker *et al.*[76] if the mean marker concentration at a position x is required, then let x' be the distance along a line through x which follows the mean concentration gradient $\nabla\bar{T}$. If $\bar{T}$ is expanded about $x'=0$ at x in a Taylor series and if terms higher than second order are neglected, then:

$$\bar{T}(x') = \bar{T}(x) + x'\bar{T}'(x) + 1/2x'^2\bar{T}''(x) \tag{4.43}$$

For the diffusing plume the laser beam is directed parallel to $\nabla\bar{T}$ and thus (4.43) can be written[76]:

$$\bar{I}_s = L/S \int_{-L/2}^{L/2} \bar{T}(x')\,dx' \tag{4.44}$$

where L is the cylindrical control volume diameter. In addition $\bar{T}'' = \nabla^2\bar{T}$ and substituting (4.43) into (4.44) and integrating yields:

$$\bar{I}_s = S[\bar{T}(x) + 1/24L^2\nabla^2\bar{T}(x)] \tag{4.45}$$

If $L^2\nabla^2\bar{T}(x)$ is much less than $24\bar{T}(x)$ then $\bar{I}_s$ is a linear measure of $\bar{T}$. For small enough control volumes this condition is usually easily satisfied.[76]

Turning now to the diffusivity of the smoke particles D^* in still air, it is estimated from the Stokes-Einstein formula with the Cunningham correction[76]:

$$D^* = kT/3\pi\mu D_p[1 + Kl/D_p] \tag{4.46}$$

where k is Boltzmann's constant, T is the temperature (°K), K is the Cunningham constant (1.8 for air), l is the molecular mean free path of the gas, D_p is the Stokes particle diameter, and μ is the dynamic viscosity. For an oil smoke, Rosensweig *et al.*[78] found the Stokes diameter to be .5 μm. This value is within the range for tobacco and incense smoke particles (i.e. .01→1 μm).[79] Becker *et al.*[76] evaluated the diffusivity for the smoke particles in room temperature air to be $D^* = 4 \cdot 10^{-10}$ m^2 sec^{-1} which is comparable to diffusivities in liquids. Hence the particles can be expected to be excellent tracers for any disturbance propagating through the air.[80]

From elementary kinetic theory of transport processes the self diffusion of marked molecules in a gas is given by Fick's first law of diffusion: $J = -D\partial c/\partial x$ where c is the molecular concentration and D is the coefficient of self-diffusion: $D = 1/3\bar{v}l$.[81] The term $\bar{v}$ is the mean molecular velocity and l is the mean free path. The experimentally measured value of D for N_2 gas (similar to air) at S.T.P. is $1.85 \cdot 10^{-5}$ m^2 sec^{-1}.[82]

Returning now to the problem of the plasma 'puff' induced turbulent diffusion of the smoke particles, it is appropriate to consider solutions to the Fickian law, equation (4.38). Expressed in spherical polar coordinates it becomes[83]:

$$\frac{\partial n}{\partial t} = D\left(\frac{1}{r^2}\frac{\partial}{\partial r}\left(r^2\frac{\partial n}{\partial r}\right) + \frac{1}{r^2\sin\theta}\frac{\partial}{\partial\theta}\left(\sin\theta\frac{\partial n}{\partial\theta}\right) + \frac{1}{r^2\sin^2\theta}\frac{\partial^2 n}{\partial\Phi^2}\right) \tag{4.47}$$

where $n = \bar{s}_0(x,y,z,t)$, $D = \varepsilon(t)$. If only cases of radial diffusion are considered then (4.47)

becomes:

$$\frac{\partial n}{\partial t} = D\left(\frac{\partial^2 n}{\partial r^2} + \frac{2}{r}\frac{\partial n}{\partial r}\right) \tag{4.48}$$

Using $u = n(r)$, the foregoing relation becomes:

$$\partial u/\partial t = D\partial^2 u/\partial r^2 \tag{4.49}$$

Consider the initial volume of illuminated smoke to be a sphere of radius r_0 and suppose the total number of particles at $0 \leq r \leq r_0$ is N and zero at $r > r_0$. Then equation (4.49) is subject to the following boundary values and initial conditions:

$u = n_0 r$, when $t = 0$, $0 < r < r_0$

$u = 0$, when $t = 0$, $r > r_0$

$u = 0$, when $r = 0$

Then the solution to (4.49) is[34]:

$$n(r) = \frac{n_0}{2r(\pi Dt)^{1/2}} \int_0^{r_0} r'\{\exp(-(r-r')^2/4Dt) - \exp(-(r+r')^2/4Dt)\}dr' \tag{4.50}$$

where n_0 is the initial concentration of smoke particles per unit volume. Equation (4.50) can be rewritten:

$$n(r) = \frac{n_0}{2r(\pi Dt)^{1/2}} \exp(-r^2/4Dt) \int_0^{r_0} r'\exp(-r'^2/4Dt)[\exp(rr'/2Dt) - \exp(-rr'/2Dt)]dr' \tag{4.51}$$

Expansion of the integrand in powers of r' and assuming a small value of r_0 results in the approximate solution[34]:

$$n(r) = \frac{N}{8(\pi Dt)^{3/2}} \exp(-r^2/4Dt)\left[1 + \left(\frac{r^2}{Dt} - 6\right)\frac{r_0^2}{40Dt}\right] \tag{4.52}$$

Considering now the scattered light signal from the dispersing smoke particles, assume the chopper wheel aperture is scanned across the expanding spherical control volume. This is illustrated in Figure 4.4. The area of the aperture projected onto the spherical surface is δA. If p is the scattered light intensity per particle then the total intensity scattered from the volume element is given by:

$$I = 2p\,\delta A \int_0^{\infty} n(r)\,dx \tag{4.53}$$

Using relation (4.52) for $n(r)$, (4.53) becomes:

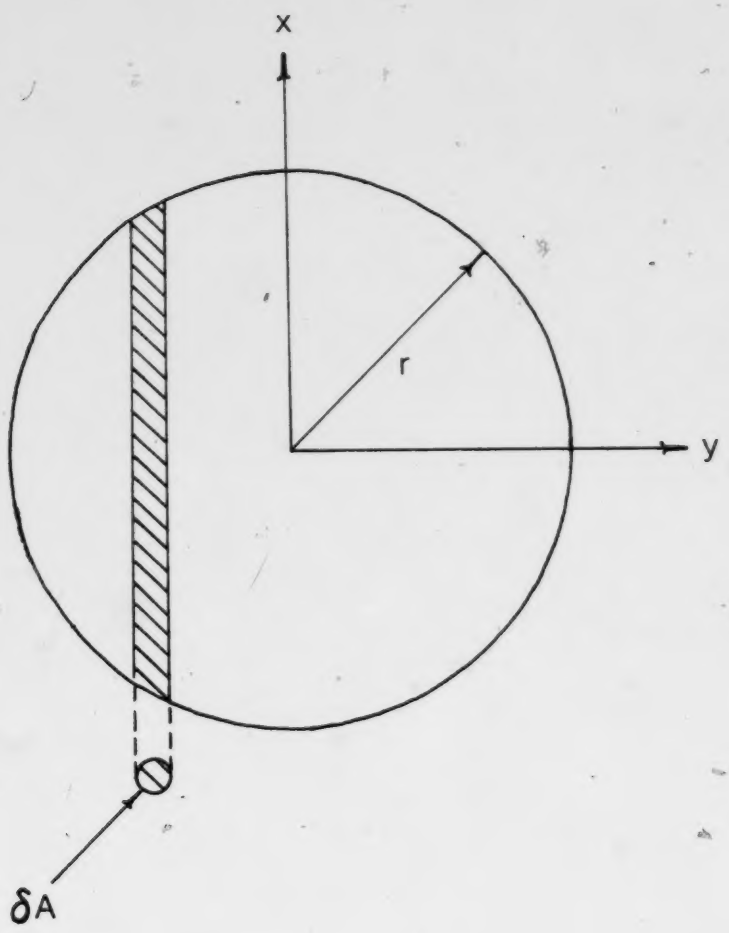

Figure 4.4 Scan Of Aperture Across Spherical Control Volume

$$I=2p\,\delta A\int_0^{\infty}\frac{N}{(8\pi Dt)^{3/2}}\exp(-r^2/4Dt)\left[1+\left(\frac{r^2}{Dt}-6\right)\frac{r_0^2}{40Dt}\right]dx \tag{4.54}$$

Using the relation $r^2=x^2+y^2$, the evaluation of I results in:

$$I=\frac{pN\,\delta A}{4\pi Dt}\exp(-y^2/4Dt)\left(1+\left(\frac{y^2}{Dt}-4\right)\frac{r_0^2}{40Dt}\right) \tag{4.55}$$

Integration of (4.55) with respect to time yields:

$$\int_0^t I\,dt'=2u_0^{-1}\int_0^{\infty}I\,dy=pN\,\delta A(4\pi Dt)^{-1}(u_0)^{-1}(4\pi Dt)^{1/2}(1-r_0^2/20Dt) \tag{4.56}$$

where $u_0=dy/dt$ is the scanning speed. At $y=0$ (i.e. along the diameter) in equation (4.55), I is maximum (I_m) and (4.56) may be written:

$$\int_0^t I\,dt'=I_m(u_0)^{-1}(4\pi Dt)^{1/2} \tag{4.57}$$

where $I_m=pN\,\delta A(4\pi Dt)^{-1}(1-r_0^2/20Dt)$. During times t for which $r_0^2/20Dt$ is much less than 1:

$$I_m=pN\,\delta A/4\pi Dt \tag{4.58}$$

From the still photographs of the dispersion process described in the next section it was apparent that once the turbulent plasma puff front reached the smoke column, a section of the latter developed a concavity in the direction of entrainment and then separated from the remaining column. Immediately upon detachment the smoke segment seemed to develop into a roughly spheroidal configuration. Furthermore, simultaneous Schlieren and still photographs which were taken of the dispersion process at later times strongly supported qualitatively the concept of a spherical expansion. The entire process just described occurred within an extremely short time after the puff front impinged upon the column.

Taking $t=t_0$ to be the time at which the smoke column segment perturbation due to the plasma puff commenced, the scattered light intensity at each instantaneous position across the segment scanned by a chopper wheel aperture is given by:

$$I_0=2pn_0x\,\delta A \tag{4.59}$$

where the x-direction is that of Figure 4.4. The area under the intensity curve is given by:

$$\int I_0\,dt=u_0^{-1}\int_{-r_0}^{r_0}I_0\,dy \tag{4.60}$$

Converting to polar coordinates, equation (4.60) becomes:

$$\int I_0\,dt=-2pnr_0^2\,\delta A/u_0\int_{-\pi/2}^{\pi/2}\sin^2\theta\,d\theta \tag{4.61}$$

Therefore,

$$\left| \int I_0 \, dt \right| = \pi r_0^3 p n_0 \, \delta A / u_0 \tag{4.62}$$

From the qualitative description of the diffusion process at early times given in the preceding paragraphs it is evident that the determination of the initial radius of the expanding spheroidal structure with any reasonable degree of precision posed an extremely difficult problem. This was overcome by extrapolating equation (4.58) (independent of r_0) to $t=t_0$ where it would represent the maximum scattered light intensity of the turbulent diffusion from an equivalent point source.[61] As is described in the next section this extrapolation was used to facilitate the determination of the diffusion constant D from the experimental data.

Continuing with this reasoning if δA is eliminated between equations (4.62) and (4.58) at $t=t_0$ then:

$$I_m = u_0 N \left| \int I_0 \, dt \right| / (4\pi^2 r_0^2 n_0 D t_0) \tag{4.63}$$

But $N=4/3\pi r_0^3 n_0$. Therefore,

$$I_m = r_0 u_0 \left| \int I_0 \, dt \right| / (3\pi D t_0) \tag{4.64}$$

Rearranging (4.64) and multiplying the numerator and denominator by I_0' where I_0' is the maximum value of I_0 (i.e. along the diameter) results in:

$$D = r_0 u_0 \left(\left| \int I_0 \, dt \right| / I_0' \right) / (3\pi t_0 (I_m / I_0')) \tag{4.65}$$

A further simplification can be applied to equation (4.65). Evidently from the relation (4.59), $I_0' = 2 r_0 p n_0 \, \delta A$ and accordingly equation (4.62) may be expressed as:

$\left| \int I_0 \, dt \right| = \pi r_0 I_0' / 2 u_0$. Substituting the latter relation into (4.65) results in:

$$D = r_0^2 / 6 t_0 \tag{4.66}$$

since $(I_m / I_0') = 1$ at $t=t_0$.

The initial period of turbulent decay is predominantly due to the decay of the energy-containing eddies. This is caused by the energy drain from these eddies via inertial interactions towards the small eddies pertinent to the dissipation wavenumber range.[15] The length of this initial period is difficult to define since the transition to other periods occurs very gradually. During this initial period the energy decay law was found from grid-generated

turbulence measurements in a wind tunnel to be: $v'^2 = c\bar{U}x^{-1}$ where $\bar{U}$ is the mean flow velocity and c is a constant.[46]

For relatively long dispersion time periods (within the initial period of decay) equation (4.17) yields for the eddy diffusivity $\epsilon = D = v'^2 L_t$ where the first subscript has been omitted to reflect the assumed isotropy of the dispersion. Therefore from the decay law for v'^2 and assuming a constant value of L for these times, the eddy diffusivity may be written as:

$$D \propto \bar{U}x^{-1} \tag{4.67}$$

4.3.3 Experimental Determination Of The Eddy Diffusivity

Before the experiments were performed it was necessary to determine the optimum vertical smoke column velocity for maximum entrainment of the smoke particles by the turbulent puff to occur. It was required that this velocity be much less than the horizontal puff propagation speed (~ 5 m sec^{-1}). Using a Sony Video Motion Analyzer and a 30 frame/sec rotary shutter camera to observe the column motion it was found that to maintain a stable and uniform vertical flow the minimum velocity that could be attained was approximately .1 m sec^{-1}. This was found to be quite sufficient for the above requirement.

A preliminary experiment was performed in order to obtain visual verification that the fluid motion in the dispersing wave was sufficiently intense and turbulent for the distribution of heat to the wave front. The dissipating plume of smoke was photographed using a Calumet pictorial camera focussed in turn onto a Polaroid Land Camera. Type 47 (3000 A.S.A.) film was used and the illumination was provided by a remotely triggerable flash unit. A series of the resulting photographs for various delay times is presented in Plate 4.1. Evidently the smoke from a small segment of the column was rapidly (~ 10^{-3} msec) and fairly evenly distributed over a much larger volume. An enlargement of a particular one of these photographs taken on ultra-high speed film (20000 A.S.A.) is shown in Plate 4.2. It gives a clear picture of the convective flows which would be expected within a puff or buoyant thermal, together with the mixing action described at the beginning of this chapter. It is also apparent that in the region

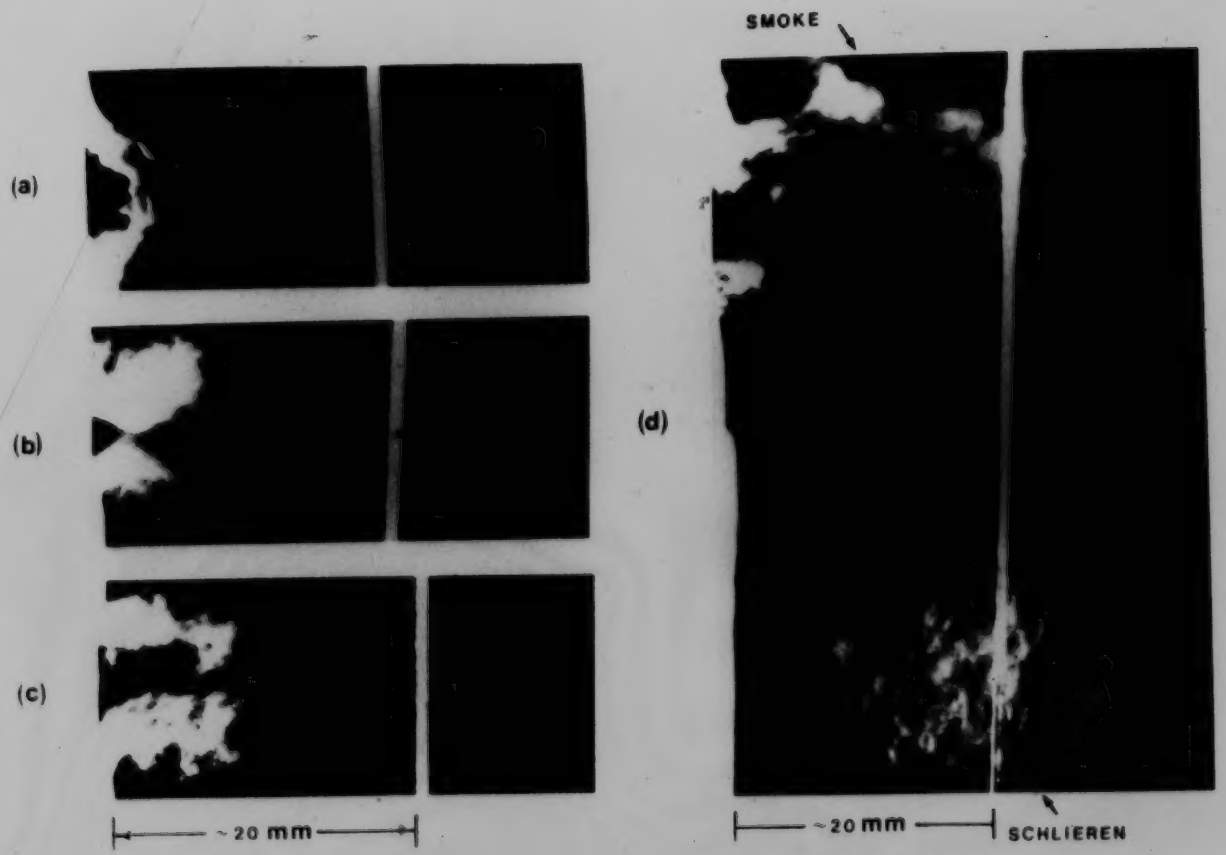

Plate 4.1. Photographs Of Smoke Dispersion At Various Delay Times. Photos (a), (b), and (c) taken at approximately 10^{-3} sec time intervals; (d): a combined smoke and Schlieren photograph.

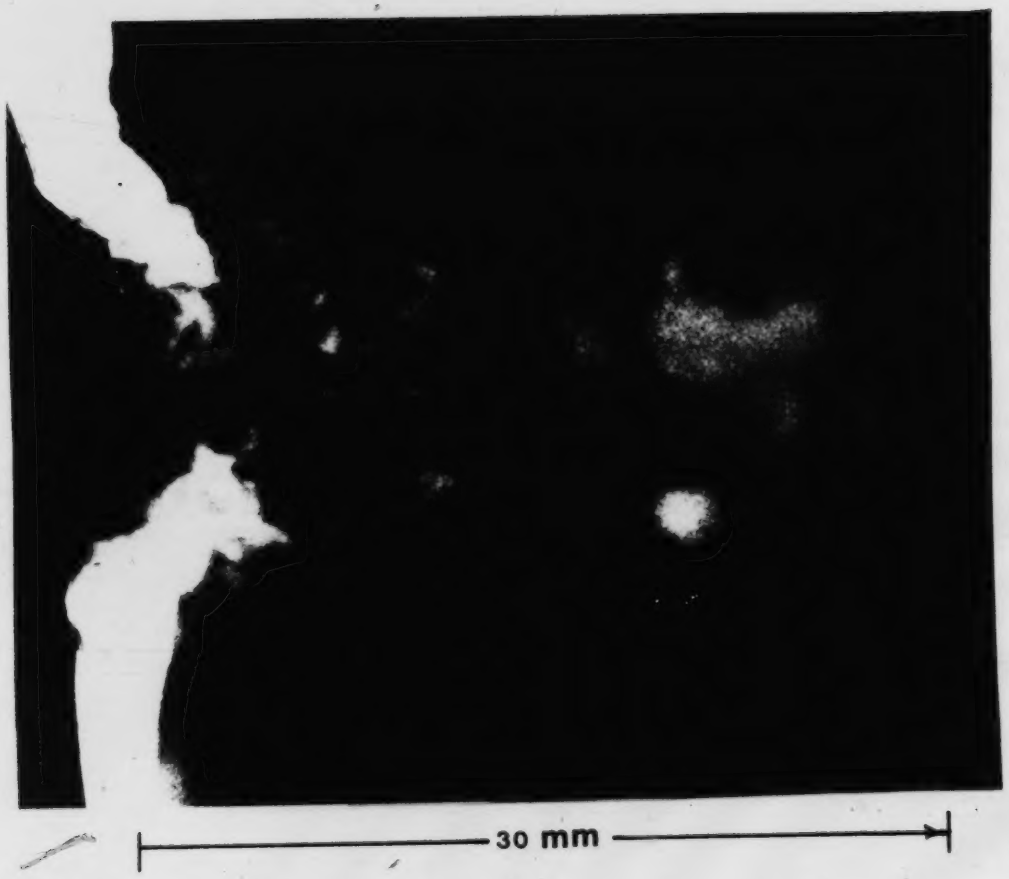

Plate 4.2 Photograph Of A Single Smoke Dispersion Event

near the igniter there is quite incomplete mixing and it seems likely that the 'hot pocket' hypothesis may be supported, particularly within about 30 mm from the plug. The work of Clements *et al.*[31] found chemical activity attributable to radicals within a similar distance.

Although the photographs provided a very useful qualitative description of the turbulent diffusion process inherent to the igniter, it was found to be particularly difficult, especially with the ultra-high speed film, to obtain a calibrated and regular (i.e. constant γ) relationship between the light intensity (smoke density) and print density using the methods of Hurter and Driffield.[17] Hence the main experimental work utilized the highly superior photomultiplier/raster system which is characterized by its ideal linear light intensity to voltage relationship.

For successive scans across an event involving the dispersing smoke particles the peak intensity profiles on the scope raster display decreased in amplitude with increasing time as is shown for example on the photograph of Plate 4.3. The photographs of the preceding experiment indicated occasional dispersions of the smoke plume in directions other than along the horizontal igniter axis. However, these occurrences were easily detected by the photomultiplier/raster system since the corresponding scattered light intensity traces were of markedly lower amplitude than for dispersions along the igniter-laser beam axis and hence they were not used in the data analysis described in the following discourse.

In order to evaluate the variation of the turbulent diffusion coefficient for various distances downstream from the plug aperture and to observe whether it depended on the impressed igniter energy (capacitor voltage), luminosity scans from the oscilloscope were recorded on the Sony Video Motion Analyzer for several parameter values. A considerable degree of irreproducibility was evident among the collected traces but this was expected due to the above mentioned deviations in the puff propagation direction. Nevertheless it was possible to obtain at least ten scans representative of the first few milliseconds of the diffusion process at each parameter setting which were apparently suitable for further analysis. These were photographed from the Sony monitor screen and the peak amplitude of the scattered light curve

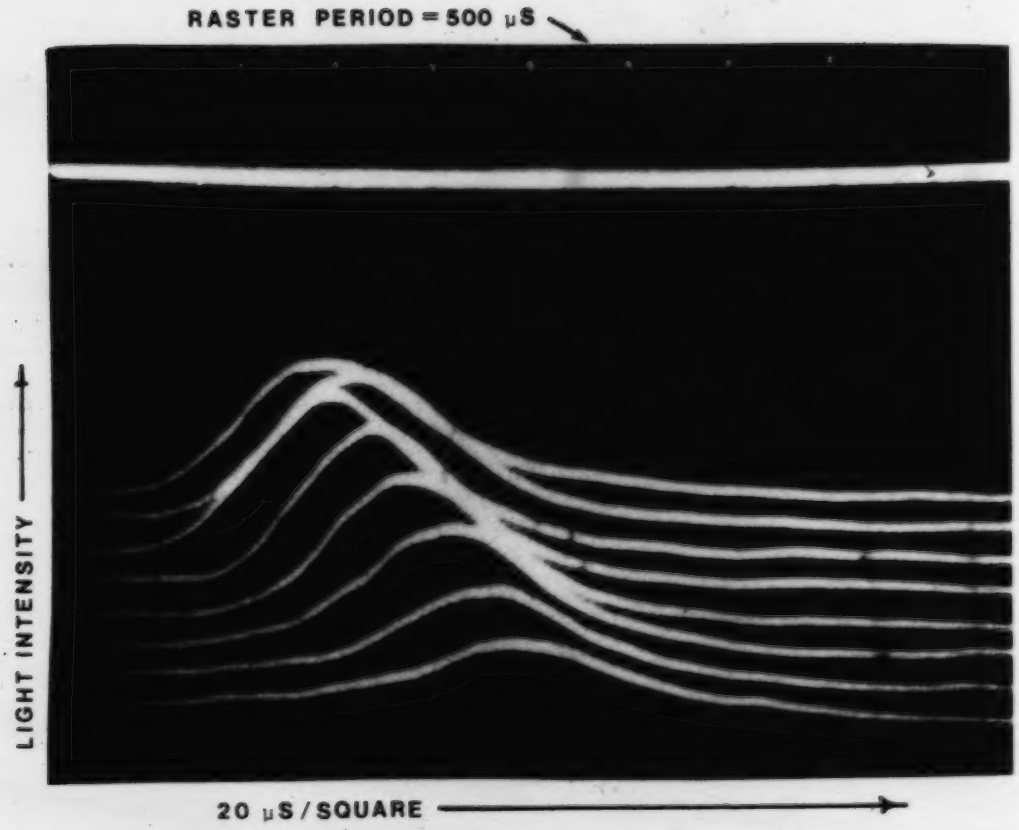

Plate 4.3 Photograph Of The Scope Raster Display For A Single Diffusion Event

at each successive scan time was calibrated. Each amplitude was then normalized with respect to the initial value (i.e. I/I_0) and averaged over the total number of runs at each parameter setting. These values were then plotted as a function of the normalized time period (t/period between traces) on a log-log graph. An example of one of these plots is shown in Figure 4.5. The normalized data were then replotted on log-log graphs with the abscissa coordinates shifted to the right until the plotted points exhibited the t^{-1} falloff described in Section 4.3.2 for the diffusion of an equivalent point source. A line of slope −1 was then drawn through the shifted points and extrapolated to $I/I_0=1$. These log-log plots are shown in Figures 4.6 and 4.7. The time t_0 corresponding to this value was then evaluated and substituted into relation (4.66) along with the initial column radius $r_0=1$ mm to obtain a value for the diffusion coefficient D. Table 4.1 presents the turbulent diffusion coefficients with the corresponding parameter settings.

4.3.4 Discussion Of The Eddy Diffusivity Results

The plotted experimental results were found to exhibit excellent agreement with the concept of a turbulent diffusion from a spherical source of finite initial radius as derived in Section 4.3.2. Figure 4.5 indicates that a definite time period elapses before the normalized scattered light intensity (concentration) decay becomes proportional to t^{-1}. This period can be deduced to be the time required for the $r_0^2/20Dt$ term in equations (4.56) and (4.57) to decay. In order to obtain a very rough approximation of the magnitude of this term when the above t^{-1} proportionality commences, assume r_0 is of the order of 1 mm and D from Table 1 (at 2.34 cm) is $4.5 \cdot 10^{-4}$ m^2 sec^{-1}. From Figure 4.5 it is evident that the normalized intensity decreases with an approximate slope of −1 beyond the range of 1.5 msec. Substitution of these values yields: $r_0^2/20Dt \simeq .07$ which is much less than unity. Although this value is very approximate especially with the aforementioned uncertainty in the initial spheroidal radius, it indicates that the turbulent diffusivity D determined from the extrapolation methods of the preceding section is within the correct order of magnitude.

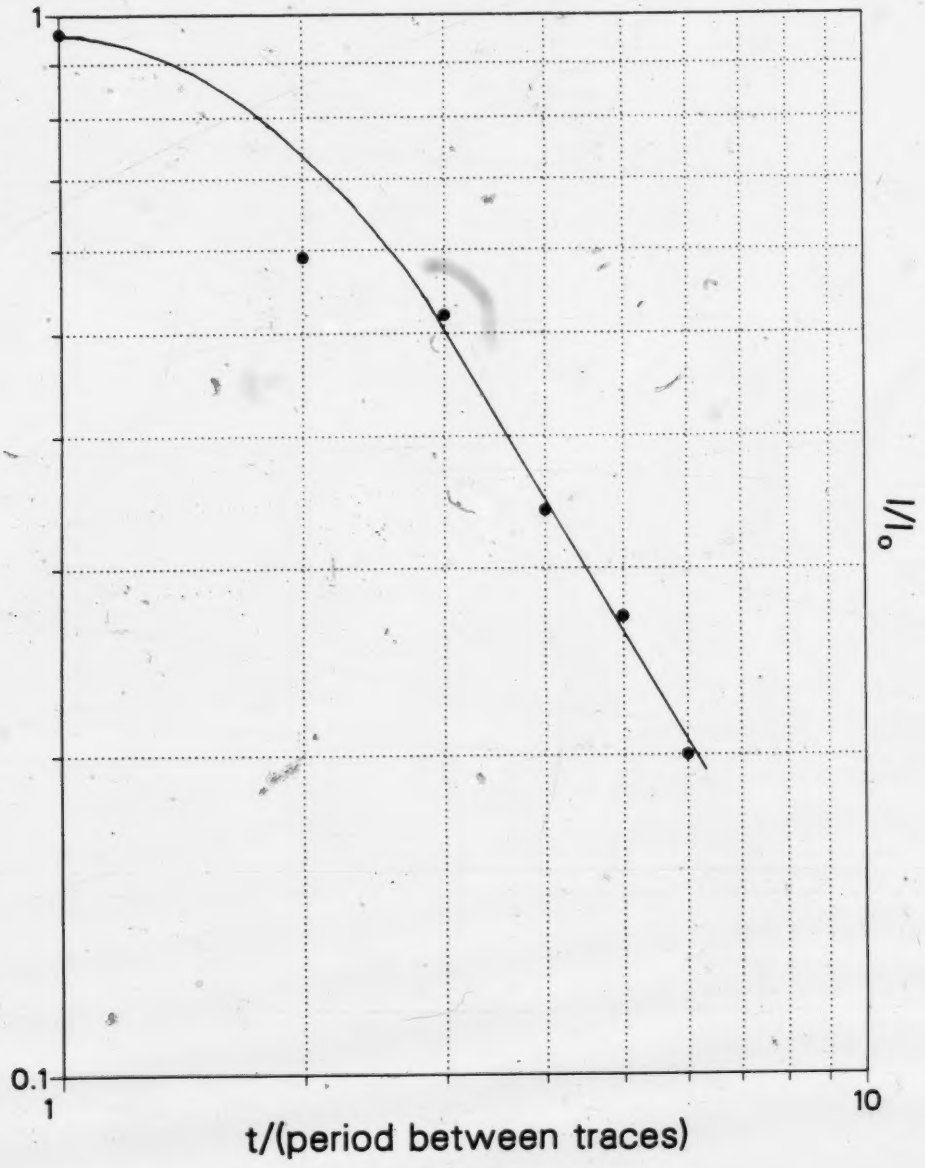

Figure 4.5 Log-Log Plot Of Normalized Scattered Light Intensity Decay With Scanning Time Period. Period between traces = .5 msec.

Distance (cm)	D (10^{-4} m^2 sec^{-1})
1.75	4.50
2.06	4.50
2.34	4.50
2.64	3.70
2.95	1.87
3.25	1.67
3.56	1.40
3.84	1.03
4.14	0.83
4.45	0.87

Voltages (V; d=1.91 cm)	D (10^{-4} m^2 sec^{-1})
250	3.70
350	3.66
450	3.47
550	3.97

Table 4.1 Turbulent Diffusion Coefficients

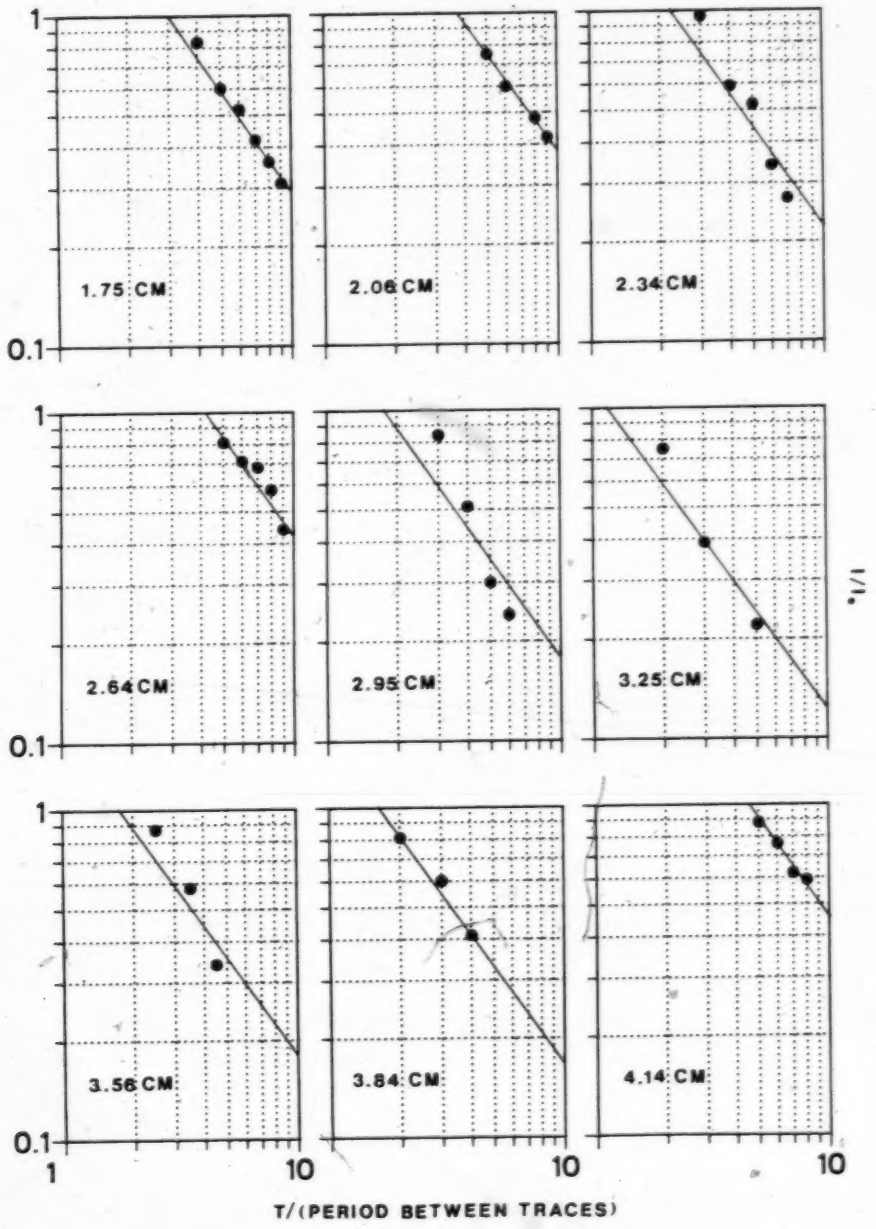

Figure 4.6 Log-Log Plots Of Shifted Data For Various Distances

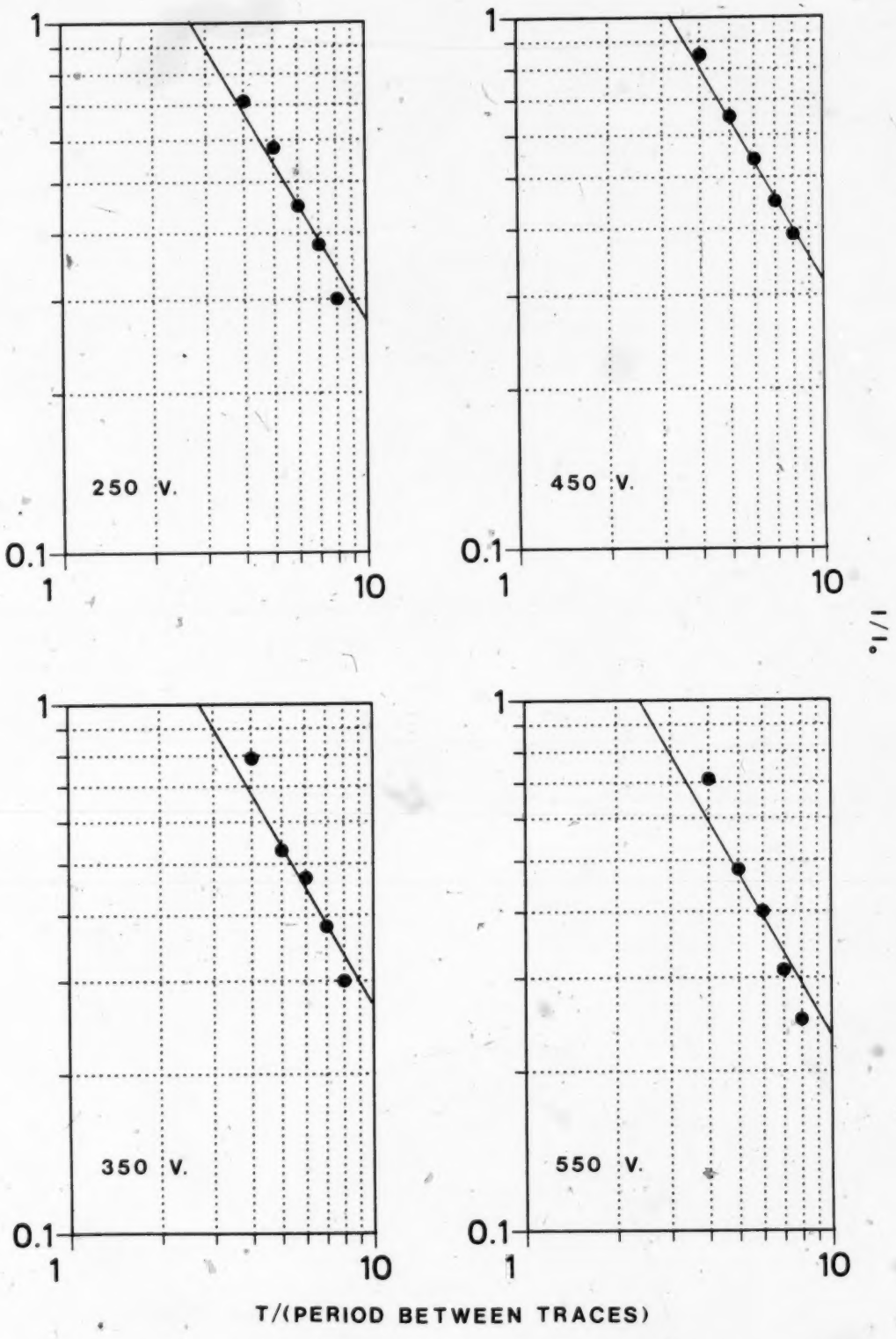

Figure 4.7 Log-Log Plots Of Shifted Data For Various Voltages

To determine whether other initial configurations were also consistent with the turbulent diffusion data, the dispersions corresponding to a plane and line source of smoke were also considered. Their expressions for the concentration falloff with time are identical[68]: $n=(n_0/4\pi Dt)\exp(-r^2/4Dt)$ but n_0 for the former source is the concentration/area while for the latter it is the concentration/length. Applying the procedure of Section 4.3.2 to this expression yields: $I \propto t^{-1/2}$. This falloff behaviour was not apparent for the experimental data and hence the viability of these theoretical models was negated.

The results of Table 1 indicate that the turbulent diffusion coefficient D decreases with increasing distances from the igniter aperture and is not dependent upon the initial igniter energy (capacitor voltage). The greatest values of D are approximately twenty-four times the still air molecular diffusivity (i.e. $1.85 \cdot 10^{-5}$ m^2 s^{-1} at S.T.P.). Towle and Sherwood[85] in their work on the turbulent air flow in the centre of ducts found similar values of D at a flow Reynolds number of 12200. They also found a marked tendency for D to decrease with increasing distances downstream of the duct inlet at low Reynolds numbers.

To determine what empirical relation existed between D and the downstream distance x, the two quantities were plotted on a log-log graph. This is presented in Figure 4.8. For $x \geq 2.3$ cm the equation of the best-fit line was found to be: $D \simeq 5.74 \cdot 10^{-9} x^{-3}$ m^2 sec^{-1}. The proportionality $D \propto x^{-3}$ implies from relation (4.67) that $U \propto x^{-2}$. From the work of Topham *et al.*[26] the relation $U \propto x^{-3}$ may be deduced for the turbulent puff cap convection velocity. The diffusion results obtained with the photomultiplier/raster system were representative of the region behind the cap. Hence the convective velocity for this region would be expected to be greater than that of the cap.

The diffusion measurements imply a turbulent enhancement of the diffusivity of at least one order of magnitude over the still air value. It is highly probable that this enhancement is of sufficient magnitude to account for the transport of the radical-rich 'hot pockets' from the plasma discharge to the relatively cold flame front region.

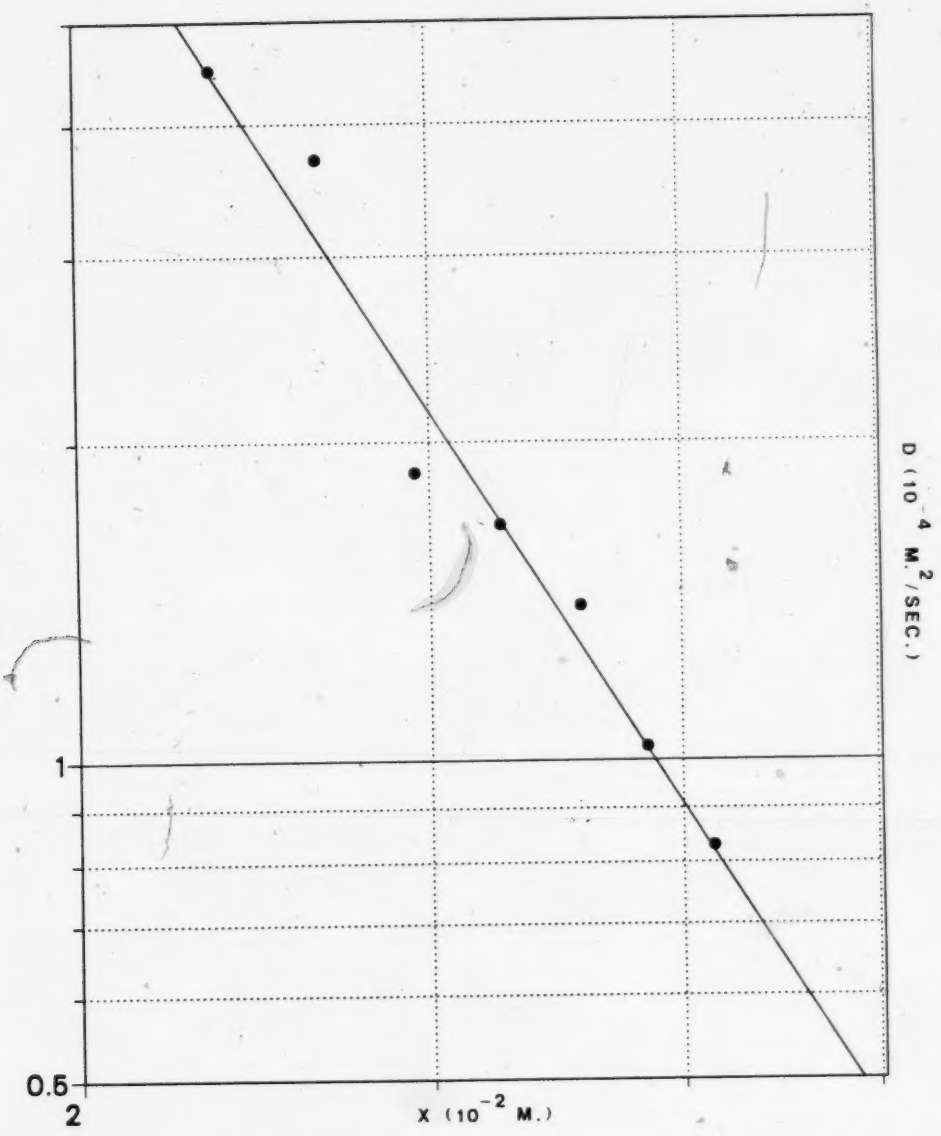

Figure 4.8 Log-Log Plot Of *D* Versus *x*

The results also support the work of Batt *et al.*[19] where the fireballs (buoyant thermals) were found to contain pockets of intense turbulent activity. The turbulent augmentation of the transport properties of the flow may also be responsible for the conventional combustion rate increase in the igniter vicinity. This is attributable particularly to the larger turbulent lengths which are effective in increasing the flame area. The extensive research of Cetegen *et al.*[21] concluded that a very substantial increase in the rate of combustion is due to this process. Additionally the flame speed is proportional to the square root of the heat conductivity and since the latter is enhanced in a turbulent flow, a corresponding increase in the speed would result.

4.4 Studies On The Relative Heat Wave And Smoke Plume Motions

It was necessary to determine the correlation between the relative motions of the heat wave and the diffusing smoke puff. To achieve this, simultaneous Schlieren and still photographs of the diffusion process were taken. From past investigations related to the plasma igniter, Schlieren photography proved to be a very useful diagnostic tool.

The optical system is illustrated in Figure 4.9 and a side view of the obstructing edge and camera is depicted in Figure 4.10. Flash photography of the smoke plume utilized the same system as that of Section 4.3.3 but differing in that the Calumet camera was tilted so that the plume image was formed on the lower half of the film. The Schlieren technique was not the conventional parallel beam, but rather involved one which was convergent (OO in Figure 4.10). The beam was reflected at a glancing angle by a small (10x3 mm) mirror which was positioned near the Schlieren focus. The mirror was also aligned with the camera lens axis and so the Schlieren image was formed in the upper half of the photographic film (within the field ÔÔ in Figure 4.10). The knife edge (E2) and mirror obstructed less than 10% of the camera lens aperture. Synchronization of the pulsed light source and flash unit was achieved using two photodiodes each directed at one of the sources and connected in turn to an oscilloscope.

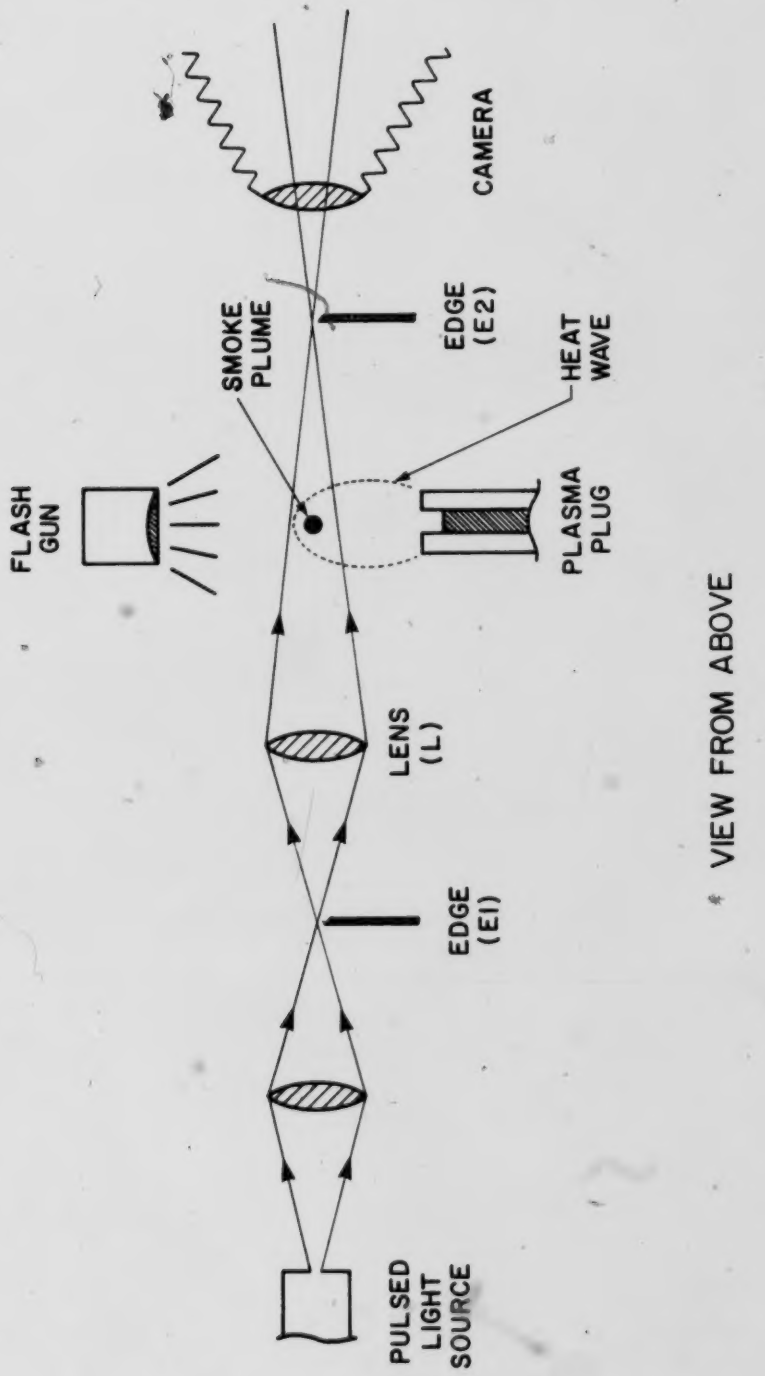

Figure 4.9 Optical Configuration For Obtaining Simultaneous Smoke And Schlieren Photographs

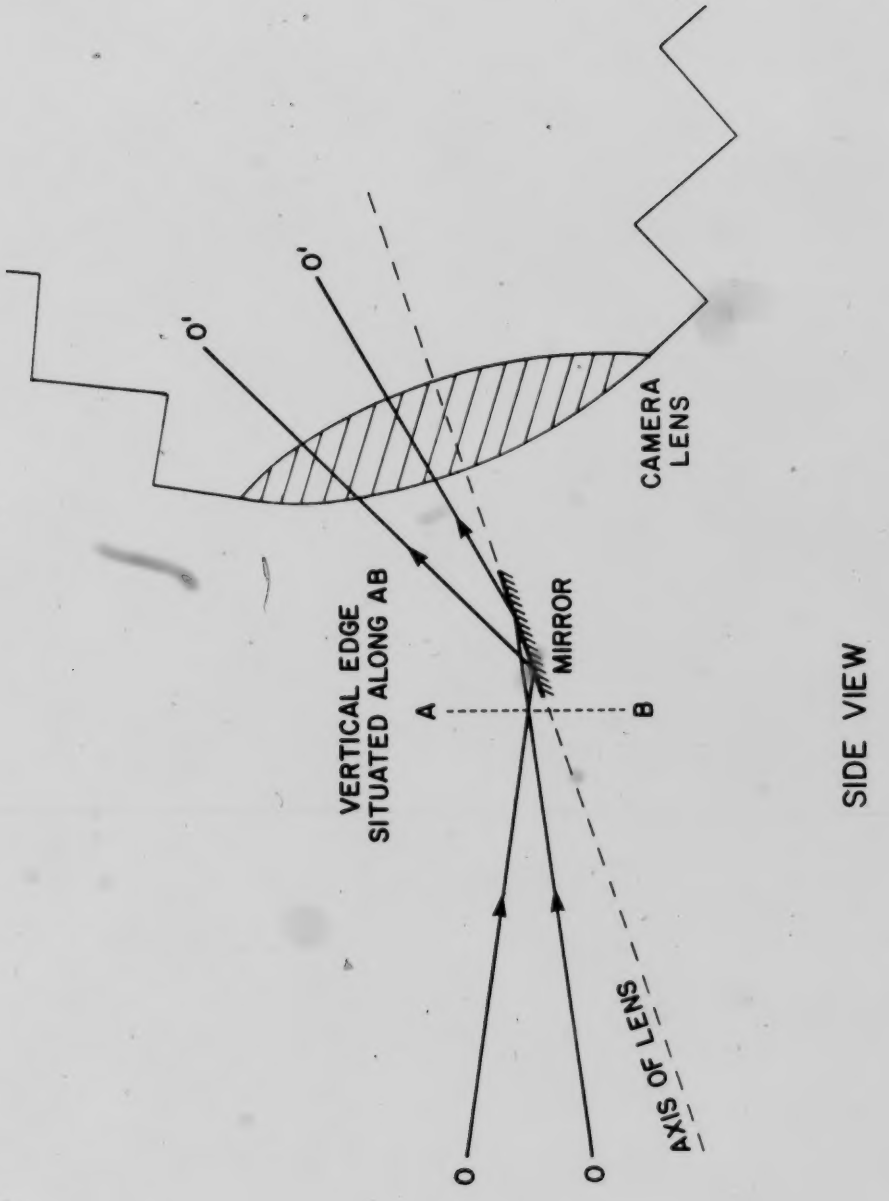

Figure 4.10 Schlieren/Mirror/Lens Configuration

With both light sources acting simultaneously two images were effectively provided at the same instant on the camera film. One was due to the very low angle forward 'scattering' (i.e. Schlieren) and the other was due to the large angle scattering of the flash. The relative intensity of the two light sources caused minimal interference between the two images. In order to align the two images for comparison of the relative progress of the heat wave and the diffusing plume, a very thin vertical wire was suspended close to the downstream side of the smoke column such that it was evident in both images on the photograph.

Several photographs were taken and in a minority of cases it appeared that the 'diffusion' wave had not progressed as far as the heat wave (Schlieren). However for the majority of the cases the two wave fronts were found to be coincident within the photographic resolution limits (1 mm). These observations could be considered to provide strong evidence that the diffusion mechanism within the heat wave is of sufficient intensity to distribute heat from the igniter cavity to the heat wave extremities. Instances where the wave fronts were non-coincident could be attributed to the experimental configuration and the aforementioned variable direction of the wave propagation. There was the possibility that the bulk of the expanding wave deviated from the igniter-laser beam axis and only enveloped the smoke column at a later time, where in turn a very misleading and delayed picture of the diffusing wave progress would have resulted. A combination Schlieren/diffusion photograph is illustrated in Plate 4.1.

4.5 Heat Conductivity Experiments

The experiments investigating the turbulent enhancement of the diffusion and heat conductivity did not deal with processes occurring at the wave front of the dispersive motion. It is expected that for the abrupt change in concentration or temperature associated with this region and more significantly at a flame front, the transport mechanism would be quite different.

For reliable transport measurements at the front (or cap) a reasonably flat working area of the surface is essential. However, from the photographs in Plates 4.1 and 4.2 there is no evidence of such an area at the front. Hence an experiment involving the measurement of the heat conductivity was performed using a flat solid surface near which similarly contoured areas of the temperature gradient could be expected to be generated. The previous work of Carleton *et al.*[23] had reported enhanced energy losses to a solid.

Figure 4.11 illustrates the experimental setup. The plasma plug generated heat wave impinged upon a flat rectangular metal surface situated 35 mm from the igniter cavity exit. An He-Ne laser beam was aligned parallel with the surface and focussed in this region to attain a very narrow beam.

For a refractive index gradient dn, an angular (Schlieren) deflection α would be produced in the beam of[89]:

$$\alpha = x\, dn/dy \tag{4.68}$$

where x is the length of the beam path through the gradient. Accordingly the photomultiplier output I would also be modified. Calibration of the output in terms of the lateral position of the edge E and hence α would permit the acquisition of a linear relationship between dT/dy and I:

$$I = \text{const.}\, dT/dy \tag{4.69}$$

The heat flux density due to conduction towards the surface will be[90]:

$$H = K\, dT/dy \tag{4.70}$$

where K is the thermal conductivity. Hence from equations (4.69) and (4.70) the relation results:

$$Q = {}_0\int^{\infty} H\, dt = \text{const.}\; K\, {}_0\int^{\infty} I\, dt \tag{4.71}$$

where Q is the total heat energy conducted across a unit area.

It was assumed in this experiment that the turbulent motion would not exist in the proximity of the wall and hence the measurement of the temperature gradient in this region would permit the determination of Q using the 'still air' value of K (i.e. $K = K_0$). The

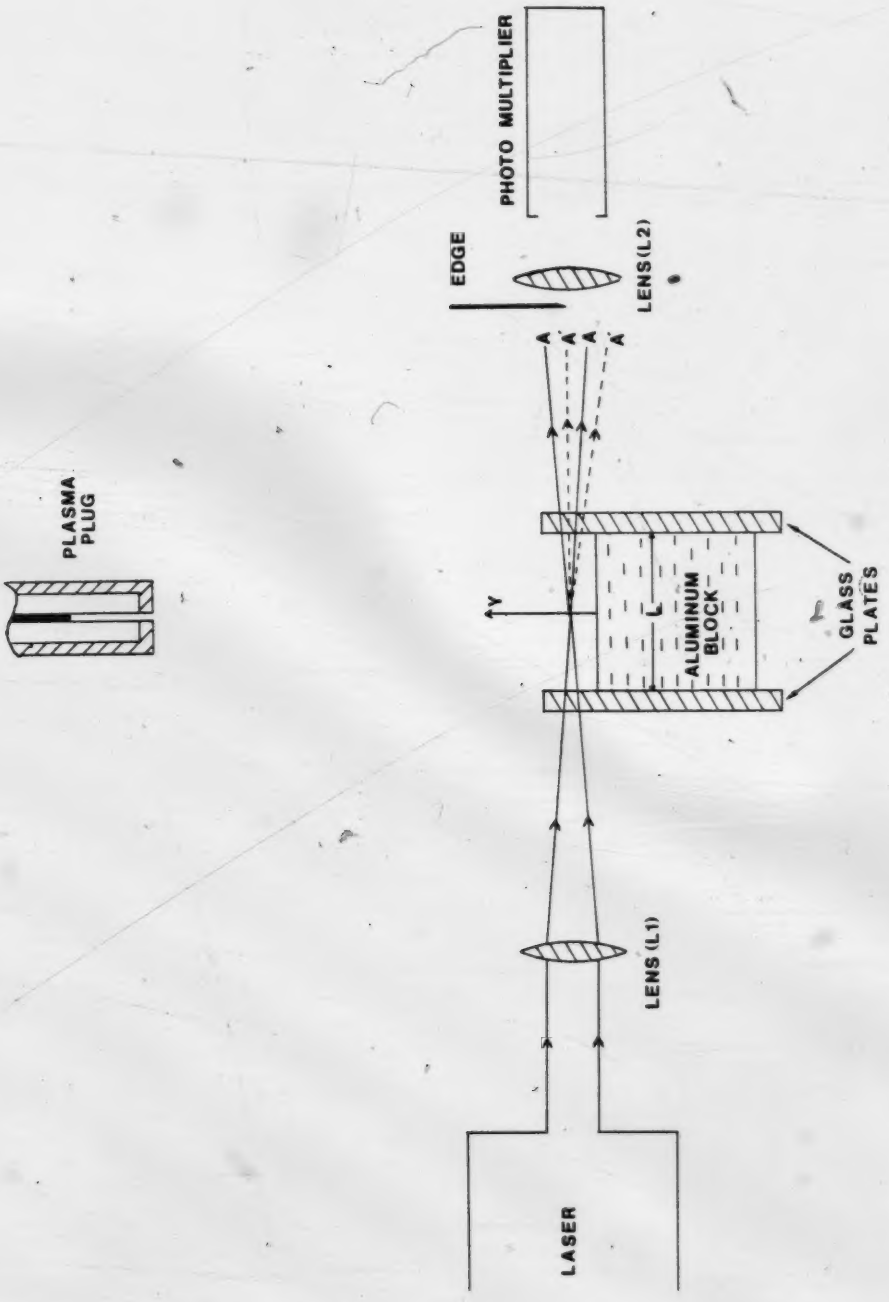

Figure 4.11 Schlieren Technique For Measuring Heat Flux Near A Wall

photomultiplier voltage oscillograms in conjunction with equation (4.71) were used to compute values of Q. This quantity is plotted in Figure 4.12 as a function of the distance y of the laser beam from the flat surface.

Each of these measurements involved a capacitive stored energy of .64 J dissipated by the igniter. From the efficiency measurements obtained in the work of Chapter 2 it was determined that less than 10% of the energy was available to the gas (i.e. $\leq$.06 J).

It is evident from the Schlieren photograph of Plate 4.1 that the total wave area is roughly equivalent to that of a sphere of 10 mm radius (i.e. ~ 10^3 mm^2). If the product of this area and the energy loss/area at the flat surface is taken, a total energy loss of approximately .15 J is obtained which, considering the degree of approximation involved in this calculation, corresponds satisfactorily to the above value of .06 J.

From Figure 4.12 there is a significant decline of the energy transport with small increases in y. If it is assumed that the effective heat conductivity retains its 'still air' value throughout the range of y, then from the same figure it is evident that the thin gas layer at the wave front ($y<.3$ mm) releases approximately 50% of the thermal energy stored in the wave. This is in contradiction to the homogenizing effect of the turbulence on the distribution of heat throughout the wave and hence the 50% energy efflux value from the outer 3% of the wave is highly unlikely. It is more reasonable to assume an effectively constant heat flux value over the wave front layer in the wall proximity and allow the conductivity to increase in value with y to ultimately attain the turbulence enhanced value expected from the diffusion measurements. Taking this constraint into account the resultant heat conductivity values can be normalized to the still air value at wall proximity, the latter value corresponding satisfactorily to the calorimetric data. The values of K/K_0 obtained in this manner are also shown in Figure 4.12.

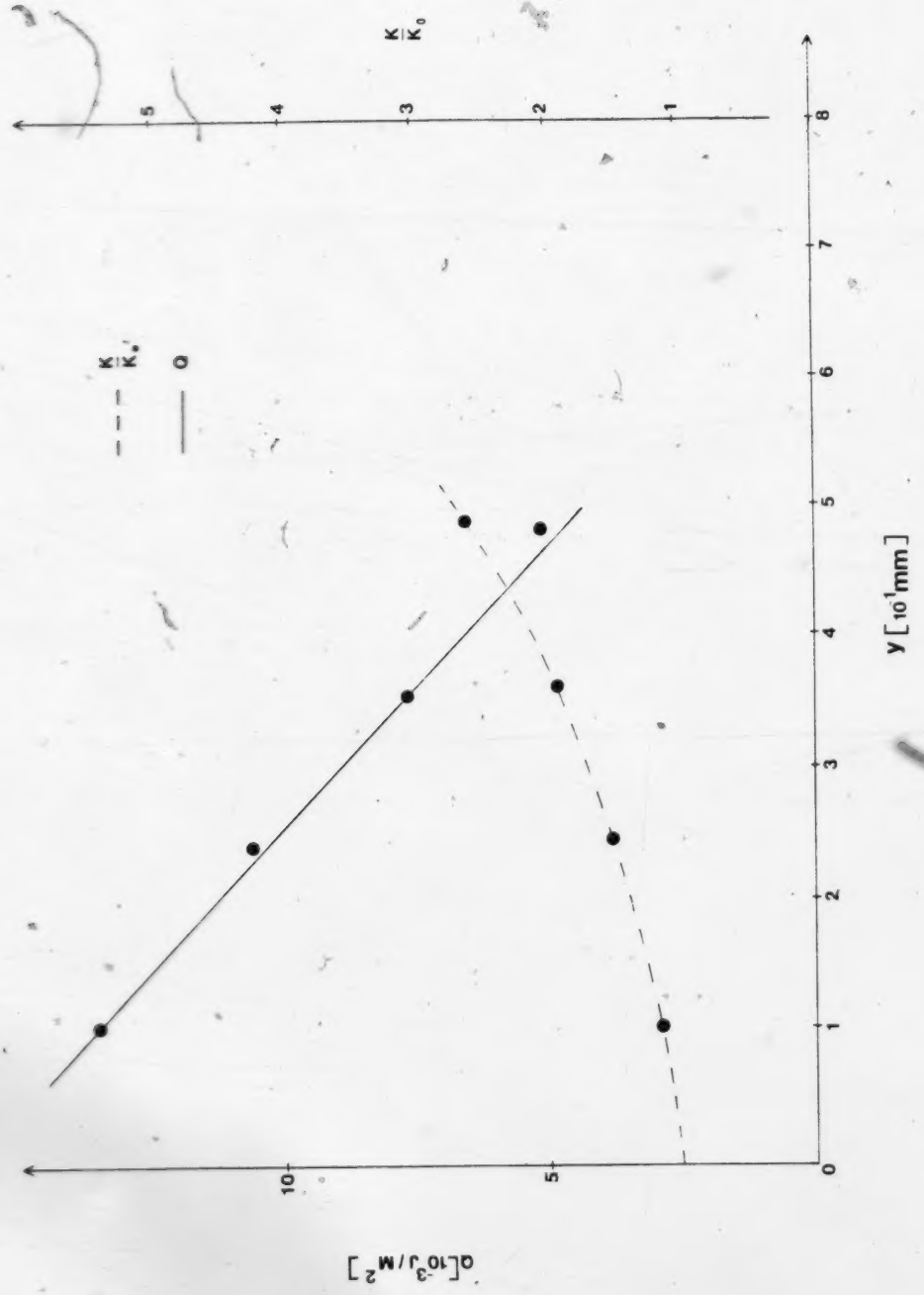

Figure 4.12 Graph Of Q And K/K_0 Versus Distance From Wall

4.6 Conclusions

In the work described in this chapter three estimates for the turbulent enhancement of the transport coefficients have been presented. The first, obtained from equation (4.1) and based on the heat distribution throughout the wave ($l \sim 50$ mm) yielded an enhancement of the order of 10^3. The second which was related to the initial dispersion of the smoke column ($l \sim 2$ mm) yielded a maximum augmentation of the order of 20. The third, related to the flame front dimensions ($l \sim .1$ mm) was found to be of the order of unity.

At one atmosphere the flame thickness of a propane-air flame is approximately .2 mm. Turbulence possessing characteristic lengths much greater than this dimension would most probably not be able to exert its full effects upon the flame front. The results of Figure 4.12 imply that the flame speed increase could be in the range of two if the restricted extent of the flame front has inhibiting properties similar to those of a solid surface. Hence the turbulent enhancement of the transport properties is dependent upon the scale length under study.

With regards to the experiments involving the determination of the diffusion coefficient, the results were found to be consistent with the concept of a turbulent diffusion from a spherical source. The diffusivity D was found to decrease with increasing downstream distances in a manner proportional to x^{-3} and this in turn implies convective velocities in the wake of the dispersing puff which are greater than that at the wave front. No variation was found between the initial igniter energies (capacitor voltages) and D. The magnitudes of the turbulent diffusion coefficients obtained indicate the existence of intense fine scale turbulence within the heat wave which may account for the transport and entrainment of the radical-rich 'hot pockets' from the plasma discharge to the relatively cold region of the flame front. The simultaneous still and Schlieren photographs of the dispersion process were found to provide further supportive evidence that the diffusion mechanism within the heat wave is of sufficient intensity to distribute heat between these regions.

The substantial modification of the flow, thermal and transport properties observed in the experiments of this chapter is very likely responsible for the combustion enhancement

evident in the igniter vicinity. Undoubtedly the conventional mechanism, the turbulent induced increase of flame area is also partially responsible for the augmentation. This conclusion was reached by Cetegen *et al.*[21]

5. Summary Of Conclusions

At the beginning of Chapter 1 it was stated that the purpose of the research described in the foregoing pages was to achieve a better understanding of the coaxial spark igniter's operating characteristics and its plasma ejection process. The work of each of Chapters 2, 3, and 4 made a unique contribution to the attainment of this goal.

In Chapter 2 the erosion results indicated that the use of low capacitances and high capacitor voltages produced minimal erosion rates. Low capacitor voltages resulted in improved efficiency. For all conditions tested the erosion rates were found to be prohibitively high for the continuous operation of igniters composed of standard materials. The expected automotive lifetimes for such an igniter were found to be less than ten hours. With regards to plasma heating, the plasma plug was found to be more efficient than either the standard gap or surface gap igniters. The measured thermal energies were in agreement with previous findings as was the energy loss distribution for the two successive stages involved in the transfer of energy.[1,23,24] It was deduced that the optimum igniter criteria to provide minimal component erosion and an effective transfer of thermal energy involved the use of low capacitances and high voltages. As indicated in Section 1.3, plasma jet igniters composed of the tested material would be viable for intermittent operation.

The work described in Chapter 3 found a quite satisfactory correspondence between the experimentally determined plasma ejection times and those deduced from a theory based on several simplifying assumptions. The experimental electric field measurements supported the validity of equation (3.10). The concept of the existence of definite plasma heating and ejection times was found to be reasonable from the transient electric field temporal behaviour and the abrupt termination of the jet luminosity respectively.

From theoretical considerations it was determined that for efficient igniter operation the plasma heating and expulsion processes would have to be of similar duration. This constraint supports the description of the plasma expansion for initial times based on the concept where the igniter cavity is considered to be analogous to the high-pressure section of a

conventional shock tube. For the later stages of the expulsion process a steady-state flow model would be more favourable.

Reasonable matching of the characteristic times of igniter operation in order to obtain optimum efficiency suggests the use of a high voltage trigger with a low voltage energy reservoir. From the results of Chapter 2 described above, this operating criterion would be detrimental to the igniter component erosion rates and hence to minimize the latter, the level of operating efficiency would have to be reduced.

The streak phography results of Chapter 3 were found to concur with those of Topham *et al.*[1] and the existence of striations propagating at highly supersonic velocities was supported by the laser spark/probe measurements. The measured values of the plasma jet front velocities were found to be consistent with those determined by Cavolowsky *et al.*[30] (i.e. 125 to 300 m sec^{-1}) at similar discharge energies. The findings of the latter also revealed the existence of the standing wave patterns observed in the streak photographs of the this work and that of Topham and associates for a similar igniter orifice diameter. Additionally Cavolowsky and co-workers suggested that the striations might represent the movement of individual pockets of high temperature plasma containing excited species. They proposed that the striations were related to the dispersion of radicals formed at initially high temperatures to considerable distances downstream where they subsequently promote chemical reaction.

The research described in Chapter 3, dealing with the plasma expansion within the igniter channel revealed that the luminous plasma did not reach the channel walls for the 1.6 mm and 3.6 mm diameters during the current discharge period. Perhaps the cavity plasma radius is constrained by a magnetic pinch effect past a certain critical radius. The composite streak photographs described in the same chapter revealed that the oscillatory motion observed in the internal channel model produced coincident striations in the external plasma jet. The exact mechanism responsible for this phenomenon has not been definitively determined.

From the studies of the plasma expulsion processes in Chapter 3 it was evident that the plasma streaming velocities behind the jet front were an order of magnitude greater than the

front velocity and hence very rapid mixing must occur at the front. It was assumed that this mixing process would be highly turbulent, consequently resulting in considerable turbulence being propagated downstream from the igniter. The investigations of Chapter 4 were inspired by this assumption and focussed on the turbulent enhancement of the flow transport properties.

In the latter chapter, the experiments performed to determine the diffusion coefficient yielded results which were consistent with the concept of a turbulent diffusion originating from a spherical source. The diffusivity D was found to vary with downstream distances as x^{-3}. This implies convective velocities in the wake of the dispersing puff which are greater than that at the wave front. The diffusivity was found to be unaffected by the initial igniter energies (capacitor voltages). The calculated magnitudes of D indicated the presence of intense fine scale turbulence within the heat wave which may account for the transport and entrainment of the radical-rich 'hot pockets' from the plasma discharge to the relatively cold flame front region. Additional supportive evidence of the intensity of the diffusion mechanism within the heat wave was provided by the simultaneous two dimensional and Schlieren photographs. The results of the heat conductivity experiments indicated that the turbulent enhancement of the transport properties depends upon the scale length under scrutiny.

The experiments of Chapter 4 indicated a substantial igniter induced modification of the flow, thermal, and transport properties and the combustion enhancement in the igniter vicinity is quite likely due to this. The turbulent induced increase of flame area would also be partially responsible.

The findings reported in Chapters 2 and 3 indicate that major difficulties are imposed upon igniter operation by the large currents used. They are greatly responsible for plug erosion and have little bearing on the energy carried by the plasma gases (i.e. less than 10% of the initial stored energy is available to the plasma jet). A means to partially remedy the latter situation would involve the design of supply circuits with smaller inherent losses. The igniter efficiency could be increased by the provision of liquid feeds or inorganic hydride cavity inserts

as mentioned at the end of Section 2.7. The transpiration cooling provided by the liquid fed plugs would also reduce the extent of the erosion process.

Several potential topics for further research were encountered in the course of the investigations. The streak photographs of Chapter 3 for the plasma expansion within the igniter channels of various diameters indicated that the luminous plasma did not reach the cavity walls during the arc discharge period for the larger diameters. No immediate justification for this is apparent and further studies are necessary. Another interesting phenomenon observed during the streak photography work was the oscillatory motion of the discharge within the igniter cavity. Further investigations of this would be justified. Other turbulence experiments using the smoke-scattered light technique could be performed to determine how enhancement of the downstream flow transport properties is affected by ambient pressure or gas composition.

References

1 Topham, D.R., Smy, P.R., and Clements, R.M., *Comb. Flame* **25**, 187-95(1975).

2 Bostick, W.H., "Plasma Motors," *Conference On Extremely High Temperatures*, (Wiley, New York, 1958).

3 Waterson, K., "Some Operating Characteristics Of Novel Ignition Devices For Hydrocarbon Air Mixtures"(D. Phil. Thesis, Oxford University, 1973).

4 Wyczalek, F.A., Frank, D.L., and Neuman, J.G., *SAE Paper* **750349**(1975).

5 Fitzgerald, D.J., *SAE Paper* **760764**(1976).

6 Asik, J.R., Piatkowski, P., Foucher, M.J., and Rado, W.G., *SAE Paper* **770355**(1977).

7 Dale, J.D., Smy, P.R., and Clements, R.M., *Comb. Flame* **31**, 173-85(1978).

8 Dale, J.D. and Oppenheim, A.K., *SAE Paper* **810146**(1981).

9 Tozzi, L. and Dabora, E.K., *19th Symp. (Internat,) On Combustion*, The Combustion Institute, 1467-74(1982).

10 Pitt, P.L. and Clements, R.M., *Comb. Sci. and Tech.* **30**, 327(1983).

11 Lawton, J. and Weinberg, F.J., *Electrical Aspects Of Combustion*, (Clarendon Press, Oxford, 1969)p.88.

12 Behbahani, D.F., Fontijn, A., Müller-Dethlefs, K., and Weinberg, F.J., *Comb. Sci. and Tech.* **27**, 123-32(1982).

13 Weinberg, F.J., *Optics Of Flames*, (Butterworths, London, 1963)p.52.

14 Ref. 11, p.41.

15 Ref. 11, p.51.

16 Orrin, J.E., Vince, I.M., and Weinberg, F.J., *Comb. Flame* **37**, 91-3(1980).

17 Harrison, A.J. and Weinberg, F.J., *Proc. Roy. Soc. (London) A* **321**, 95-103(1971).

18 Hilliard, J.C. and Weinberg, F.J., *Nature* **259**, 556-7(1976).

19 Bradley, D. and Critchley, I.L., *Comb. Flame* **22**, 143-52(1974).

20 Oppenheim, A.K., Teichman, K.Y., Hom, K., and Stewart, H.E., *SAE Paper* **780637**(1978).

21 Cetegen, B., Teichman, K.Y., Weinberg, F.J., and Oppenheim, A.K., *SAE Paper* **800042**(1980).

22 Orrin, J.E., Vince, I.M., and Weinberg, F.J., *18th Symp. (Internat.) On Combustion*, The Combustion Institute, 1755-64(1981).

23 Carleton, F.B., Vince, I.M., and Weinberg, F.J., *19th Symp. (Internat.) On Combustion*, The Combustion Institute, 1523-31(1982).

24 Clements, R.M., Smy, P.R., and Dale, J.D., *Comb. Flame* **42**, 287-95(1981).

25 Grant, J.F., Marram, E.P., and McIlwain, M.E., *Comb. Sci. and Tech.* **30**, 171-84(1983).

26 Topham, D.R., Zhang, J.X., Clements, R.M., and Smy, P.R., *J. Phys. D* **15**, L65-7(1982).

27 Zhang, J.X., Clements, R.M., and Smy, P.R., *Comb. Flame* **50**, 99-106(1983).

28 Jagoda, I.J. and Weinberg, F.J., *J. Phys. D* **13**, 551-61(1980).

29 Behbahani, D.F., Warris, A.M., and Weinberg, F.J., *Comb. Sci. and Tech.* **30**, 289(1983).

30 Cavolowsky, J., Hom, K., Oppenheim, A.K., and Weinberg, F.J., "On The Structure Of Pulsed Plasma Jets,"(Submitted for publication)(1983).

31 Clements, R.M., Smy, P.R., Topham, D.R., Vince, I.M., Vovelle, C., and Weinberg, F.J., Comb. Flame **57**, 265-74(1984).

32 Vince, I.M., Vovelle, C., and Weinberg, F.J., *Comb. Flame*, **56**, 105-112(1984).

33 Pitt, P.L., Ridley, J.D., and Clements, R.M., *Comb. Sci. and Tech.* **35**, 277-85(1984).

34 Cobine, J.D., *Gaseous Conductors*, (Dover, New York, 1958)p.301.

35 Turner, C., Turner, H.W., and Frey, F., *Report* **5119**, ERA, Leatherhead(1966).

36 Turner, C. and Turner, H.W., *Proc. 4th Int. Res. Symp. On Electric Contact Phenomena*, Swansea(1968)p.196.

37 Holm, R., *J. Appl. Phys.* **20**, 715-16(1949).

38 Cobine, J.D. and Burger, E.E., *J. Appl. Phys.* **26**, 895-900(1955).

39 Belkin, G.S., *Sov. Phys.-Tech. Phys.* **15**, 1167-70(1971).

40 Niemeyer, L., *IEEE Trans. Power Appar. Syst.* **PAS-97**, 950-8(1978).

41 Ogurtsova, N.N., Podmoshenskii, I.V., and Rogovtsev, P.N., *High Temp.* **9**, 430-5(1971).

42 Luikov, A.V., *Analytical Heat Diffusion Theory*, (Academic Press, New York, 1968)p.170.

43 Bradley, D. and Gupta, M.L., *Comb. Flame* **40**, 47-63(1981).

44 Offenberger, A.A., Smy, P.R., and Burnett, N.H., *Rev. Sci. Instrum.* **46**, 317-21(1975).

45 Hoyaux, M.F., *Arc Physics*, (Springer-Verlag, New York, 1968)p.36.

46 Ernst, K.A., Kopainsky, J.G., and Maecker, H.H., *IEEE Trans. Plasma Sci.* **PS-4**, 3-17(1973).

47 Ernst, K.A., Kopainsky, J.G., and Mentel, J., *Z. Phys.* **265**, 253-65(1973).

48 Ref. 45, p.43.

49 Spitzer, L. and Härm, R., *Phys. Rev.* **89**, 977-81(1953).

50 Menard, W.A., and Horton, T.E., *NASA Technical Report* **32/1408**, Jet Propulsion Laboratory, Pasadena(1969).

51 Landau, L.D. and Lifshitz, E.M., *Fluid Mechanics*, (Pergamon Press, New York, 1982)p.56.

52 Yos, J.M., *Space System Division Report* **Z220**, Avco Corporation, Wilmington, Ma.(1967).

53 Gaydon, A.G. and Hurle, I.R., *The Shock Tube In High Temperature Chemical Physics*, (Reinhold, New York, 1963)p.62.

54 Resler, E.L., Lin, S.C., and Kantrowitz, A., *J. Appl. Phys.* **23**, 1390-4(1952).

55 Alpher, R.A. and White, D.R., *J. Fluid Mech.* **3**, 457-60(1958).

56 Smy, P.R., *Adv. Phys.* **25**, 517-53(1976).

57 Dewey, J.M., *Ernst Mach Institute Report No.* **2/73**(1973).

58 Braginskii, S.I., *Sov. Phys.-JETP* **34**, 1068-74(1958).

59 Batt, R.G., Bigoni, R.A., and Rowland, D.J., *J. Fluid Mech.* **141**, 1-25(1984).

60 Bendat, J.S. and Piersol, A.G., *Measurement And Analysis Of Random Data*, (Wiley, New York, 1966)p.11.

61 Hinze, J.O., *Turbulence*, 2nd ed., (McGraw-Hill, New York, 1975)p.5.

62 Frenkiel, F.N., *Advances In Applied Mechanics*, vol. 3, (Academic Press, New York, 1953)p.70.

63 Bradshaw, P., *An Introduction To Turbulence And Its Measurement*, (Pergamon Press, Oxford, 1975)p.187.

64 Phillips, O.M., *Ann. Rev. Fluid Mech.* **1**, 245-64(1969).

65 Taylor, G.I., *Proc. London Math. Soc.* **20**, 196(1921).

66 Ref. 61, p.54.

67 Ref. 61, p.359.

68 Crank, J., *The Mathematics Of Diffusion*, (Clarendon Press, Oxford, 1957)p.4.

69 Ref. 61, p.385.

70 Taylor, G.I., *Proc. Roy. Soc. (London) A* **151**, 421-44(1935).

71 Birch, A.D., Brown, D.R., Dodson, M.G., and Thomas, J.R., *J. Fluid Mech.* **88**, 431-49(1978).

72 Ref. 61, p.400.

73 Ref. 62, p.100.

74 Ref. 63, p.37.

75 Ref. 61, p.229.

76 Becker, H.A., Hottel, H.C., and Williams, G.C., *J. Fluid Mech.* **30**, 259-84(1967).

77 von Kármán, Th., *Trans. Am. Soc. Mech. Engrs.* **61**, 705-10(1939).

78 Rosensweig, R.E., Hottel, H.C., and Williams, G.C., *Chem. Eng. Sci.* **15**, 111-29(1961).

79 Weast, R.C., ed., *Handbook Of Chemistry And Physics*, 60th ed., (CRC Press, Boca Raton, 1979)p.F-283.

80 Becker, H.A., Hottel, H.C., and Williams, G.C., *J. Fluid Mech.* **30**, 285-303(1967).

81 Jost, W., *Diffusion In Solids, Liquids, And Gases*, (Academic Press, New York, 1952)p.2.

82 Reif, F., *Fundamentals Of Statistical And Thermal Physics*, (McGraw-Hill, New York, 1965)p.485.

83 Carslaw, H.S. and Jaeger, J.C., *Conduction Of Heat In Solids*, 2nd ed., (Clarendon Press, Oxford, 1980)p.17.

84 Ref. 83, p.257.

85 Ref. 61, p.259.

86 Batchelor, G.K., *The Theory Of Homogeneous Turbulence*, (Cambridge University Press, Cambridge, 1982)p.151.

87 Todd, H.N. and Zakia, R.D., *Photographic Sensitometry*, (Morgan and Morgan, Inc., New York, 1969)p.56.

88 Towle, W.L. and Sherwood, T.K., *Ind. Eng. Chem.* **31**, 457-62(1939).

89 Ref. 13, p.15.

90 Ref. 83, p.7.

Vita

Name: Dennis Joseph Simeoni

Birthplace: Victoria, British Columbia

Year of Birth: 1954

Academic Background:

University of Victoria
Victoria, British Columbia
B.Sc. (Physics) 1979

University of Alberta
Edmonton, Alberta
Ph.d Candidate (Electrical Engineering)
1979-84

Honours and Awards:

Province of British Columbia Government Scholarship 1972
University of Alberta Graduate Teaching/Research Assistantship 1979-83

Related Experience:

Teaching Assistant
University of Alberta
1979-83

Publications:

(1) Smy, P.R., Clements, R.M., Dale, J.D., Simeoni, D., and Topham, D.R., "Plasma Expulsion From The Plasma Jet Igniter," *J. Phys. D* **15**, 2227-39(1982).

(2) Smy, P.R., Clements, R.M., Simeoni, D., and Topham, D.R., "Efficiency And Erosion Characteristics Of The Plasma Jet Igniter," *J. Phys. D* **16**, 783-91(1983).